REPAIR AND REGENERATION OF THE ANTERIOR CRUCIATE LIGAMENT USING BIOLOGICAL AND MECHANICAL AUGMENTATION

by

Jonquil Revé Mau

Bachelor of Science, Georgia Institute of Technology, 2010

Master of Science, North Carolina Agricultural and Technical State University, 2012

Submitted to the Graduate Faculty of

Swanson School of Engineering in partial fulfillment

of the requirements for the degree of

Doctor of Philosophy

University of Pittsburgh

2018

UNIVERSITY OF PITTSBURGH

SWANSON SCHOOL OF ENGINEERING

This dissertation was presented

by

Jonquil Revé Mau

It was defended on

June 26, 2017

and approved by

Steven D. Abramowitch, Ph.D., Associate Professor, Department of Bioengineering

Stephen F. Badylak, D.V.M., Ph.D., M.D., Professor, Department of Surgery

Prashant N. Kumta, Ph.D., Edward R. Weidlein Chair Professor, Department of Bioengineering

Patrick J. McMahon, M.D., Adjunct Associate Professor, Department of Bioengineering

Dissertation Director: Savio L-Y. Woo, Ph.D., D.Sc. (Hon), D.Eng. (Hon), Distinguished University Professor, Department of Bioengineering

REPAIR AND REGENERATION OF THE ANTERIOR CRUCIATE LIGAMENT USING BIOLOGICAL AND MECHANICAL AUGMENTATION

Jonquil Revé Mau, Ph.D.

University of Pittsburgh, 2018

The anterior cruciate ligament (ACL) is the most commonly injured ligament of the knee with well over 200,000 injuries in the US annually. Surgical reconstruction is a widely used treatment option that involves replacing the ACL with a soft tissue graft. ACL reconstruction is often associated with problems such as pain and long-term follow-up studies have shown that up to 25% of patients have experienced unsatisfactory results that include prevalence of osteoarthritis.

In recent years, there has been a renewed interest in regenerating the ACL as an alternative treatment option. In our research center, an innovative approach was developed using an extracellular matrix (ECM) sheet and hydrogel along with a novel metallic implant made of magnesium (Mg) designed to connect the two ends of a torn ACL. The biological augmentation provided by the ECM scaffolds has been shown to incite and accelerate new tissue growth. The mechanical augmentation provided by the Mg ring can restore stability to the knee immediately post-operatively and load the healing ligament throughout the healing process preventing disuse atrophy of the insertion sites. Additionally, the repair construct can be resorbed by the body as the healing tissue begins to bear load.

The objective of this research was to continue the development of ECM + Mg ring repair. First, single crystal Mg was coated using micro-arc oxidation to engineer a degradation rate

appropriate for the ACL healing application and the corrosion, coating, and surface properties of this novel material-coating combination were characterized. Then, a long-term study of ECM + Mg ring repair of a surgically transected ACL in a goat model was performed to examine if the advantages persist up to 26 weeks. The joint stability, ligament function and structural properties of the femur-ACL-tibia complex were measured. Finally, the Mg ring was redesigned for the human ACL and evaluated using finite element analysis and in human cadaveric knees.

This dissertation research has found exciting results that a goat ACL can heal successfully with a combined biological and mechanical augmentation approach and suggests further study of ACL healing in humans. In the end, such an approach could lead to an alternative treatment for ACL injuries.

TABLE OF CONTENTS

LIST OF TABLES

LIST OF FIGURES

PREFACE

"So teach us to number our days, that we may apply our hearts unto wisdom."

Psalm 90:12

In 2011, Dr. Harvey Borovetz, chair of the Department of Bioengineering at the University of Pittsburgh (Pitt) at the time, was visiting North Carolina A&T State University (NCAT) in Greensboro, NC where I was a student of their newly established Bioengineering graduate program. My professor, Dr. Devdas Pai, asked Dr. Borovetz if he knew of a summer research opportunity at Pitt in which I could participate. Dr. Borovetz said he would reach out to some labs. After a short time, we received notice that Dr. Savio L-Y. Woo of the world renowned Musculoskeletal Research Center (MSRC) had a vacancy for a summer research internship. At that time, I could have never imagined the unique opportunity that lay ahead would blossom into two summers of research while I completed my masters at NCAT and another four and a half years of doctoral studies under the support and mentorship of Dr. Woo. Throughout my graduate career at Pitt, there have been so many people who have contributed to my work and I would like to formally acknowledge them.

First, I would like to thank Dr. Woo. Thank you for accepting me as a summer student back in 2011 and 2012 and as a doctoral student in 2013 even after you weren't accepting any

more student. It's an indescribable honor to be the last student of your career. You have shaped my thinking and practice as a researcher and engineer. Your philosophy will forever inspire me to achieve higher and be better in everything that I do.

My experience at Pitt has been like none other because of the family I have formed with the staff and students of the MSRC. To previous graduate students, Dr. Kwang Kim and Dr. Katie Farraro; orthopaedic surgery fellows, Matteo Tei, Andrea Speziali, Norihiro Sasaki, Antonio Pastrone, Chris Chiang, and Huijun Kang; predoctoral fellow Huizhi Wang; undergraduate research students, Kit-Yu Leung, Sara Orr, Dhir Patwa, Seth Cordts, Lindsay Hess, Lewis Gross, Chak Yuk Yu, Sean Mackey, Yajnesh Vedanaparti, and Ian Moran; and executive assistant and friend Diann DeCenzo: I appreciate you all and the work we have done together.

There have been many collaborators who have taught me so much about what it means to be a part of a multi-disciplinary team. I would like to thank Dr. Steven Abramowitch (Dr. Bill Barone, Dr. Katrina Knight, Deanna Easley), Dr. Prashant Kumta (Dr. Abhijit Roy, Dr. Da-Tren Chou, Jingyao Wu, John Ohodnicki), Dr. Stephen Badylak (Scott Johnson, Jenna Dziki, Madeline Cramer), Dr. Patrick McMahon, Andy Holmes of the Swanson Center for Product Innovation, Dr. Bob Wagner and the Division of Laboratory Animal Resources staff, and NATON Medical Group. I would like to acknowledge the support of Dr. Harvey Borovetz, Dr. Sanjeev Shroff and the Department of Bioengineering, Dr. Sylvanus Wosu and the Department of Diversity, Dr. Jaganathan Sankar, Dr. William Wagner, Dr. Matthew McCullough, Dr. Devdas Pai, Dr. Yeoheung Yun, Dr. Vesselin Shanov and the NSF Engineering Research Center for Revolutionizing Metallic Biomaterials (ERC-RMB), Max Fedor and Suneera Bhatia and the Coulter Translational Research Partners II Program, the Biomechanics in Regenerative Medicine

(BiRM) training program, and Dr. Paul Monga and the Cellular Approaches to Tissue Engineering and Regeneration (CATER) training program.

Finally, I must thank my friends and family. I appreciate my longtime friends in Atlanta and my new friends in Pittsburgh. The Hillcrest SDA Church has been an amazing support system. My biggest motivators and cheerleaders have been my mother, Phyllis Haskins, and my husband, Edwin Mau. Thank you!

1.0 MOTIVATION

The anterior cruciate ligament (ACL) is a major stabilizer of the knee, aiding in the control of the 6 degrees of freedom (DOF) of knee motion [1, 2]. It is the most often injured knee ligament with well over 200,000 injuries in the United States per year and associated costs exceeding $2 billion [3, 4]. ACL injures commonly occur during sporting and work related activities and can lead to functional instability and long-term complications such as meniscal injuries, failure of secondary stabilizers, and the early onset of osteoarthritis [5].

There are several treatment options for ACL injuries including conservative (nonsurgical) treatment and surgical reconstruction. Nonsurgical therapy includes bracing and rehabilitation protocols that aim to regain joint mobility and improve neuromuscular function to obtain compensatory functional stability [6, 7]. The most common treatment is ACL reconstruction (ACLR) and is selected for nearly two-thirds of all ACL injury patients. ACLR is an arthroscopic procedure where the injured ACL is removed and replaced with a soft tissue graft. While ACLR is able to restore joint stability in the short-term, there are consistent reports of unsatisfactory outcomes in the long-term including problems with pain, especially at the graft donor site. Also, long-term follow-up studies have shown that 20% to 25% of patients have an increased risk in developing osteoarthritis [8-11]. Additionally, there are over 9,000 scientific journal articles on ACLR aiming to make improvements to various components of the surgical

procedure, suggesting that an ideal surgical procedure yielding good short- and long-term outcomes has yet to be developed.

An advantageous alternative to ACLR is to heal the native ACL. This approach to treating ACL injuries would have many advantages over ACLR, including preservation of its complex anatomy, insertion sites, proprioceptive nerve fibers, and biomechanical properties. Patients could also avoid the problems associated with donor site morbidity seen with ACLR because healing the ACL would eliminate the need for graft harvesting and large bone tunnels in the femur and tibia. However, the ACL has a limited potential for healing, even in the case of incomplete rupture [12]. For this reason, suture repair, a surgical technique that attempts to reconnect the torn ends of the ACL to permit healing, has been an inferior option demonstrating no difference to conservative treatment [13-15].

With recent advances in tissue engineering, there has been a renewed interest in ACL healing. Previous ACL healing studies have focused their efforts on biological strategies such as mesenchymal stem cells [16], growth factors [17], platelet-rich plasma [18], and extracellular matrix (ECM) bioscaffolds [19]. The results of these studies have demonstrated an ability to increase new tissue growth but do not successfully restore the joint stability and biomechanical properties of the normal ACL suggesting that biological augmentation alone is not sufficient [18, 19]. This knowledge has been the motivation for our innovative approach to ACL healing called "ECM + Mg-ring repair" which combines biological augmentation and mechanical augmentation using ECM scaffolds and a resorbable metallic implant. The feasibility of ECM + Mg-ring repair has been demonstrated at time zero and in short-term preclinical studies [20, 21]. This approach has been shown to both accelerate new tissue growth and restore joint stability [20, 21]. With such promising results, it is evident that ACL healing is still a promising treatment option.

Thus, the overall objective of this dissertation research was to characterize the Mg material used for the implant, complete a long-term study of ECM + Mg-ring repair of a transected ACL in a goat model and use the acquired knowledge to further develop the Mg-ring device for human application.

2.0 BACKGROUND

2.1 BIOLOGY AND BIOMECHANICS OF LIGAMENTS

Ligaments are bands of soft connective tissues composed of closely packed, parallel collagen fiber bundles that connect bone to bone. These unique tissues serve essential roles in the musculoskeletal system by transferring tensile loads to maintain stability and guide motion of diarthrodial joints. Knowledge of the biology and biomechanics of ligaments provide insight to how ligaments function in response to physiological and pathological loading.

2.1.1 Biochemical Composition and Histological Structure

Ligaments have low vascularity and low cellularity with less than 5% of the total volume occupied by cells [22-25]. The cells in these tissues are called fibroblasts and function to maintain and remodel the extracellular matrix (ECM) in which they reside. Ligaments consist of both the fibrillar components including collagen and elastin and the nonfibrillar components such as proteoglycans, glycolipids, and water (65% to 70% of total weight). The collagen fibers are organized and well-oriented along the longitudinal direction with fibroblasts arranged in rows along the fibers [26, 27].

Approximately 70% to 80% of the dry weight of normal ligament is composed of type I collagen. Histologically, collagen fibers display a regular wavy appearance, or crimp pattern,

under unloaded conditions [23, 25, 28, 29]. Under transmission electron microscopy, a bimodal distribution of collagen fibril size can be observed with a smaller group of fibrils measuring between 40 and 75 nm in diameter and the larger fibrils between 100 and 150 nm in diameter [30-33]. The smaller fibrils are located in the spaces between the larger fibrils allowing for optimal fibril packing [34]. This bimodal distribution is functionally significant because the incorporation of a high number of small diameter fibrils ensures better binding between fibers by virtue of their higher surface to volume ratio while the larger diameter fibrils provide the stiffness and strength requirements. Collagen also has the ability to form covalent intramolecular and intermolecular crosslinks, which are key to its tensile strength characteristics and resistance to chemical or enzymatic breakdown [35-37].

There are many other collagen types, including III, V, IX, X, XI, and XII, present in much less amounts but still play important roles in maintaining the structure and function of ligaments. For example, type III collagen is involved in tissue healing and remodeling [38] and type V collagen exists in association with type I collagen and serves as a regulator of collagen crosslinking and fibril diameter [39, 40]. Furthermore, type XII collagen provides lubrication between collagen fibers [41]. Collagen types IX, X, and XI exist with type II collagen at the fibrocartilaginous zone of the ligament-bone interface [42-44] and function to minimize the stress concentrations when loads are transmitted from soft tissue into bone [45, 46].

Elastin, which is present in ligaments in a few percent by weight, allows the tissue to return to its prestretched length following physiological loading. The ground substance constituents of ligaments make up only a small percentage of the total dry tissue weight but are nevertheless quite significant because of their ability to imbibe water. The water and proteoglycans provide lubrication and spacing that are crucial to the gliding function of fibers in

the tissue matrix. Ligaments display time- and history-dependent viscoelastic properties that reflect the complex interactions between proteins, ground substance, and water Collectively, these constituents serve to maintain fiber orientation and separation for optimal function [47].

At the ultrastructural level, ligaments have a hierarchal organization composed of fibrils, fibers, subfascicular units, fasciculi, and the tissue itself (Figure 1) [48]. Ligaments are surrounded by a loose areolar connective tissue, referred to as periligament [49, 50]. This ensheathment facilitates gliding movements of fibers allowing them to stretch and bend against each other and the parallel arrangements of fibers allows forces to be channeled in specific directions [48].

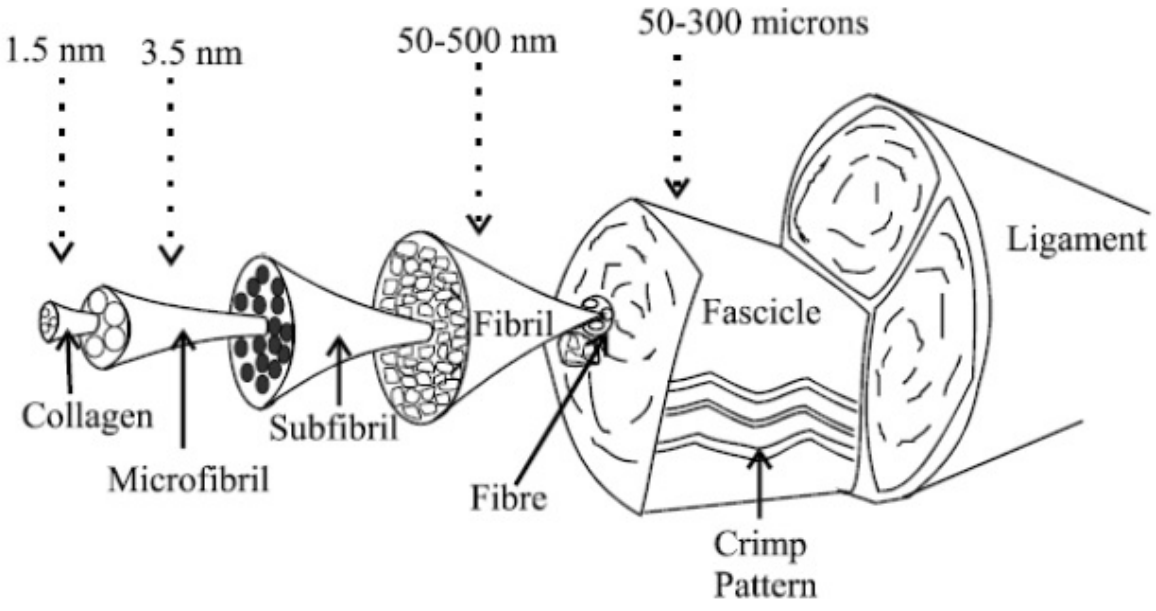

Figure 1: A schematic of the structural hierarchy of ligament [51]

Ligament insertions to bone distribute and dissipate forces by transmitting them through the fibrocartilage to bone. There are two types of insertions: direct and indirect. Direct

insertions are more common having four distinct phases in the transition from ligaments to bone: ligament, fibrocartilage, mineralized fibrocartilage, and bone [45, 52, 53]. The size of each zone varies with particular ligaments; however, the total length of the transition zone is usually much less than 1 mm. Indirect insertions are more complex morphologically as there are distinct superficial and deep fibers. The superficial fibers are connected to the periosteum, whereas the deeper fibers, called Sharpey fibers, are anchored directly to the bone [45, 53, 54]. Indirect insertions usually occur when the ligaments attach to bone after crossing the epiphyseal plate.

2.1.2 Tensile Properties of Ligaments

The primary functions of ligaments are to maintain the proper anatomic alignment of the skeleton and guide joint movements. They also transmit forces along their longitudinal axis. Thus, their biomechanical properties are measured via uniaxial tensile testing to obtain structural and mechanical properties.

2.1.2.1 Structural Properties of Bone-Ligament-Bone Complex

Uniaxial tensile testing of ligaments can be complex as there are many factors that have been shown to affect the outcome. Isolated ligaments are difficult to test independently due to the short length of the ligament substance and the common problem of specimen slippage from clamps. As a result, uniaxial tensile tests are generally performed using the entire bone-ligament-bone complex (e.g. femur-ACL-tibia complex or FATC) with ligament insertion sites left anatomically intact. The bones are clamped such that the ligament can be aligned to the applied tensile load. Using a materials testing machine, a load is applied along the longitudinal axis of the ligament at a prescribed rate until failure. A resulting load-elongation curve is

obtained (Figure 2). Generally, the curve has a nonlinear toe region characteristic of the recruitment and uncrimping of collagen fibers, the linear region, and the failure region. The parameters that describe the structural properties of the specimen include the ultimate load, the ultimate elongation, linear stiffness, and energy absorbed at failure. The ultimate load is the maximal force applied to the specimen and the corresponding elongation is the ultimate elongation or elongation at failure. The linear stiffness is the slope of the linear region and energy absorbed at failure is the area underneath the curve. The parameters reflect behavior of the entire bone-ligament-bone complex which includes tissue geometry, orientation of collagen fibers to applied loads as well as the contribution of the bony insertions [55].

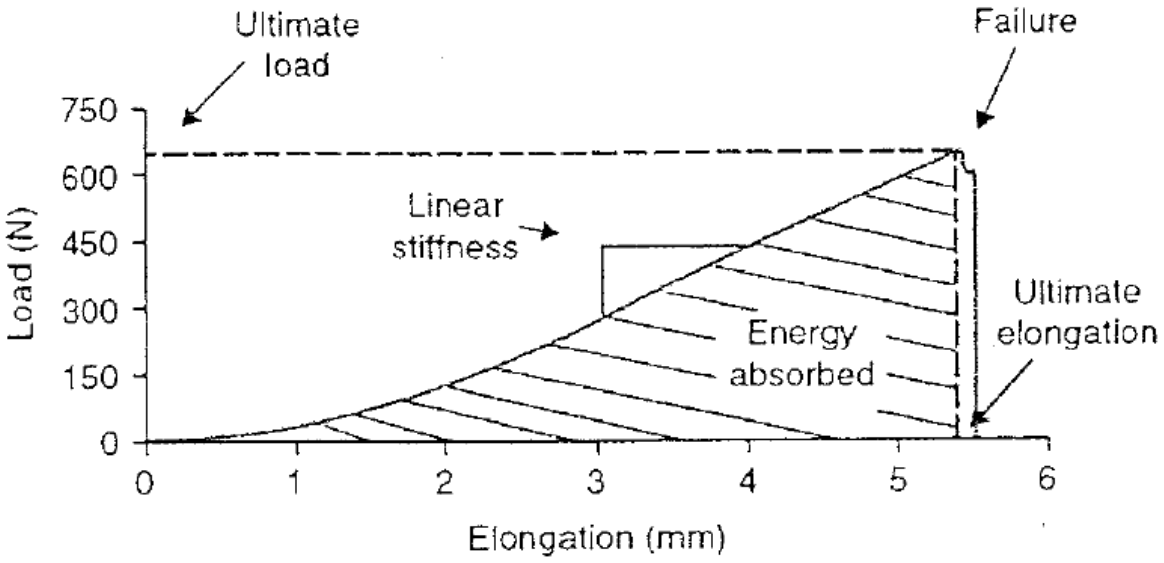

Figure 2: A typical load-elongation curve from uniaxial tensile testing of a bone-ligament-bone complex representing its structural properties [56]

Structural properties of a bone-ligament-bone complex are sensitive to testing conditions. Specimen orientation during tensile testing, for example, has been shown to significantly affect

the structural properties. When human FATCs were tested in an anatomical orientation where the angles of insertion at the femur and tibia are preserved, stiffness and ultimate load of FATCs were significantly higher compared to those tested in a nonanatomical orientation where it was aligned along the tibial axis [57]. Specimen storage method [58] and testing temperature [59], as well as donor age [57] and activity level [60, 61] were also found to be significant factors affecting structural properties.

2.1.2.2 Mechanical Properties of Ligament Substance

The mechanical properties of a ligament can also be obtained from the same uniaxial tensile test. A stress-strain relationship is obtained by normalizing the tensile load by the cross-sectional area (i.e. stress) and by normalizing the change in elongation in a defined region of the ligament substance by the initial length (i.e. strain). The parameters that describe the mechanical properties of the specimen include the tensile strength, ultimate strain, tangent modulus, and strain energy density of the ligament substance can be determined (Figure 3). Tensile strength is the maximal stress and the corresponding strain is the ultimate strain. The tangent modulus is the slope of the linear region of the stress-stain curve and the strain energy density is the area underneath the stress-strain curve. These parameters describe the specimen independent of its size and geometry.

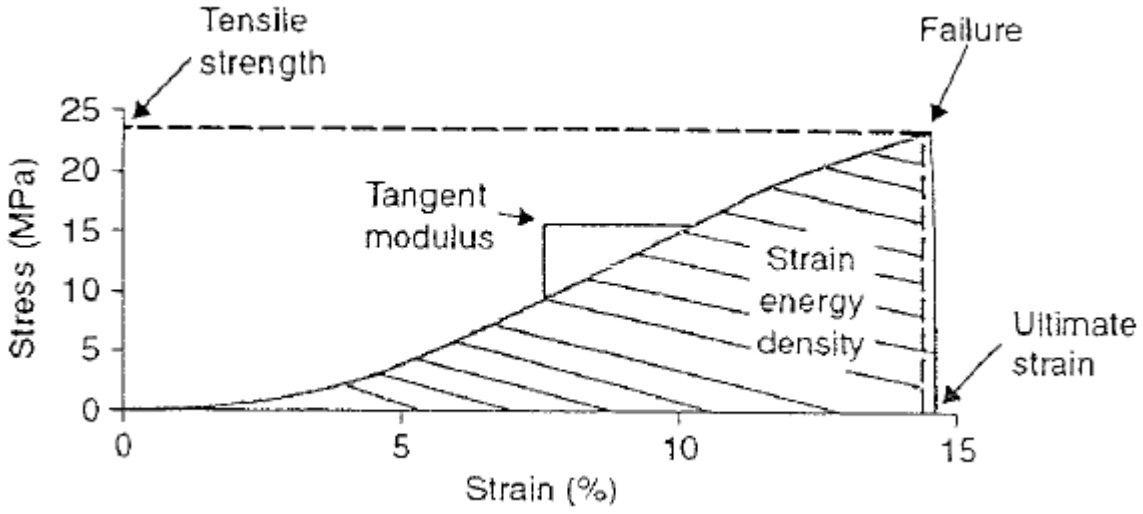

Figure 3: A typical stress-strain curve from uniaxial tensile testing representing the mechanical properties of a ligament[56]

An accurate measurement of the cross sectional area is required for stress calculations. To reduce errors associated with oversimplification of the complex shape and distortion of the specimen shape via contact measurement methods (i.e. calipers), noncontact methods have been used [62-65]. In our research center, the laser reflectance system has been adopted as a method to measure both the cross-sectional area and the shape of soft tissues [66]. The second obstacle to overcome when determining the mechanical properties of a ligament is accurate measurements of tissue strain during experimental protocols. The use of the clamp-to-clamp distance to determine the initial length of the specimen for calculations of stretch or strain can lead to errors in strain measurement because the clamp imposes an artificial boundary condition on the tissue as well as local damage [67]. To avoid these errors, optical techniques utilizing markers and video tracking have been developed [58, 68-72]. The change from the gauge length to its current position can be output in terms of percent strain and used in calculating the mechanical properties [58, 71, 73-76].

2.1.3 Role of Ligament in Joint Function

It is important to understand the role of ligaments in the context of the joint function as a whole along with the aforementioned tensile properties. Joint motion is governed by the direction and magnitude of externally applied loads, ligament forces, contact between joint surfaces, and muscle activity. For the knee, motions include a combination of translations: proximal-distal, medial-lateral, and anterior-posterior, and rotations: internal-external, flexion-extension and varus-valgus. These translations and rotations describe motion in 6 degrees of freedom (DOF).

In order to assess joint stability and ligament function, methods for measuring knee kinematics as well as the in-situ forces in the knee ligaments in response to external loading conditions have been developed. Due to the difficulty of achieving 6 DOF knee motion experimentally, early experiments on ligament function were performed on material testing machines limited to a single degree of freedom [77, 78]. An external load would be applied to a cadaveric knee and the resulting translation would be measured. Then, in-situ forces in the ligament, such as the ACL, would be measured by repeating the motion after transection of the ligament and calculating its in-situ forces using the principle of superposition. However, by constraining DOF, results from these experiments could not reflect the true function of the ligament. Gradually, systems with more DOF were developed [79, 80], prior to the introduction of noncontact 6 DOF systems.

Linkage systems were the first type of system to permit 6 DOF of knee motion to measure forces in ligaments indirectly [81]. By fixing the knee flexion angle, the remaining 5 DOF tibia-femoral motion of a knee and the in-situ forces in ligaments were determined through sequential cutting [82]. However, a serious limitation of all linkage systems was that they could

not repeat the starting position or the multiple DOF path of motion once the ligament was transected.

A robotic/universal force-moment sensor (UFS) testing system was developed to study knee kinematics as well as directly measure the in-situ forces in the knee ligaments in response to external loading conditions (Figure 4) [83]. The limitations associated with linkage systems were eliminated with the development this testing system that can be operated in force, position, or hybrid control. For example, the starting position and path of motion could be repeated throughout the experiment and the in-situ forces in the ligament could be determined in response to externally applied loads using the principle of superposition. The robotic/UFS testing system is also advantageous because it provides all of its data for a single specimen, thus eliminating interspecimen variation and allowing the greater statistical power by enabling the use of repeated measures analysis of variance (ANOVA). This powerful system has now been adopted by laboratories worldwide, which have generated an abundance of new knowledge about knee ligaments and joint function. As it pertains to the ACL, it has been particularly important for determining the function of the ACL and other knee ligaments including joint kinematics [84], in-situ forces [85], the effect of knee motion and external loading on the length of the ACL [81], the effect of joint constraints on the in-situ load distribution in the ACL [86], and the interdependence of the medial meniscus and ACL [87, 88].

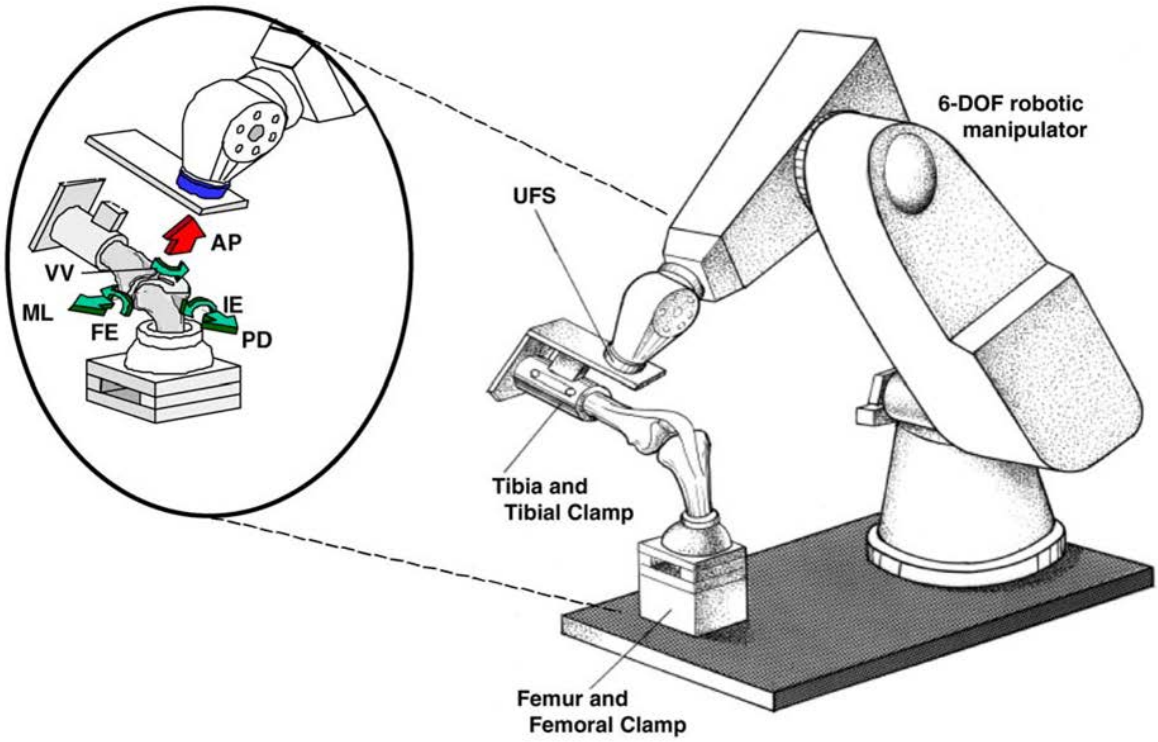

Figure 4: A schematic illustrating a knee joint being tested on the robotic/universal force-moment sensor (UFS) testing system at preselected angles of knee flexion, providing 5-degree of freedom joint motion (AP – anterior-posterior, PD – proximal-distal, ML – medial-lateral, VV – varus-valgus, IE – internal-external, FE – flexion-extension) [89]

2.2 LIGAMENT INJURIES AND CLINICAL MANAGEMENT

Orthopaedic soft tissue injuries are common with an estimated 800,000 surgeries performed each year [90]. More specifically, the ACL is the most often injured knee ligament with well over 200,000 injuries in the United States with associated costs exceeding $2 billion [3, 4]. There are

several treatment options for ACL injuries including conservative (nonsurgical) treatment and surgical repair and reconstruction.

2.2.1 ACL Anatomy and Physiology

The ACL is a major stabilizer of the knee, aiding in the control of the 6 DOF of knee motion (Figure 5) [77]. The primary function of the ACL is to restrain anterior translation of the tibia with respect to the femur with secondary roles in internal-external and varus-valgus rotations [2, 85, 91-95]. It is located in the center of the tibiofemoral joint where it crosses from its femoral attachment on the medial surface of the lateral condyle to its tibial attachment on the tibial plateau in front of and lateral to the anterior tibial spine [96, 97]. The ACL consists of two bundles, the anteromedial (AM) and posterolateral (PL) bundles. The AM bundle is tighter in flexion and the PL bundle is tighter in extension [82, 94, 95]. This double bundle structure allows the ACL to function throughout all angles of flexion. While the ACL is located intraraticularly, it remains extra-synovial throughout its course [97, 98]. The synovium is a thin connective tissue that lines the ACL and protects it from the synovial fluid. The synovium encompasses a network of nerve and blood vessels that are the primary source of nutrition for the ACL [98-104].

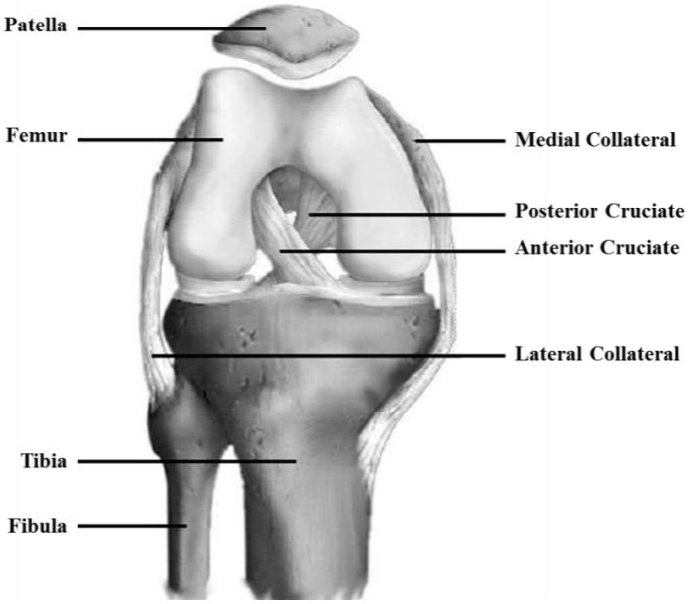

Figure 5: Anterior view of the flexed knee, showing the bones and major stabilizing ligaments

2.2.2 Incidences and Consequences of ACL Injuries

The ACL is the most frequently injured ligament in the knee [3, 4, 105-107]. ACL injuries commonly occur during sports and work related activities as a result of contact or noncontact mechanisms [3, 4, 107]. Contact injuries result from direct impact from an object or individual such as a football tackle while noncontact injuries involves sudden deceleration, an abrupt change in direction, or jump landing [3, 4, 107]. A midsubstance tear of the ACL has limited potential to heal on its own and can lead to chronic knee instability and long term complications such as meniscal injuries, failure of secondary stabilizers, and the early onset of osteoarthrosis [5, 87, 108-111].

2.2.3 Clinical Management of ACL Injuries

The primary goals of clinical treatment of an ACL injury are to eliminate pain and restore ligament function and knee stability. Also, treatments should manage short term symptoms such as pain as well as delay the onset of osteoarthritis. Conservative treatments and surgery are among the treatment options.

2.2.3.1 Conservative Treatment

About one-third of ACL injuries are managed with conservative (nonsurgical) treatments. These treatments includes bracing and rehabilitation protocols that aim to regain joint mobility and improve neuromuscular function to obtain compensatory functional stability [6, 7]. More specifically, they aim to strengthen the hamstrings and quadriceps muscles and restore balance and knee range of motion [112].

The use of conservative treatment following ACL injury has been debated. Some have reported that the modification of physical activity and rehabilitation restore neuromuscular function led to good long term knee function [113, 114], while others have found less favorable results. Anterior and rotatory instability have been reported in a large number of patients, as well as subsequent injury to other structures in the knee [12, 115, 116]. Additionally, many conservatively treated patients will eventually seek surgical treatment to manage complications. Thus, due to the long term consequences and risks associated with ACL deficiency, as well as the higher activity levels of younger patients, those who may be satisfactorily treated with non-surgical intervention include but are not limited to those who are willing to avoid high risk activities and those who are more than 40 years of age [5].

2.2.3.2 Surgical Repair

Due to poor results following conservative treatment, clinicians have investigated surgical treatment options for ACL injuries. In the 1960s, surgical techniques were developed to repair an injured ACL by reapproximating the torn ends using sutures [15, 117-119]. However, due to the ACL's limited innate healing capacity, these studies achieved limited success. Feagin et al. conducted a study of West Point cadets who underwent suture repair after ACL injury and by 5 years post-surgery, the majority of patients experienced poor functional outcomes, including reinjury, instability, and impairment of daily activities [9]. Similarly, Sandberg et al. demonstrated no difference between suture repair and conservative treatment of the ACL [15], while Engebretson at al. showed that replacing the injured ACL with a soft tissue graft (ACL reconstruction) provided significantly improved functional outcomes [120]. As a result, there began a shift in surgical treatment to ACL reconstruction, which was able to immediately restore strength and stability to the joint.

2.2.3.3 ACL Reconstruction

ACLR has become the gold standard of treatment for ACL injuries for its ability to restore knee stability. Also, many patients hope to prevent the early development of osteoarthritis that is inevitable with an ACL deficient joint.

ACLR is an arthroscopic procedure where the damaged ACL is removed and replaced with a soft tissue autograft or allograft. The replacement graft is often securely fixed into femoral and tibial bone tunnels using interference screws. The bone-patellar tendon-bone (BPTB) graft had been used widely because of its high strength [121]. Also, it has bone blocks on both ends that could facilitate initial fixation in the bone tunnels and good osteointegration. Follow-up studies have shown good short and mid-term outcomes after ACLR with a BPTB

graft [122-124]. However, post-operative complications, such as patellar tendon ruptures, arthrofibrosis, loss of quadriceps function, anterior knee pain, and extension deficits were reported [125, 126]. More recently, the hamstring tendon (semitendinosus and gracilis) [127-129] and quadriceps tendon [84, 130-133] grafts have increased in popularity because of the ease of graft harvesting and smaller incision as well as reduced postoperative issues such as donor site morbidity and knee extensions deficits.

Regardless of graft choice, there is a prevalence of osteoarthritis after ACLR [109, 134-136]. The long term degenerative effects on ACL reconstruction are likely caused by the inability of the ACL replacement graft to replicate the biomechanical function of the native ACL. It is not possible to replicate the complex anatomy and function of the native ACL with a soft tissue graft. Additionally, the strength of the grafts do not match the stiffness of the ACL [57, 121]. These reasons along with inherent healing challenges lead to altered knee kinematics resulting in degenerative effects including degeneration of the articular cartilage.

2.2.3.4 Rationale for Alternative Treatments

ACLR has been the most widely chosen treatment option for ACL injuries. Clinicians and researchers have sought to improve surgical reconstruction techniques including the graft options, fixation strategies, surgical techniques, healing enhancements, and so on. While ACLR can restore joint stability in the short-term, there is a prevalence of osteoarthritis and other complications in the long-term. Recently, it has become obvious that more treatment options are needed, especially when a number of new biological interventions have become feasible.

An advantageous alternative treatment is to heal or regenerate the native ACL as opposed to replacing it. This approach to treating ACL injuries would have many advantages over ACLR, including preservation of its complex anatomy, insertion sites, proprioceptive nerve

fibers, and biomechanical properties. Patients could also avoid the problems associated with donor site morbidity seen with ACLR because healing the ACL would eliminate the need for graft harvesting and large bone tunnels in the femur and tibia. Furthermore, by preserving the ACL's structure and biomechanical function, healing the ACL could delay the development of osteoarthritis. Thus, we continue to research and develop an innovative approach involving tissue engineering strategies to heal ACL injuries.

2.2.4 Ligament Healing

Ligaments have been shown to exhibit varying and unique healing responses following injury. For example, the ACL and posterior cruciate ligament (PCL) have a low healing capacity while the medical collateral ligament (MCL) has a good healing response, even without surgical treatment [137-140]. There are many factors that influence the healing response such as mechanical forces, vascularity and nutrition, location in the body (intra-articular versus extra-articular), and cellularity modulation of the healing process. Thus, it is helpful to understand the healing process of ligaments that exhibit a better natural healing response in order to understand how to heal the ACL.

2.2.4.1 Phases of Ligament Healing

The events of healing of ligaments can be roughly divided into four overlapping phases: hemorrhage, inflammation, repair (proliferation), and remodeling. Minutes after the ligament injury, blood collects and forms a platelet-rich fibrin clot at the injury site and the hemorrhagic and inflammatory phases occur over several days. In the hemorrhage phase, a cascade of cellular events occurs that include release of cytokines within the clot followed by the appearance of

polymonomuclear leukocytes and lymphocytes. These cells respond to autocrine and paracrine signals to expand the inflammatory response and recruit other types of cells to the wound [141].

The reparative phase follows over the next couple of weeks to months. During this phase, fibroblasts recruited to the injury site start forming healing tissue. Growth factors, including transforming growth factor-β (TGF-β) and platelet-derived growth factor (PDGF) isoforms, are involved in modulating the healing [142]. Meanwhile, increased neovascularization brings in circulating cells and nutrients to further enhance the healing process. The blood clot quickly turns into newly formed healing tissue that is composed of an aggregation of cells surrounded by a matrix. But, its histomorphological appearance and biochemical composition is different from that of an uninjured ligament. Notably, there is a homogenous distribution of smaller diameter collagen fibrils which is in stark contrast to the bimodal distribution of the normal ligament [33, 143, 144]. Biochemically, it contains elevated amount of proteoglycans, a higher ratio of type V to type I collagen, and a decrease in the number of mature collagen cross links.

Then the remodeling phase follows for months to years after the injury. In this phase, cellularity and levels of collagen type III are decreased while the matrix is realigned in response to loading applied to the tissues. On the other hand, the diameter of collagen fibrils remains small while the level of collagen type V remains elevated for years after injury [143-147]. Interestingly, the type V collagen has been shown to play a central role in the regulation of the lateral aggregation of smaller collagen fibrils. Thus, an elevated type V collagen could be associated with the inferior mechanical properties of healing tissue [148, 149].

2.2.4.2 MCL Healing

The healing process of the MCL follows this general healing pathway as described above. Thus, it serves as a good model for the study of histological, biochemical, and biomechanical changes with time. It has been shown that the process of MCL healing is greatly impacted by treatment [150-154]. Laboratory and clinical studies have shown controlled mobilization is superior to immobilization [153, 155, 156]. As a result, nonoperative repairs have a better outcome to surgical repairs. In our research center, a severe "mop-end" injury model of the rabbit MCL that tears its midsubstance while simultaneously damaging its insertion sites has been developed and used to compare nonoperative treatment without mobilization to surgical repair with a brief period of mobilization [156]. After 12 weeks of healing, there were no significant differences in varus-valgus knee rotation, in-situ force of the MCL, or tensile properties between repaired and non-repaired MCL [156]. Based on these studies, clinical management (i.e. bracing) with early controlled range of motion exercises as soon as pain subsides is suggested [157, 158].

While the MCL heals with non-operative treatment and the stiffness of the healing femur-MCL-tibia complex (FMTC) begins to approach normal levels, the CSA of the healed tissue continues to increase with time, measuring as much two and a half times its normal size by 52 weeks after injury [155]. Meanwhile, the mechanical properties of the healing MCL remain consistently low when compared to those for the normal ligament and do not improve with time. In other words, the healing process involves making a larger quantity of lesser quality ligamentous tissue. Moreover, studies also show that the rate of healing of the ligament is asynchronous with the insertion sites because of its anatomical and morphological complexity.

There is also evidence that activity level could influence the rate of healing [159]. A goat model was used because it has more robust activity as well as larger size than the rabbit. With

this model, the stiffness and ultimate load of the healing goat FMTC are closer to control values at earlier time periods than those from the rabbit model.

2.2.5 Challenges for ACL Healing

Unlike the MCL, an extra-articular ligament, the ACL does not undergo the normal phases of healing after injury. It has been observed that the remnants of ACL degenerates rapidly after injury [160, 161]. There are several biological and mechanical factors that influence this process [162-166]. First, numerous studies have reported the lower intrinsic healing capacity of the ACL compared the MCL [167-169], and reduced cellular proliferation [170], ECM production [170], gene expression [171, 172], migration [173], and less vascularity [22, 101] have all been identified as contributing factors. Additionally, the synovium surrounding the ACL contains vasculature and nerves. When the synovium is disrupted, it takes 3-6 weeks to regenerate following ACL injury [100, 164, 174]. Without the synovium, the synovial fluid can enter the injury site and prevent hematoma formation, and limit the initial step of ligament healing. Further, it has been shown that the two ends of a ruptured ACL retract and form a large gap between them; thus, making it more difficult to restore continuous tissue [164]. The gap between the torn ends is further exaggerated by the lack of mechanical stabilization following injury and causes altered loading and kinematics.

These multiple factors explain why ACL healing is challenging. Thus, creating an appropriate environment in which the ACL could heal is essential as well as addressing the biological and mechanical factors that affect the healing response. Therefore, this dissertation research aims to address some of these healing complexities to achieve ACL healing.

2.2.6 New Approaches to ACL Healing

Just as the challenges to ACL healing have been due to biological and mechanical factors, strategies for healing the ACL have been developed similarly. With the advances in tissue engineering and regeneration, many biological approaches to ACL healing have been developed resulting in new tissue formation to a varying degree. In general, the ACL healing rate is slow and the lack of loading to the healing ACL has deleterious effects on its attachments to bone. Thus, mechanical augmentation that could maintain joint stability while simultaneously loading the healing ACL has been used in combination with biological augmentation to incite more robust tissue healing.

2.2.6.1 Biological Augmentation

Steadman and coworkers developed a microfracture technique that involves making multiple holes in the subchondral bone at its femoral attachment to encourage release of marrow elements to form hematoma and provide an enriched environment for ACL healing [175]. They have used this approach to successfully treat active patients over 40 years of age [175]. With clinical evidence for the potential of ACL healing other biological strategies have been employed for “hard to heal” soft tissues including hyaluronic acid, growth factors, mesenchymal stem cells, platelet-rich plasma (PRP), and ECM bioscaffolds for partial ACL defects as well as full ACL transection [16, 17, 19, 163, 166, 176]. These studies have shown that biological augmentation could increase vascularity, more tissue formation and improved biomechanical properties of the healing ACL. Clinically, patients with partial ACL tears with suture repair and bone marrow plasma were able to return to sports 4-5 months and experienced good healing up to 2 years based on MRI scans [177].

In addition to early work on biological augmentation to heal partial ACL injuries, Murray et al. have used collagen-platelet-rich plasma (C-PRP) as a bioscaffold for healing a fully transected and sutured porcine ACL [178]. At 4 weeks, the linear stiffness under uniaxial tension, the load at yield and at failure were more than 2 times that of the suture repaired control group [178]. These improvements persisted up to 3 months post-operatively with a 320% increase in linear stiffness and a 76% greater yield load than suture repair alone [18].

The potential advantages of using porcine small intestinal submucosa (SIS) ECM to heal the transected ACL were examined [19, 179, 180]. The ACL was first surgically transected and then underwent suture repair. Then, and ECM-SIS sheet was used to wrap around the injury site before injecting ECM hydrogel into the transected site (Figure 6). Suture repair alone served as the control group. After 12 weeks, the CSA of the ACL following ECM-SIS treatment was 4.5 times over that of the suture repair group (127 ± 90% vs. 34 ± 25%, respectively). The function of each stifle joint was assessed using the robotic/UFS testing system. The anterior-posterior tibial translation for the ECM-treated group, in response to a 67-N anterior-posterior tibial load, had statistically significant improvement as compared to those for the suture repair control. At 30° of joint flexion, the anterior-posterior tibial translation was 8.6 ± 2.0 mm which was less than that of the control group. The in-situ force in the healing ACL was found to be nearly 2 times higher than that of the control group. Similar results were found at 60° and 90° of joint flexion.

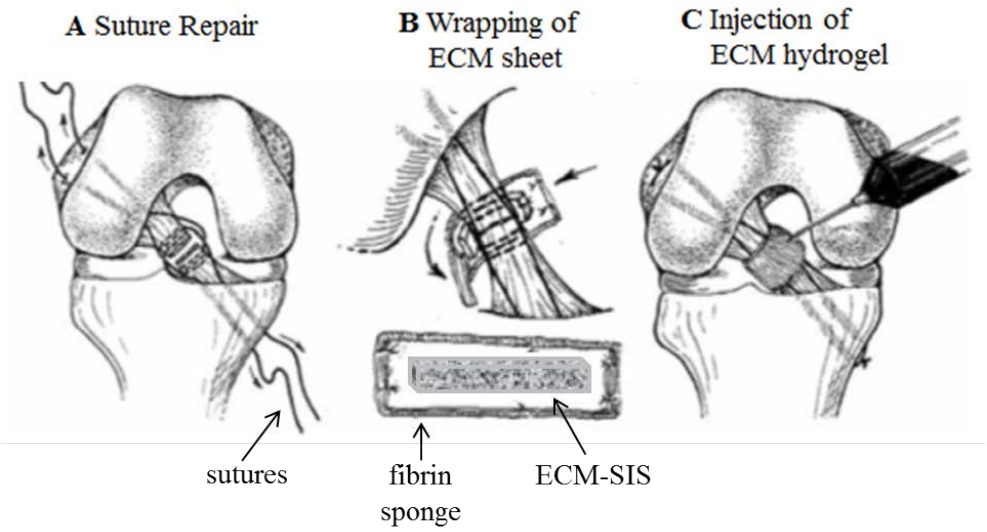

Figure 6: Illustrations of the ECM-SIS treatment for a transected ACL in a goat model [19]

Afterward, the healing ACL was exposed and an abundance of continuous neo-tissue formation could be seen, but there was hypertrophy. Histologically, the healing ACL had an organized collagen matrix with spindle-shaped cells. Tensile testing of the FATC was done and the stiffness for the treated group was 2.4 times that of the suture repair control group. These results suggest biological augmentation could indeed enhance ACL healing [19].

A preliminary experiment involving a longer time point (26 weeks) was also conducted. In this case, the healing of the ACL continued as its collagen fibers had become completely aligned and packed. During tensile testing, the mode of failure was at the femoral insertion site rather than the original transection site. While the healed ACL had become stronger, the insertion sites became weakened due to the lack of adequate loading of the entire FATC during the slow healing process. These results also suggested that some form of mechanical loading of the ACL during its healing would be needed to limit the deleterious effects of disuse atrophy of its femoral and/or tibial insertion sites.

2.2.6.2 Mechanical Augmentation

Literature has suggested that mechanical augmentation by means of sutures could help stabilize the knee with an injured ACL. Fleming et al. used suture augmentation, in which sutures were passed from bone to bone in a porcine model to reduce anterior joint laxity [181]. In our research center, we have also used sutures for mechanical augmentation in a series of goat experiments. Our first study was to determine the best location of the tunnels for suture (#2 Fiberwire sutures) augmentation on stifle joint stability following complete ACL transection [182]. We found that placing the sutures from the anterior footprint of the femoral origin to the medial aspect of the tibial footprint, the anterior tibial translation as measured by the robotic/UFS testing system was restored to within 3 mm of the intact joint following suture augmentation and the in-situ force was similar to that of the intact ACL (Figure 7). Furthermore, these data represented 54-76% improvement over suture repair. It was concluded that suture augmentation, when placed close to the ACL insertion, could provide good initial joint stability which could aid ACL healing. Another study also showed the relative contribution of the soft tissues in resisting the anterior tibial load [183]. Under 67-N anterior tibial load, the ACL provided the dominant support in the intact joint. In the case of ACL-deficiency, the MCL and medial meniscus carried significant loads. At 30° of joint flexion, these loads reached up to 36% and 53% of the intact ACL, respectively. Following suture repair of the ACL, the in-situ force was 81% of the intact ACL while that for the augmentation sutures was 103%. Similar results were seen for 60° and 90° of joint flexion[183]. It could be concluded that suture augmentation had provided sufficient initial joints stability and concomitantly lowered the loads on the MCL as well as the medial meniscus and potentially, reduced their chance of injury from overloading.

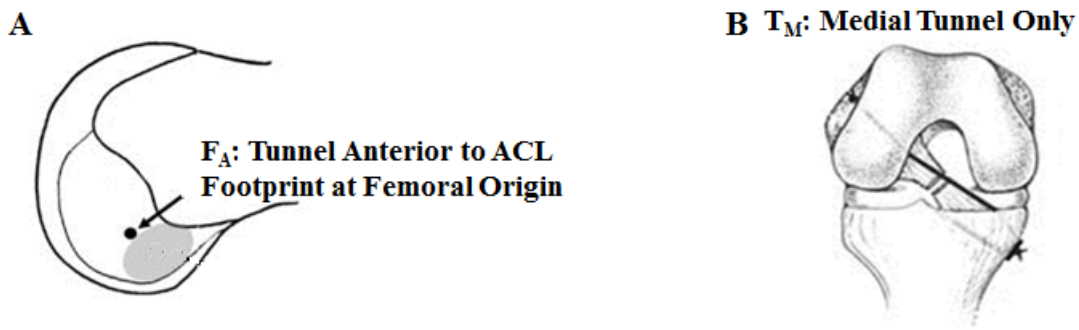

Figure 7: Diagram of tunnel locations for augmentation sutures. A) F_A is located anterior to the ACL footprint at the femoral origin and B) T_M is located medial to the footprint at the tibial insertion [182]

Finally, an in-vivo study was done to see whether suture augmentation could actually heal a surgically transected ACL [184]. After 12 weeks, the anterior-posterior tibial translation for the suture augmentation group was about 20% lower than that of the suture repair group while the in-situ force in the healing ACL was more than 50% higher that the suture repaired ACL. Upon dissection, the ACL was found to heal with significant neo-tissue formation. In terms of the structural properties of the FATC, the linear stiffness was 75% greater than that of the suture repair group. It was concluded that suture augmentation could provide the needed stability to the stifle joint for the intrinsic healing of the ACL to take place. In addition, such augmentation would reduce the forces carried by secondary structures in an ACL deficient stifle joint in order to help avoid injury to the MCL and medial meniscus.

2.2.6.3 Combined Biological and Mechanical Augmentation

With the knowledge that biological and mechanical augmentation could each individually enhance ACL healing, we then asked the research question whether their combination may work synergistically to further accelerate the healing process. It was hypothesized that since the

mechanical augmentation would stabilize the knee immediately after surgery, it could help the biological augmentation to stimulate and accelerate the ACL healing.

For this purpose, we designed a novel Mg-based ring to bridge the gap between the two torn ends of the ACL (Figure 8). It serves as an internal splint for mechanical augmentation while simultaneously load the healing ACL as well as its insertion sites to prevent disuse atrophy. The function of the Mg ring repaired ACL was first evaluated in an *in vitro* study using a goat model. Following the application of a Mg ring, the anterior tibial translation of the repaired ACL was reduced by 60-70% from the ACL deficient state as measured by the robotic/UFS testing system. This was within approximately 3 mm of that of the intact joint [185]. Mg ring repair could also restore the in-situ forces of the repaired ACL to within ± 5 N of the levels of the intact ACL [185]. These data suggest that the Mg ring is indeed a suitable device for mechanical augmentation.

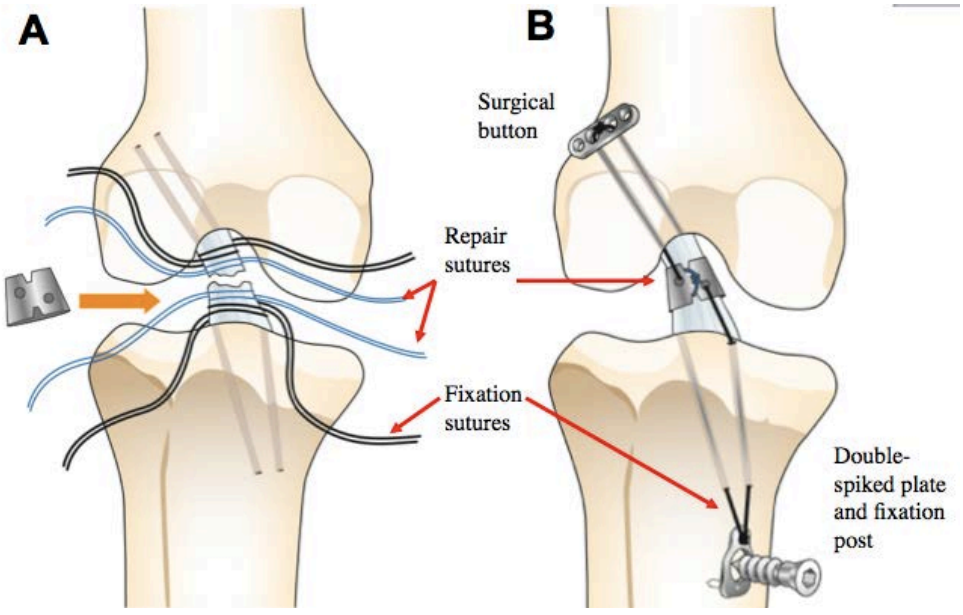

Figure 8: Mg ring repair of the ACL including bone tunnels and placement of repair and fixation sutures (A) and fixation of the ring using commercially available orthopaedic devices (B) [20]

With the promising *in vitro* results, the Mg ring was used in combination with ECM bioscaffolds in an *in vivo* animal study [186]. Since Mg is a biodegradable and bioresorbable material, it is hypothesized that the Mg ring would degrade as the ACL healing progresses and its mechanical function could be replaced by the healing ACL (Figure 9) [20]. After surgical transection, the Mg ring was sutured to connect the stumps of the ACL followed by wrapping the transection site with an ECM sheet and injection with ECM hydrogel [186]. After 6 weeks of healing, the device had degraded about 40% and translucent healing tissue was seen [186]. By 12 weeks, the function of the stifle joint as determined by the robotic/UFS testing system in response to a 67 N anterior-posterior tibial load, the anterior-posterior tibial translation of the Mg ring repaired group were 9.8 ± 1.5, 4.0 ± 1.5, and 3.4 ± 1.3 mm at 30°, 60°, and 90° of joint flexion, respectively and these values were lower than that of the suture repair group (11.8 ± 3.4, 14.4 ± 4.2, 10.8 mm, respectively $p < 0.05$). The in-situ forces carried by the ECM + Mg ring repair group were approximately twice that of the suture repair group. Similarly, the structural properties of the FATC for ECM + Mg ring repair group showed that stiffness and ultimate load reached 77 ± 33 N/mm and 371 ± 240 N, respectively. These values were 3 times greater than the suture repair group [186]. These results also compared favorably to those following ACL reconstruction in the same animal model. The stiffness and ultimate load values were 1.5 to 1.8 times higher than those following ACL reconstruction (37.2 ± 22 N/mm and 268.8 ± 175.8 N, respectively) in a goat model at 12 weeks [186, 187]. These results are exciting as the combined biological and mechanical augmentation therapy has worked in synergy to accelerate ACL healing. This dissertation includes the study of ECM + Mg ring repair after 26 weeks of healing to determine if these benefits will persist.

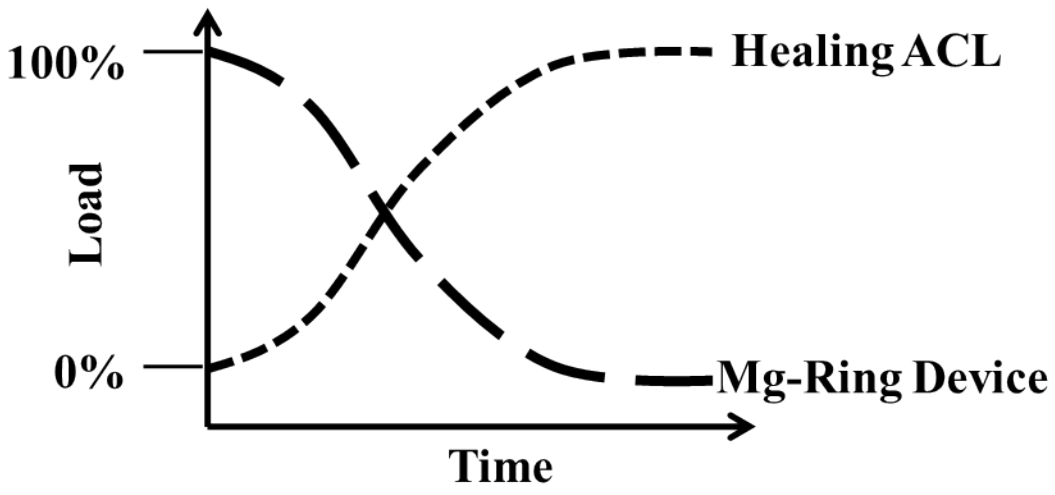

Figure 9: The Mg-based ring was hypothesized to degrade with time while the healing ACL would gradually bear the loading

2.3 MAGNESIUM AS A BIOMATERIAL FOR ORTHOPAEDIC APPLICATIONS

2.3.1 Bioresorbable Orthopaedic Biomaterials

Biomaterials are used in orthopaedic surgery for bone substitutes, fixation and stabilization of fractured bones, ligament and tendon reconstruction procedures, total joint arthroplasties, and so on. Historically, non-degradable metals, namely stainless steel and titanium alloys, have been used because they possess good mechanical strength, biocompatibility, and corrosion resistance [188]. However, because they remain in the body permanently, secondary surgeries are required for their removal. In addition, due to wear processes, they sometimes release toxic metallic particles into the body that could lead to a cytotoxic response [125, 189-191].

With the advent of functional tissue engineering, bioresorbable materials have gained much attention and their usage has increased, as they could be replaced by the patient's own tissue as well as be used for delivery of bioactive molecules to improve healing of various hard and soft tissues. These biomaterials are chosen based on the needed properties for the desired application, including specific mechanical properties, porosity, degradation profiles, biocompatibility, and adherence and incorporation into adjacent tissue [192].

For the repair or replacement of ligaments and tendons, there are a number of options for biomaterials such as fibrous collagen, ECM, silk, and synthetic polymer scaffolds that have been explored and used [193, 194]. In addition, hydrogels have become an attractive option to fill irregularly-shaped voids and aid in the delivery of cells, growth factors, and other bioactive molecules [195]. For regeneration of the soft tissue-to-bone interface (e.g. ACL insertion to femur), polymers have become a popular choice as they can be engineered to possess multi-phasic properties [196].

However, polymer materials may not be an ideal choice for some orthopaedic applications. When poly-L-lactic acid (PLLA) interference screws were used for graft fixation during ACLR, the devices often fractured during implantation due to their brittleness [197]. Furthermore, their rate of degradation varied greatly between patients and in most cases was very slow, with the screw remaining mostly intact even after 2 years [198]. Also, after degradation, the void left was not filled with regenerating bone. A 10 year follow-up study showed that an osseous cyst had formed after complete degradation of an interference screw [199]. Recently developed composite materials such as PLLA with tri-calcium phosphate (TCP) particles are designed to address the inadequate osteointegration, but results have been mixed as some studies reported improved results [198] while other reported poor integration [200].

2.3.2 Historical Use of Mg for Orthopaedic Implants

The history of biodegradable Mg implants started shortly after the discovery of elemental Mg by Sir Humphrey Davy in 1808 [201]. The most influential pioneer was the physician Erwin Payr from Austria whose versatile clinical applications and reports inspired the advancement of the field of biodegradable Mg implants to various surgical areas. In 1900, Payr introduced the idea of using Mg plates and sheets in joint arthroplasties to regain or preserve joint motion. Inspired by Payr, Chlumsky used Mg to regain motion in stiff joints (e.g. knee ankylosis) [201]. More specifically, he interposed 0.1-0.8 mm thick Mg sheets between freshly separated bone surfaces in the knee joints of dogs and rabbits [201]. The Mg sheets were completely corroded after 18 days and the joint motion was restored after bony separation of ankylotic joints in animals and humans [201].

Payr also proposed possible Mg implants in orthopaedic applications including fixator pins, nails, wires, pegs, cramps, sheets and plates. Following suit, Lambotte investigated the use of a Mg nails as well as a Mg plate and screw fixation for treatment of bone fractures of children resulting in good to total restoration of the joint function with no pain in the operated area [201]. It was also noted that Mg seemed to be a promoter of bone formation and healing [201]. Similarly, Maier investigated pins made of spindle-shaped Mg sheets in two humerus fractures in humans and Troitskii and Tsitrin reported the successful treatments of 34 cases of pseudoarthritis with a plate and screw combination made of a Mg-Cd alloy [201].

Nearly all patients benefited from the treatment with Mg implants. While most patients had no pain and almost no infections were observed during post-operative follow-up, they experienced subcutaneous gas cavities caused by rapid implant corrosion [201]. Since the problem of controlling the corrosion of Mg *in vivo* had not been sufficiently addressed, many

surgeons had turned to use the more corrosion-resistant materials, such as stainless steel [201]. Thus, Mg was no longer seriously considered as a biomaterial.

2.3.3 Recent Advances in Mg-Based Materials

In recent years, there has been a renewed interest in the use Mg and its alloys for orthopaedic applications because of advances in alloying, processing, and coating to engineer desirable mechanical properties, corrosion rates, and biocompatibility. As a lightweight metal with mechanical properties similar to natural bone, a natural ionic presence with significant functional roles in biological systems, and *in vivo* degradation via corrosion in the electrolytic environment of the body, Mg-based implants have the potential to serve as biocompatible, osteoconductive, degradable implants for load-bearing applications. A search of Web of Science using "magnesium" and "stainless steel" as search queries under the category "biomaterials" revealed that the number of publications on Mg has exponentially increased in the past ten years, compared to those on stainless steel (Figure 10).

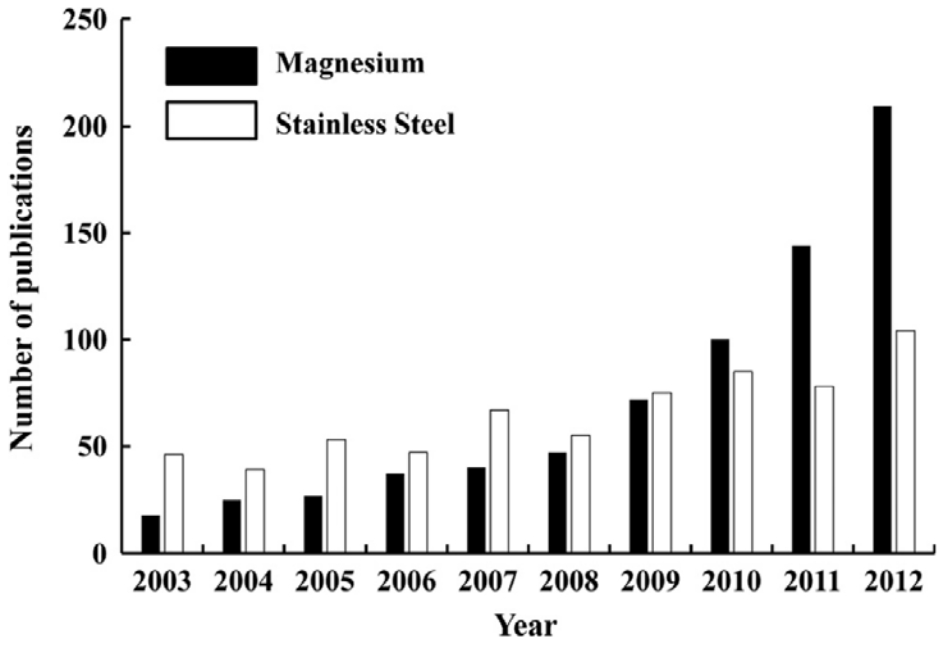

Figure 10: Histogram showing the number of publications each year on research on Mg and its alloys and stainless steel as biomaterials [20]

2.3.3.1 Mechanical Properties

Mg-based materials have significantly lower moduli than titanium-based materials (41-45 GPa vs. 110-117 GPa) [202]. As a result, their mechanical properties are closer to those of cortical bone and could reduce the level of stress shielding. In terms of tensile strength, Mg-based materials are 3-16 times stronger than polymers (160-250 MPa vs 16-69 MPa). They are also more ductile and have higher ultimate strain that reaches up to 16% which could reduce the risk of device fracture during implantation.

However, pure Mg may not possesses mechanical properties strong enough for load-bearing applications [203]. Alloying of Mg with various elements has led to the development of many materials with greatly enhanced mechanical properties. With enhanced mechanical properties, Mg alloys are better suited for orthopaedic applications. The most common Mg alloys are those including aluminum (Al), which increases the corrosion resistance by forming an

insoluble layer of Al_2O_3 on its surface when exposed to simulated body fluid (SBF) [204]. Al has commonly been alloyed with zinc (Zn) to produce popular alloys AZ31 (3% Al, 1% Zn), AZ61 (6% Al, 1% Zn), and AZ91 (9% Al, 1% Zn) [204-206]. Calcium (Ca) has also commonly been used as an alloying element in Mg alloys particularly attractive for bone healing applications [207, 208]. Additionally, rare earth metals such as yttrium (Y), zirconium (Zr), and neodymium (Nd) have been used in Mg alloys due to their improvements on the mechanical properties, creep resistance, and corrosion rate of Mg [64, 209-211].

Other strategies have been employed to modify the microstructure of the Mg material to change its properties in addition to alloying. For example, a Mg calcium phosphate scaffold was designed to be porous in order to have its mechanical properties similar to those of cancellous bone, thus making it ideal to be used as a bone substitute [212]. Others have investigated the growth of monocrystalline forms of Mg (single crystal Mg), which has improved ductility and exhibits superplastic behavior [213-217].

2.3.3.2 Controlled Degradation

The corrosion mechanism of Mg is very complex. When subject to aqueous environments, Mg and its alloys are known to degrade via an electrochemical reaction producing magnesium hydroxide and hydrogen gas (Figure 11). The overall corrosion reaction of Mg in aqueous environments is below:

$$Mg_{(s)} + 2H_2O_{(aq)} \rightarrow Mg(OH)_{2(s)} + H_{2(g)} \quad (overall\ reaction)$$

$$Mg_{(aq)} \rightarrow Mg^{2+} + 2e^- \quad (anodic\ reaction)$$

$$2H_2O_{(aq)} + 2e^- \rightarrow H_{2(g)} + 2OH^-_{(aq)} \quad (cathodic\ reaction)$$

The production of OH^- causes a pH increase which favors the formation of Mg hydroxide layer by the precipitation reaction.

$$Mg^{2+}_{(aq)} + 2OH^-_{(aq)} \rightarrow Mg(OH)_{2(s)} \qquad (product\ formation)$$

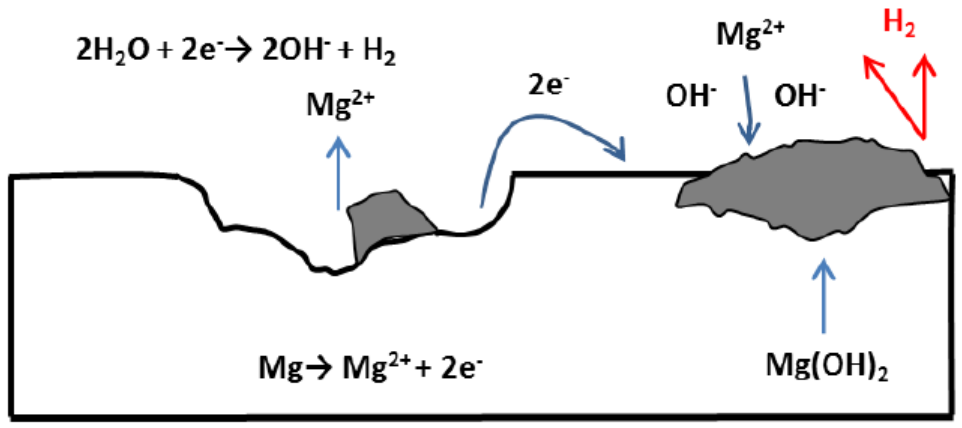

Figure 11: Schematic of reactions between Mg in an aqueous environment [218]

In addition to the challenges in understanding the corrosion mechanisms of Mg alloys in biological environments, there is the issue of controlling the corrosion rate and mode. The initial corrosion rate of Mg alloys is often too fast, and a highly reactive Mg alloy surface can be harmful for the biological environment. Strong hydrogen bubbling takes place when a bare Mg alloy sample is introduced to any type of simulated body fluid. Combined with this, local alkalization in the vicinity of the surface can be observed. So while the general corrosion rate needs to be tailored to match the desired lifetime of the device, it is even more desirable to have a controlled time-dependence of the corrosion rate. For instance, initial slow corrosion would allow development of a stable bio-interface and would enable the mechanical integrity of the device to be maintained for the required period. This should be followed by faster dissolution and finally by a complete removal of the implant by soluble corrosion products. Exploration of

novel alloys as well as surface modification approaches have been developed for the control of biodegradation of Mg alloys. The challenge in both strategies is to combine optimization of the corrosion behavior with the tailored and desired performance for the specific targeted application [219].

Alloy development for biodegradable implants requires consideration of tailored corrosion behavior, suitable mechanical properties, excellent biocompatibility, and if possible even desired bioactivity [219]. By meticulous control of alloy chemistry (alloying elements and impurities), processing, heat treatments and resulting microstructures, significant progress has been made in the development of novel alloys with promising *in vitro* and *in vivo* properties [220]. One alloy system of interest for biodegradable implants is Mg alloyed with Y, Zr, and rare earth elements, but Mg-Ca and Mg-Ca-Zn alloys have also been investigated. Other alloying elements explored are Ca, Mn, Zn, and Sr, which are expected to lead to additional beneficial biological effects [221]. For biodegradable Mg alloys, degradation rates of ultra-high purity Mg have been shown to be very low both *in vitro* and *in vivo* [222].

The different approaches studied for coatings and surface modification of biodegradable Mg alloys include anodization, CaP coatings, biodegradable polymers and so on [219]. A suitable coating for degradable Mg based implants should initially offer good protection to mitigate the negative effects related to fast burst of dissolution of a freshly implanted device, then degrade in a controllable manner, and finally enable complete dissolution of the coating and the underlying substrate. The required time-profile of degradation of course depends on the targeted application. One drawback in the design of coatings for tailored degradation is the unknowns between a test of degradation rate in the laboratory and true performance of the coating *in vivo* [219].

2.3.3.3 Biocompatibility

Mg is essential to human metabolism and is naturally found in bone tissue [223-228]. It is the fourth most abundant cation in the human body, with an estimated 1 mol of Mg stored in the body of an adult, with approximately half of the total physiological Mg stored in bone tissue [224]. Mg is a co-factor for many enzymes, and stabilizes the structures of DNA and RNA [223]. The level of Mg in the extracellular fluid ranges between 0.7 and 1.05 mmol/L, where homeostasis is maintained by the kidneys and intestines [224]. While serum Mg levels exceeding 1.05 mmol/L can lead to muscular paralysis, hypotension and respiratory distress [226], and cardiac arrest occurs for severely high serum levels of 6-7 mmol/L, the incidence of hyper-Mg is rare due to the efficient excretion of the element in the urine [224, 226, 227].

Witte et al. explored the *in vivo* degradation of Mg-based alloys, comparing two alloys containing only Al and Zn, and two alloys with rare earth element combinations [211, 229]. The Al-Zn alloys contained 3 wt% Al and 1 wt% Zn (AZ31), and 9 wt% aluminum and 1 wt% Zn (AZ91). The first rare-earth alloy was composed of 4 wt% Y and 3 wt% of a rare earth metal mixture consisting of Nd, Ce, and Dy (WE43). The final rare-earth alloy consisted of 4 wt% Li, 4 wt% Al and 2 wt% of a rare earth element mixture of Ce, La, Nd, and Pr (LAE442). The implants consisted of rods 1.5 mm in diameter and 20 mm in length, inserted into the femur of guinea pigs. The implants were harvested at 6 and 18 weeks. Complete degradation was observed in 18 weeks [229]. Significantly increased bone area was observed in all groups at week 6 and 19, in comparison to the polymer control [211]. Adverse effects due to the formation of subcutaneous gas were not observed.

Li et al. conducted a preliminary *in vitro* assessment of the cytotoxicity of pure and surface treated Mg using bone marrow cells of mice [227]. The results show positive cell

proliferation and viability after 72 hours of incubation with Mg and no sign of growth inhibition. These studies along with numerous others support the viability of Mg-based materials as lightweight, degradable, biologically compatible and biologically active (i.e. osteoconductive) orthopaedic implants[202].

2.3.3.4 Suitability with Imaging Modalities

Mg alloys do not interfere with magnetic resonance imaging unlike other metallic materials, such as titanium or stainless steel alloys. Ernsterger et al. evaluated artifacts caused by Mg-based intervertebral discs and observed minimal interference by Mg-based discs was comparable to that of the polymer control [230]. At the same time, Mg-based alloys can be imaged *in vivo* using computed tomography allowing accurate assessment of device degradation and bone formation [231].

2.3.4 Rationale for Use of Mg for Regeneration of the ACL

Mg and its alloys possess advantageous properties with excellent potential for mechanical augmentation of an injured ACL. They are lightweight and possess suitable mechanical properties such that they could withstand loading *in vivo*. Additionally, their ductility could allow for small deformations to conform to the anatomy of the knee and potentially prevent damage to the cartilage, menisci, and other structures. Also, a Mg alloy and surface coating combination could be strategically selected to tailor a corrosion rate desirable for ACL healing applications and allow for the gradual transfer of loading from the implant to the healing ACL throughout the healing process (3-6 months). Finally, the known biocompatibility of Mg would be attractive for the clinical translation of a Mg implant for ACL healing.

3.0 OBJECTIVES

3.1 BROAD GOALS

An advantageous alternative treatment option to ACLR is to heal the injured ACL which allows for the preservation of the normal ACL anatomy and function and eliminates the need for graft harvesting. In our research center, an innovative approach to healing the ACL was developed using an extracellular matrix (ECM) sheet and hydrogel along with a novel metallic implant made of magnesium (Mg) and shaped like a cylinder, or a Mg ring designed to bridge the gap between the two ends of a torn ACL. The biological augmentation provided by the ECM scaffolds has been shown to incite and accelerate new tissue growth. The mechanical augmentation provided by the Mg ring can restore stability to the knee joint immediately post-operatively and load the healing ligament throughout the healing process preventing disuse atrophy of the insertion sites. Additionally, the entire ECM + Mg ring repair construct can be resorbed by the body as the healing tissue begins to bear load. Short term preclinical studies in the goat model have yielded promising results demonstrating feasibility of ECM + Mg ring repair of an injured ACL. The overall goal of this dissertation is to further develop and evaluate ACM + Mg ring repair through the completion of the Specific Aims.

3.2 SPECIFIC AIMS AND HYPOTHESES

Specific Aim 1: *To characterize single crystal Mg coated via micro arc oxidation.* Previous studies of ECM + Mg ring repair in a goat model have shown that an implant made with single crystal (SC) Mg coated via micro arc oxidation can be completely resorbed by 12 weeks and yield favorable results. Thus, resorption of the Mg ring implant by 12 weeks *in vivo* is an adequate degradation rate for the application of ACL healing. This was achieved by matching SC Mg coated via micro arc oxidation to the *in vitro* degradation rate of Mg ring implant used in a previous *in vivo* study in a goat model for 12 weeks of healing. Additionally, characterization of the *in vitro* corrosion, coating surface and structural properties was conducted.

Specific Aim 2: *To evaluate ECM + Mg ring repair after implantation and long-term healing in a goat model.* ECM + Mg ring repair of surgically transected goat ACL was performed and evaluated after 26 weeks of healing. Cytology and total protein content of synovial fluid were used to assess the biocompatibility of the treatment. Gross morphology and histology were used to observe the healing ACL in terms of collagen fiber morphology and cellular response. Joint kinematics and in-situ forces in the healing ACL were measured to quantify the function of the ACL. The structural properties of the healing femur-ACL-tibia complex (FATC) were obtained and used to assess tissue quality and failure mode. *Based on the outcomes from earlier work using ECM + Mg ting repair, it was hypothesized that the advantages of ECM + Mg ring repair would persist to 26 weeks characterized by continuous collagen fibers without atrophy of the insertion sites as evident by failure mode.*

Specific Aim 3: *To develop and evaluate the Mg ring implant for use in humans.* In preparation for future use in humans, the Mg ring implant was scaled up considering the anatomy of the human ACL. Then, the redesigned implant for use in humans was machined and implanted into human cadaver knee specimen to evaluate its ability to restore joint stability and load the ACL immediately post-operatively. Lastly, a finite element model of the implant in the human knee was developed for further observation of the von Mises stress values and concentrations within the model and evaluation of future deign iterations of the implant. *It was hypothesized that Mg ring repair would be able to restore anterior tibial translation of the Mg ring repaired ACL within 5 mm of that of the intact joint under externally-applied loads and in-situ force in the repaired ACL to levels ± 20 N to that of the intact ACL.*

4.0 MATERIAL CHARACTERIZATION

4.1 INTRODUCTION

The Mg material used for the application of ACL healing was chosen for its clinical relevance and previous preclinical use. Specifically, a monocrystalline or single crystal (SC) Mg substrate was found to be most suitable because of its lack of grain boundaries resulting in higher ductility that could be advantageous for the Mg ring implant. Additionally, the purity of single crystal Mg without alloying elements as well as minimization of the defect concentration in particular, dislocations (edge, screw) and stacking faults is highly relevant clinically to achieve the desired mechanical ductility, strength and bio corrosion.

As ACL healing is relatively slow and takes weeks, a strategy that allows for slow corrosion initially and development of a stable bio-interface that would enable the mechanical integrity of the implant to be maintained for a required period of 6 to 12 weeks is needed. Afterward, a faster dissolution and finally a complete resorption of the implant by soluble corrosion products would be desired. With the selection of SC Mg as the metallic substrate, a micro arc oxidation (MAO) coating strategy was selected. While there are several types of surface modification approaches including CaP coatings and biodegradable polymers, MAO could provide the aforementioned properties [232].

Micro arc oxidation (also known as anodization and plasma electrolytic oxidation) is an electrolytic passivation process that is used to increase the thickness of the natural oxide layer on the surface of metals. A metal is placed in an electrolytic solution and a voltage is applied resulting in high temperatures and a sparking phenomenon. The sparking contributes to the porosity that is characteristic of MAO coatings (Figure 12). There is an outer porous layer and an inner barrier layer. The outer porous layer does not contribute to corrosion protection as the pores act as passages for corrosive media. The inner barrier layer however is often considered to have a major influence on the corrosion resistance as this layer is denser and compact with fewer pores [232].

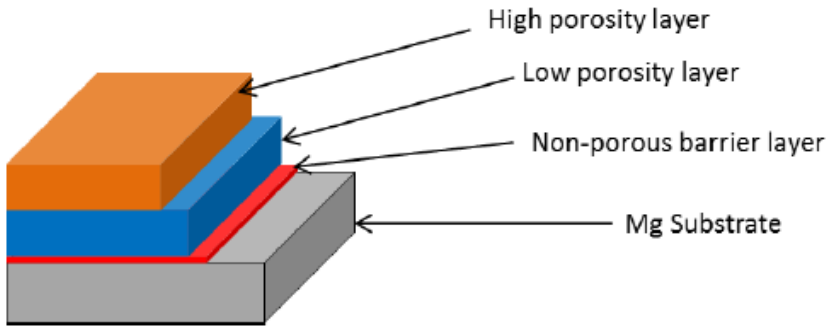

Figure 12: Schematic description of coating prepared using MAO process [218]

Specific Aim 1 includes the use of hydrogen evolution measurement to quantify the corrosion profile used in a previous *in vivo* study in a goat model after 12 weeks of healing referred to as "healing study" in subsequent sections. Then, SC coated for various periods of time also underwent hydrogen evolution measurement to match the corrosion profile of the Mg ring implant used in the "healing study". Additionally, this novel material-coating combination underwent *in vitro* immersion testing to determine the corrosion behavior as determined by Mg

ion concentration, pH, and change in mass. The coating and surface properties were also characterized.

4.2 METHODS

4.2.1 Preparation of Metallic Substrates

The corrosion, coating, and surface properties of MAO coated SC were characterized. The actual Mg ring implants were used for characterization specific to the geometry of the device and to determine the *in vitro* corrosion rate that could be used as a standard for future device development. Disks were used for understanding how the properties varied independent of the shape such as corrosion rate as a result of coating time or substrate material.

4.2.1.1 Mg Ring Implants

SC Mg cylinders were machined into the geometry of the Mg ring implant (Figure 13) at the Swanson Center for Product Innovation (SCPI). To produce the implants, the inner and outer diameters were first turned using a lathe. Then surface holes and other features were added using CNC milling with a custom-made mandrill. These Mg ring implants were used for hydrogen evolution measurements and subsequent *in vivo* studies (Figure 14).

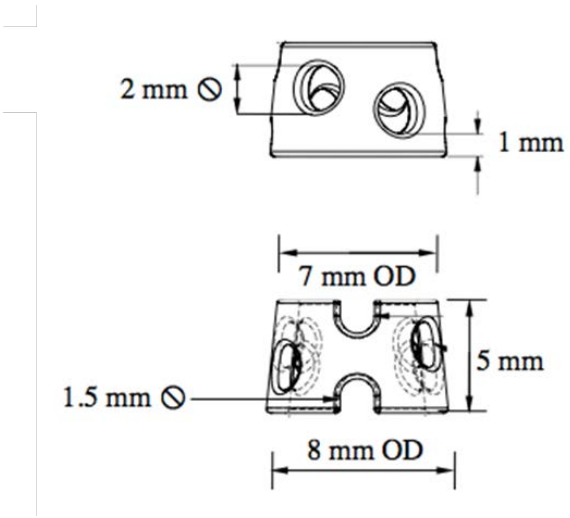

Figure 13: Geometry of the Mg ring implant[21]

Figure 14: Mg ring implants manufactured with single crystal Mg

4.2.1.2 Pure Mg Disks

Commercially available 99.9% Mg (Goodfellow Corporation, Coraopolis, PA) and SC Mg obtained from the Institute of Solid State Physics (Beijing, China) were used. Cylindrical samples of 10 mm diameter by 1 mm thickness (prior to polishing) with a 1 mm diameter hole were machined by the University of Pittsburgh's Swanson Center for Product Innovation (SCPI). The samples were successively polished using 320-grit, 600-grit, and 1200-grit silicon carbide

(SiC) abrasive paper. After polishing, the samples were rinsed with ethanol and air dried. These Mg disks were used for *in vitro* immersion testing.

4.2.2 Micro Arc Oxidation Coating

Each of the Mg samples underwent micro arc oxidation coating in a 6 M Na_3PO_4 + 8 M $Na_2SiO_3 \cdot 5H_2O$ + 4 M KF electrolytic solution prepared using deionized water and continuously stirred with a magnetic stirrer. The coatings were formed in a stainless steel container (1 L of solution used) surrounded by an ice bath (Figure 15). The Mg samples were immersed in the electrolytic solution using a 0.25 mm titanium wire passed through the 1 mm diameter hole at one end and the titanium wire was attached to the pulse source at the other end. Using an adjustable DC pulse source, the coatings were obtained under constant applied potential of 300V for 2 and 5 minutes with the uncoated samples as the control. After coating, the samples were rinsed with ethanol, air dried, and stored in a desiccator.

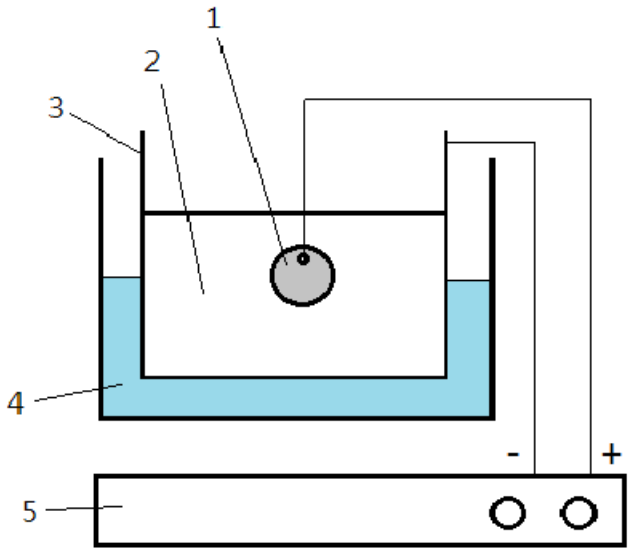

Figure 15: The setup for MAO coating: 1) Mg sample, 2) electrolytic solution, 3) stainless steel container, 4) ice bath, and 5) power source

4.2.3 Corrosion Characterization

Techniques used for exploring the corrosion behavior of metallic materials in general, including Mg, involve immersing the samples in a corrosive solution [219]. There are numerous methods for measuring the corrosion rate of Mg in aqueous solutions, which can be used independently or simultaneously. These include weight loss (mass loss), hydrogen collection, electrochemical and non-electrochemical methods as well as chemical analysis of the solution. Due to the simplicity and availability of resources, non-electrochemical methods were used for the characterization of the MAO coated SC substrates. Weight loss measurements are well established and hydrogen collection methods can be readily used for monitoring the instantaneous corrosion rate even in real time [219].

4.2.3.1 Hydrogen Evolution Measurement

Hydrogen evolution measurements were taken for Mg ring implants from the previous 12 week *in vivo* study or "healing study" as well as SC Mg (Institute of Solid State Physics, Beijing, China), uncoated and samples coated (Section 4.2.2) for 2, 5, and 10 minutes (N=2 each). The samples were placed in Hanks' Balanced Salt Solution (Sigma Aldrich, St. Louis, MO) at 37°C. The samples were suspended within 1L beaker of HBSS solution underneath an inverted funnel. A burette was placed over the top of the funnel above the samples to capture the hydrogen released (Figure 16). All beakers, funnels and burettes were glass to prevent hydrogen permeation. The samples were suspended to ensure full surface exposure and the inverted funnels were elevated to prevent ion accumulation within the funnel volume. The solution level in each burette was measured intermittently for 2 weeks. The corrosion rate can be calculated from hydrogen evolution from the following relationship:

$$CR = \frac{K \times W}{A \times T \times D}$$

where K is 8.76×10^4, W is mass loss (g), A is exposed area (cm^2), T is time of exposure (h), and D is the density of the material (g/cm^3).

$$\Delta W = \frac{1.085\, V_H}{P_{ATM}}$$

where ΔW is change in mass (mg), V_H is the volume of hydrogen evolved (mL), and P_{ATM} is atmospheric pressure.

To further elucidate the corrosion properties of the Mg ring implant used in the previous 12 weeks of healing study, change in mass was calculated and microCT images were obtained after hydrogen evolution testing.

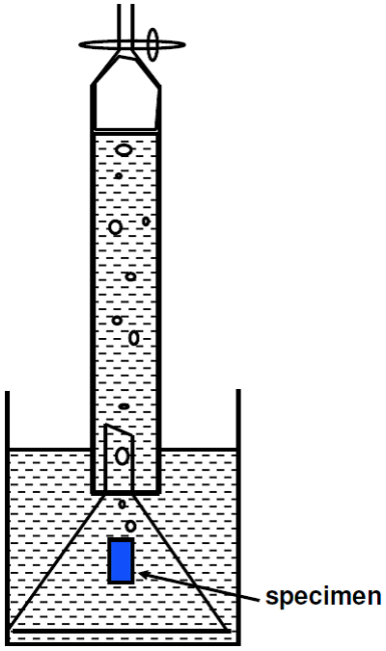

Figure 16: Hydrogen evolution measurement setup

4.2.3.2 *In Vitro* Immersion Testing

In vitro corrosion studies were conducted using HBSS (Sigma Aldrich, St. Louis, MO) as the immersion solution (initial pH of 7.4). The Mg disk samples were placed in 50 mL polypropylene tubes (Falcon Blue Max, BD, Franklin Lakes, NJ) with 50 mL of HBSS. The samples were placed inside an incubator which was maintained at 37°C. The Mg ion concentration of the solution, pH of the solution, and mass of the samples were measured daily for 7 days and weekly for 4 weeks.

4.2.4 Coating Characterization

In order to know how the coating process changes the surface of the Mg substrate, scanning electron microscopy (SEM) was used to observe the surface morphology of the Mg substrate. The Mg disks were coated with palladium for 90 seconds. Scanning electron microscopy (SEM)

(JOEL JSM-6610LV) was used to characterize the surface morphology of the coated surfaces. The porosity of the coating was determined from the SEM images using Image J (NIH, Bethesda, MD).

4.2.5 Surface Characterization

Lastly, the MAO coating changes the surface qualities of the Mg substrate. The hardness, roughness, and hydrophilicity were characterized in order to quantify the changes and give insight to the potential cellular response to the MA coating. Vickers microhardness was measured using a microindenter (LM800 Microhardness Tester, LECO Corporation, Saint Joseph, MI) whereby a sharp indenter tip applied a load of 50 g to the surface of the sample with a 10 second dwell time (Figure 17). The indentation created by the square pyramidal diamond indenter was measured using optical microscopy. The Vickers Pyramid number (HV) was determined by F/A, where F is the force applied to the diamond indenter in kilograms-force and A is the surface area of the resulting indentation in square millimeters. A was determined by the formula:

$$A = \frac{d^2}{2\sin(\frac{136°}{2})}$$

where d is the average length of the diagonal length left by the indenter in millimeters. The HV number was then calculated by:

$$HV = \frac{F}{A} = \frac{2\ \sin(\frac{136°}{2})F}{d^2}$$

where F is in kgf.

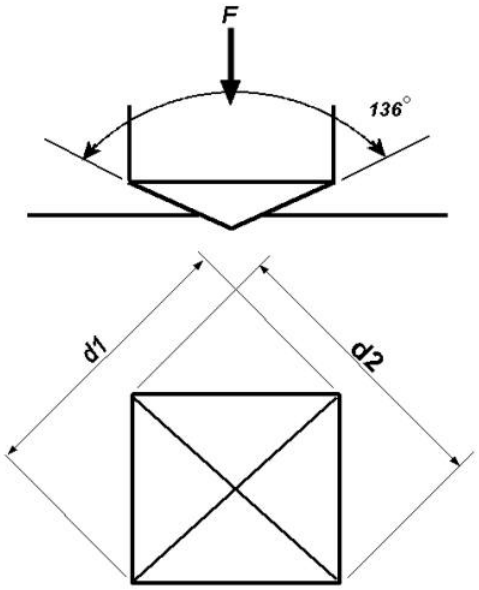

Figure 17: Schematic of Vickers Hardness testing

The surface roughness was measured by means of a surface profiler (KLA Tencor, Alpha Step IQ) and the average roughness (R_a) was obtained. Hydrophilicity was quantified using contact angle measurements using a tensiometer. Contact angles were measured with a system equipped with a microscope and a camera. A 5 μl droplet of distilled water was suspended from the tip of the microliter syringe. The syringe tip advanced toward the surface until the droplet made contact with the surface. Images were collected with the camera and the contact angle between the drop and the surface was measured by the software.

4.2.6 Data Analysis

The porosity, coating thickness, Mg concentration, average roughness, hardness, and contact angle were averaged between samples and expressed as a mean ± standard deviation. Two-way

ANOVA was used to compare the values in response to the independent factors, substrate type (SC Mg and 99.9% Mg) and coating time (2 and 5 minutes). Statistical significance was defined as $p<0.05$. This data was used to identify if there is an ideal material-coating combination that is able to achieve the desired corrosion rate with properties most attractive to cellular contact (i.e. harder, rougher, more hydrophilic).

4.3 RESULTS

4.3.1 Hydrogen Evolution Measurement

The hydrogen evolution measurement of Mg ring implants from the previous "healing study" was obtained (Figure 18). The glassware for one of the implants broke after 1 week reducing the intended time of exposure. However, the corrosion profiles of both samples were similar. There was minimal corrosion for the first 60 hours. Then the corrosion increased up to more than 5 mL of hydrogen gas. Table 1 gives the weight before and after the Mg ring implants were immersed in HBSS for up to 2 weeks. There is no change in mass because the physical degradation of the Mg ring implants was not greater than the accumulation of corrosion products (Figure 19).

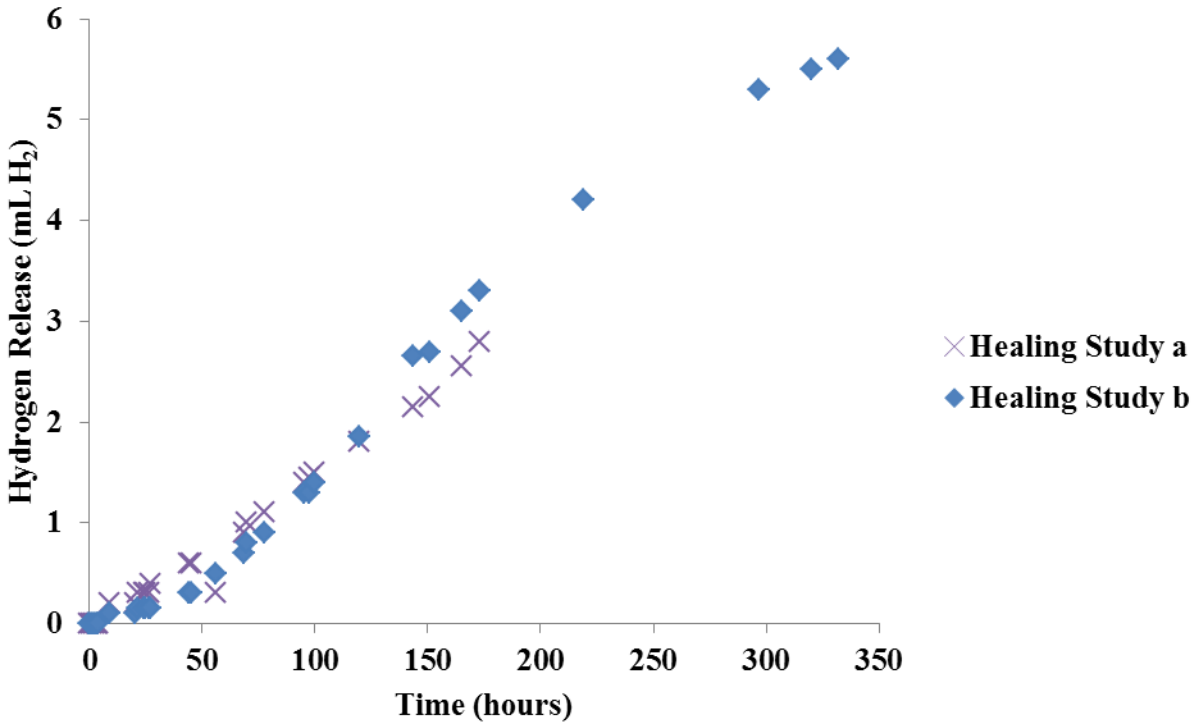

Figure 18: Hydrogen evolution measurements of Mg ring implants (from previous 12 weeks of healing study or "Healing Study") immersed in HBSS for 2 weeks

After completion of the hydrogen evolution measurement, microCT images of the corroded Mg ring implants were taken and the percent corrosion was quantified. After 2 weeks immersed in HBSS, the microCT images (Figure 20) indicated that the MAO coated Mg ring implant degraded 13% compared to the pre-immersion images.

Table 1: Weight of Mg ring implants before and after immersion in HBSS

Sample	Weight (g) Before Immersion	Weight (g) After Immersion
Healing Study a	0.087	0.088
Healing Study b	0.087	0.085

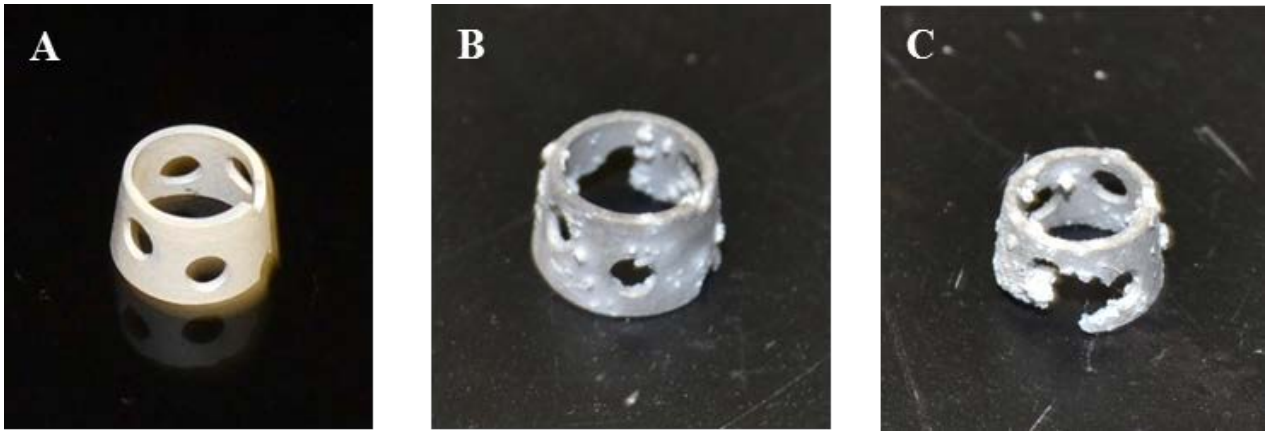

Figure 19: Photographs of the MAO coated Mg ring implants from the previous "healing study" before hydrogen evolution measurements (A) and after immersion in HBSS (B&C)

After completion of the hydrogen evolution measurement, microCT images of the corroded Mg ring implants were taken and the percent corrosion was quantified. After 2 weeks immersed in HBSS, the microCT images (Figure 20) indicated that the MAO coated Mg ring implant degraded 13% compared to the pre-immersion images.

After completion of the hydrogen evolution measurement, microCT images of the corroded Mg ring implants were taken and the percent corrosion was quantified. After 2 weeks immersed in HBSS, the microCT images (Figure 20) indicated that the MAO coated Mg ring implant degraded 13% compared to the pre-immersion images.

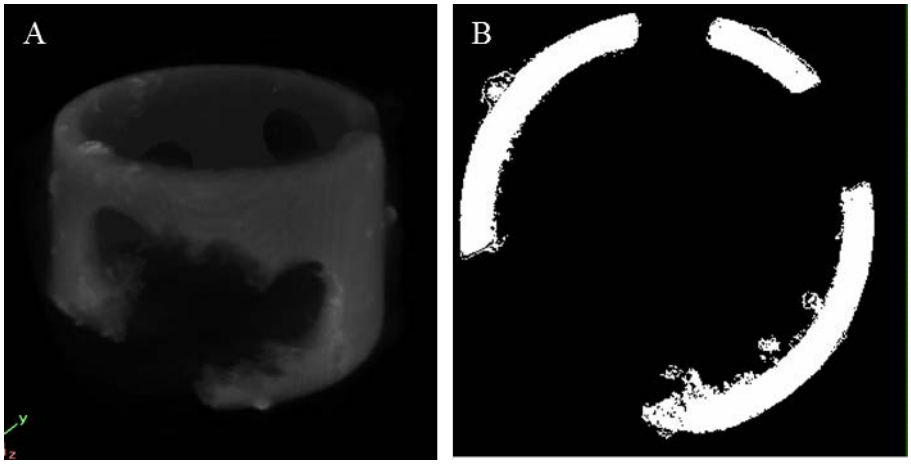

Figure 20: Micro CT reconstruction (A) and cross section (B) of corroded Mg ring implant

The uncoated Mg ring implants and those coated for 2, 5 and 10 minutes underwent hydrogen evolution in attempts the match the corrosion profile of the implants from the previous "healing study" (Figure 21). The 2 uncoated samples had similar corrosion profile with fast corrosion with an approximate 1 mL of hydrogen gas evolved within the first 60 hours followed by minimal to no corrosion for the remaining time of exposure. For the 2 minute coated implants, there was variation between the corrosion profiles of the 2 samples with sample *2 min a* having more hydrogen gas evolved than the "healing study" samples and sample *2 min b* having less hydrogen gas evolved. A similar trend is seen with the 5 minute coated samples with sample *5 min a* having more hydrogen gas evolved than the "healing study" samples and sample *5 min b* having less hydrogen gas evolved. The Mg ring implants coated for 10 minutes has less hydrogen gas evolved than those of the previous "healing study" as well as those coated for 2 minutes and 5 minutes excluding sample *5 min b*. The Mg ring implants coated for 2 minutes and 5 minutes had hydrogen evolution profiles closest to those of the previous "healing study."

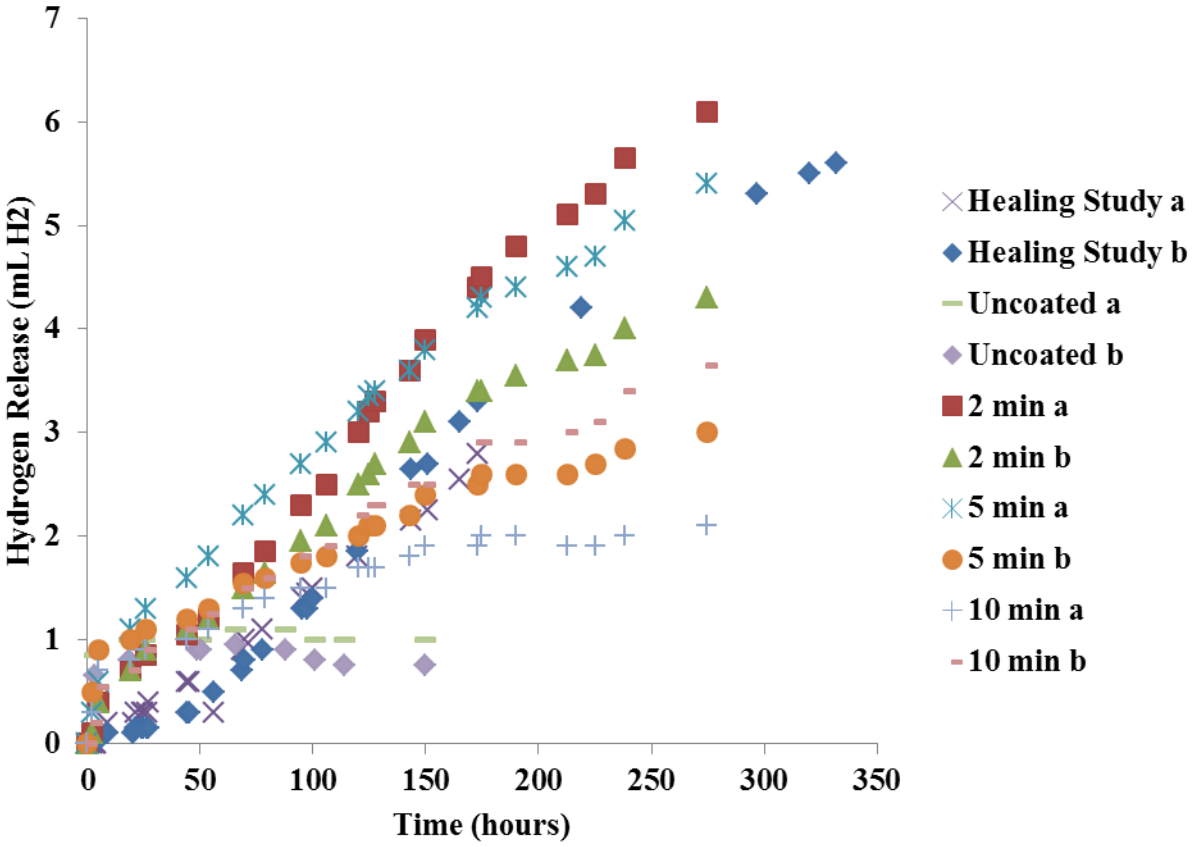

Figure 21: Hydrogen evolution measurement of Mg ring implants from the previous "healing study" as well as those uncoated and coated for 2, 5, and 10 minutes

4.3.2 *In Vitro* Degradation

In vitro degradation testing on SC and 99.9% Mg coated for 2 minutes, 5 minutes as well as uncoated disks was conducted (Figure 22). This describes the corrosion of the substrates in HBSS for up to 4 weeks. The Mg ion concentration in the HBSS after immersion of the SC samples depicts minimal change in Mg ion concentration over the 4 week time period (Figure 23). The uncoated samples had Mg ion concentration greater than the other samples at each time point. There was no significant difference between the Mg ion concentration of the 2 minute and

5 minute samples. A similar trend was seen with the change in pH values of the HBSS solution after the Mg disks had been immersed up to 28 days (Figure 24). The uncoated samples had a greater change in pH than the 2 minutes and 5 minute samples while there was no significant difference between the change in pH of the 2 minute and 5 minute samples.

Figure 22: Photograph of Mg disk sample before and after MAO coating

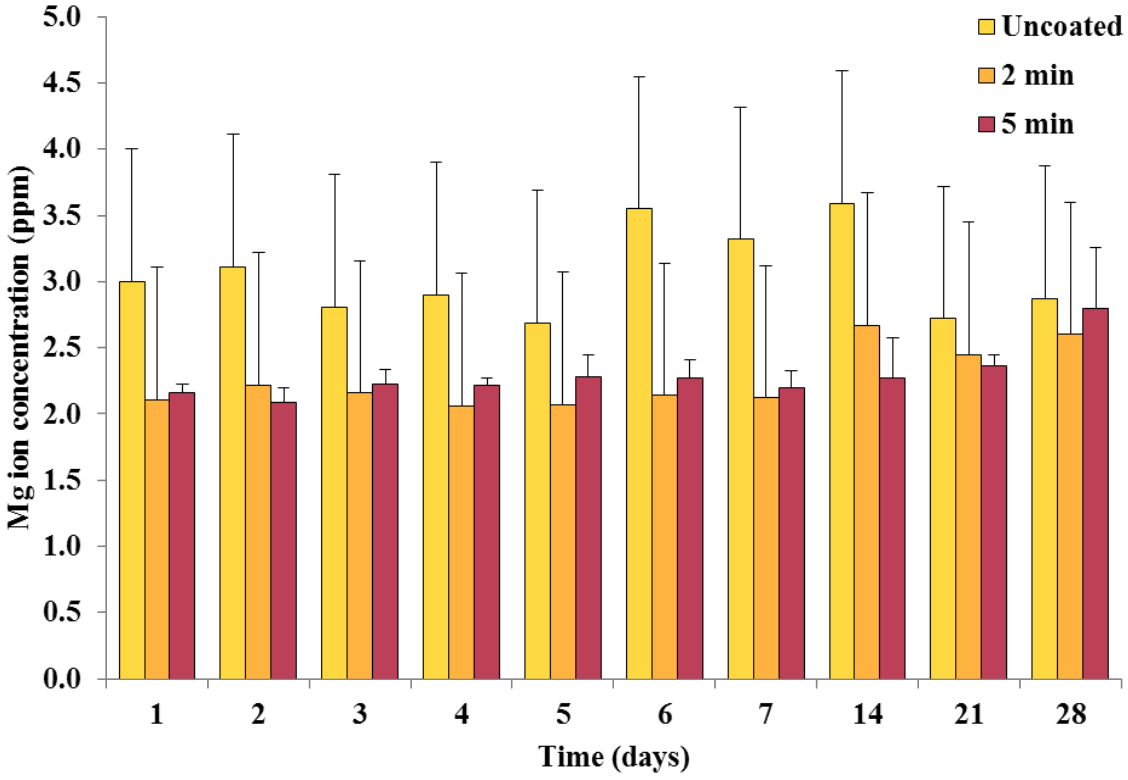

Figure 23: Mg ion concentration (ppm) in HBSS after in vitro corrosion testing of SC Mg disks

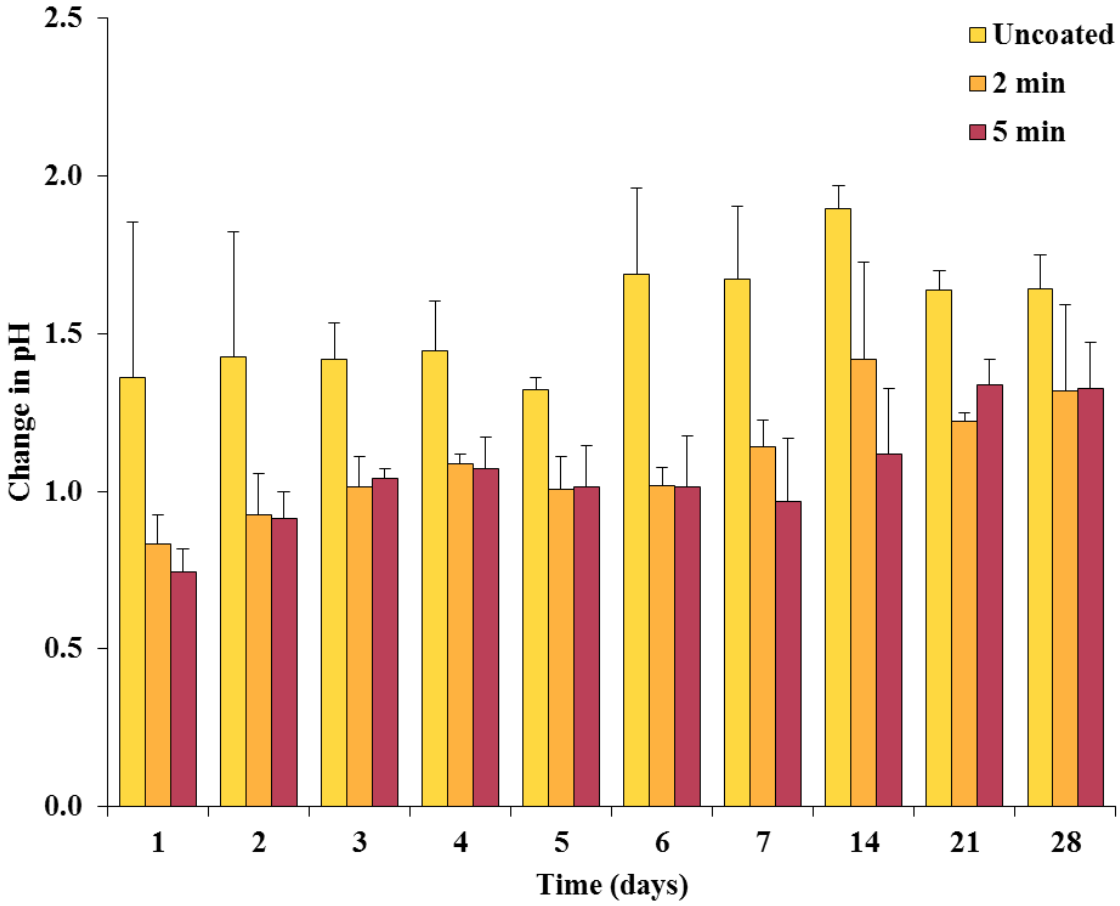

Figure 24: Change in pH of HBSS after in vitro corrosion testing of SC Mg disks

Lastly, the percent change in mass of the SC samples was recorded (Figure 25). The approximate initial mass of the uncoated SC samples was 0.12 g. The percent mass of the uncoated SC samples increased up to 2%, an estimated 2.4 mg, the first 3 days and didn't vary much the remaining 4 week time period. There was less than 1% increase in the mass of the 2 min and 5 minute samples over the 4 week duration. The percent increase in mass as opposed to decrease as a result of corrosion is due to the accumulation of corrosion products with minimal to no physical mass loss.

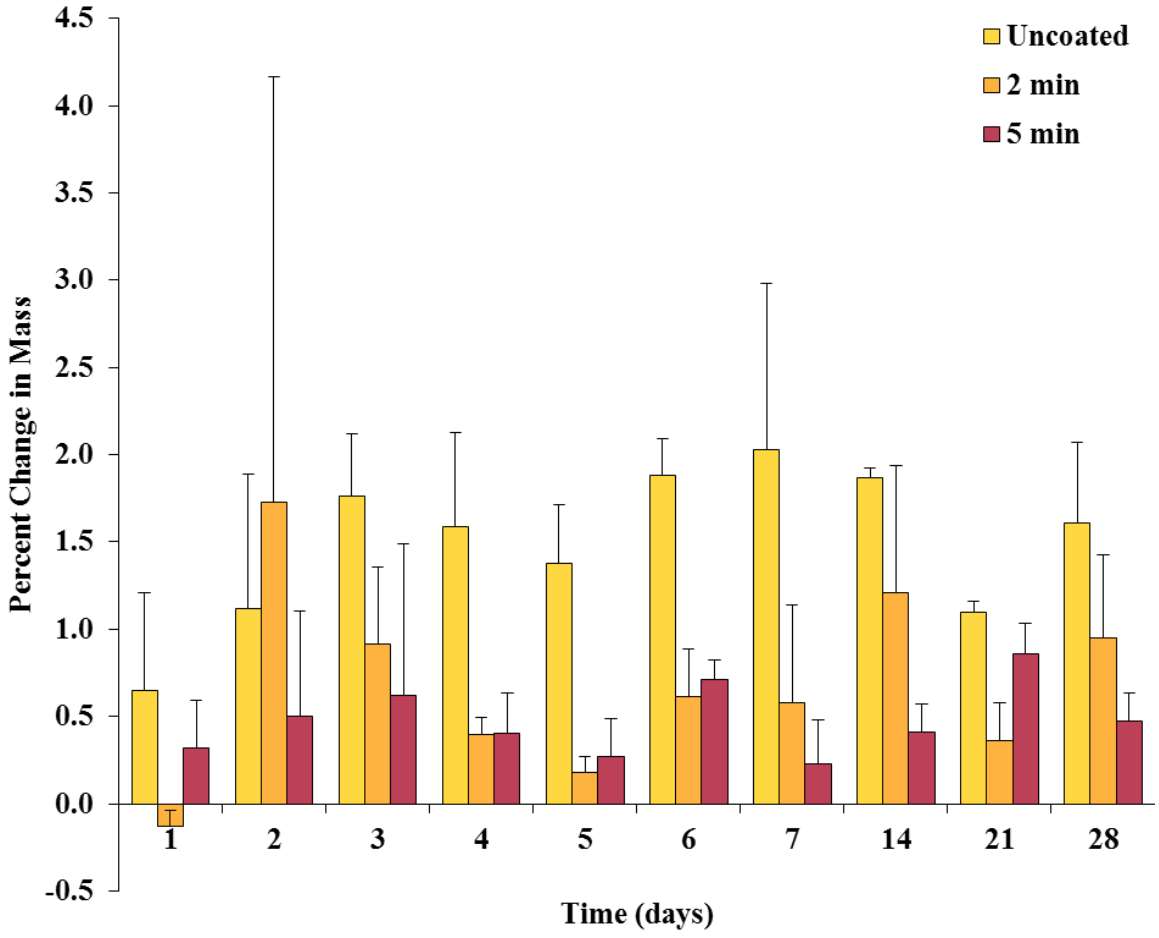

Figure 25: Percent change in mass of SC Mg disks after in vitro corrosion testing

The in vitro degradation testing was also performed on the 99.9% Mg as a commercially available control (Figure 26). For the uncoated, 2 minutes, and 5 minute samples, the Mg ion concentration steadily increased over the 4 weeks ranging between 2 ppm at 1 day to 10 ppm after 4 weeks immersed in HBSS. The uncoated samples and the 5 minute coated samples had comparable Mg ion concentrations up to 2 weeks. The 2 minutes samples had the least amount of Mg ion concentration suggesting a slower corrosion rate.

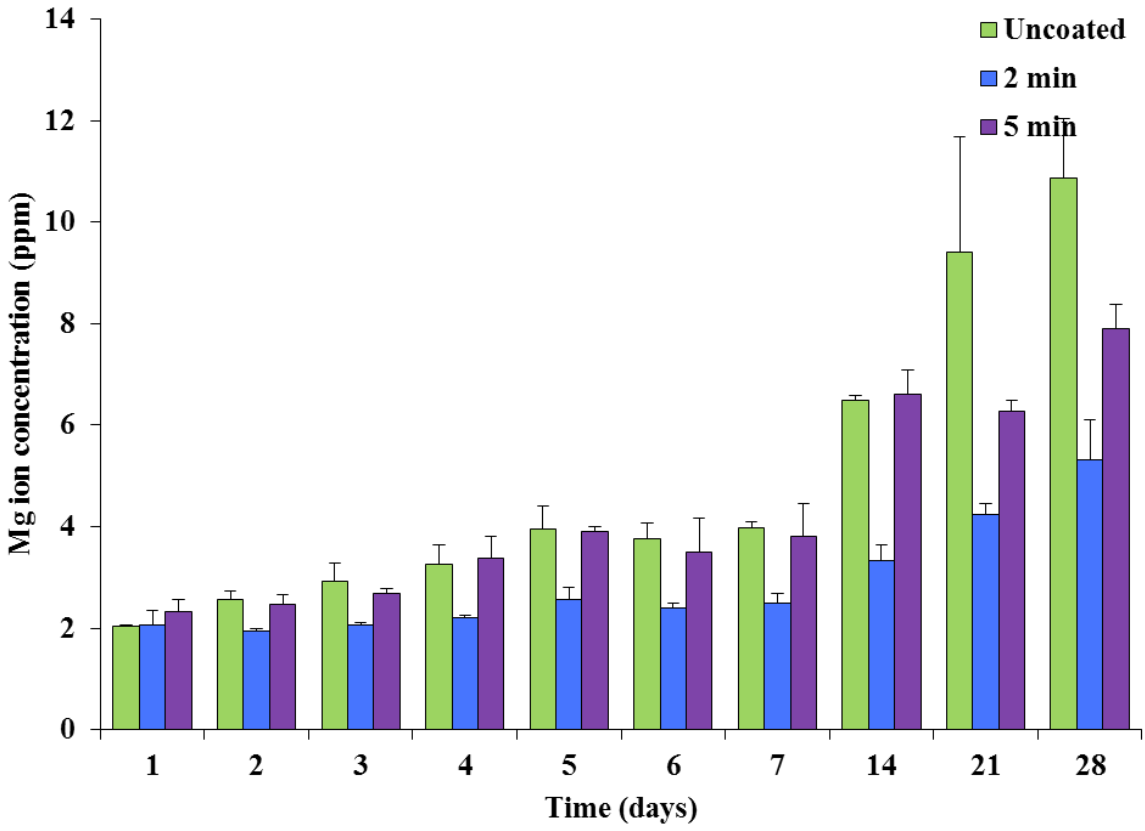

Figure 26: Mg ion concentration (ppm) in HBSS after in vitro corrosion testing of 99.9% Mg disks

A similar trend was seen with the change in pH of the HBSS after the 99.9% Mg samples were immersed in HBSS for 4 weeks (Figure 27). There was a steady increase in the change in pH from about 8.4 to 10 (initial pH of HBSS is 7.4). There was no significant different between the change in pH of the uncoated, 2 minute, and 5 minute groups. The Mg ion concentration and change in pH indicate a steady degradation of the samples over 4 weeks of interest.

Finally, the change in mass of the 99.9% Mg uncoated, 2 minutes, and 5 minutes showed an initial increase in mass over the first 1-2 weeks followed by a decrease in mass which is an indication that the physical mass loss has become greater than the accumulation of corrosion products (Figure 28). The trend in change in mass was similar to that of the Mg ion concentration and change in pH where the 2 minute samples had the slowest corrosion rate.

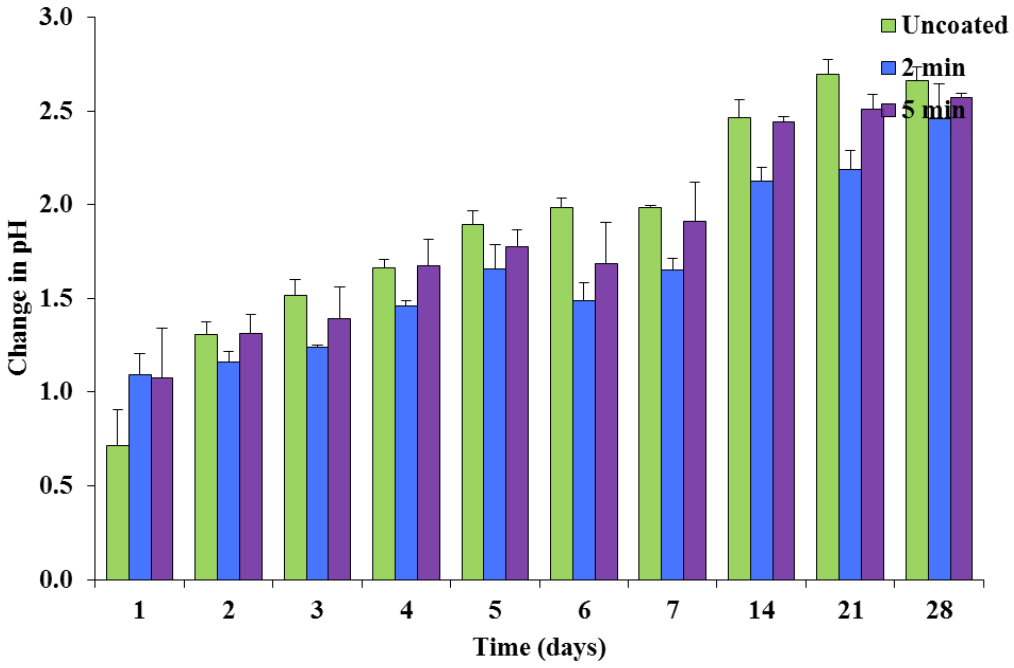

Figure 27: Change in pH of HBSS after in vitro corrosion testing of 99.9% Mg disks

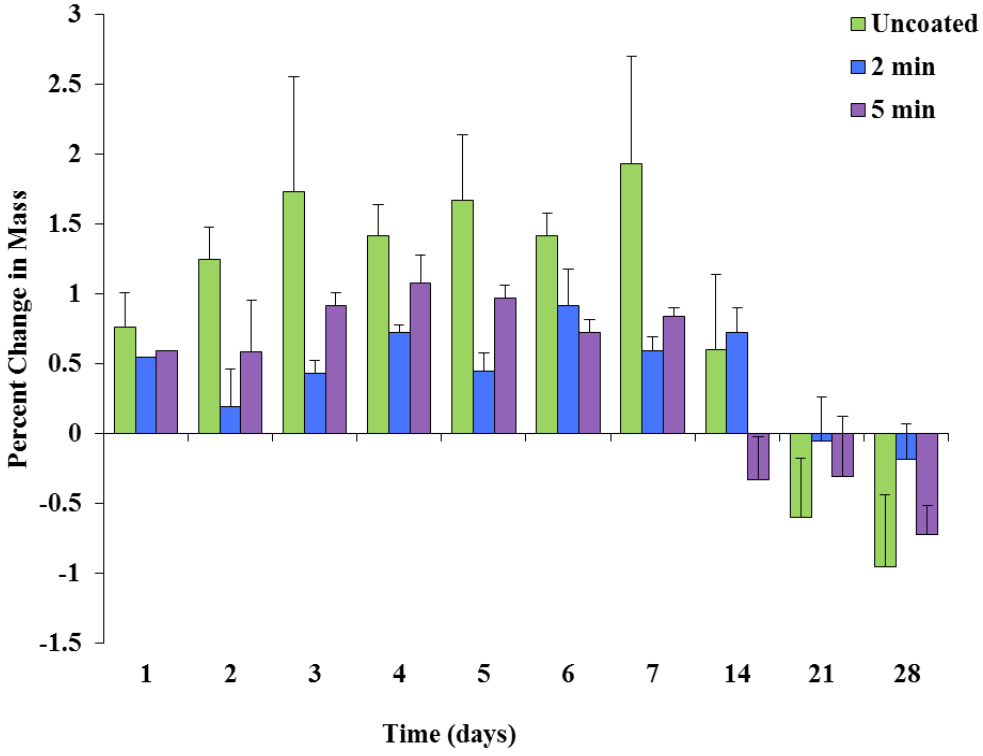

Figure 28: Percent change in mass of 99.9% Mg disks after in vitro corrosion testing

4.3.3 Surface Morphology

The SEM images of the uncoated, 2 minute, and 5 minutes samples of SC Mg as well as the 99.9% Mg control were recorded highlighting the characteristic porous surface of MAO coating (Figure 29). The uncoated samples were not porous. The porosity of the SC Mg 2 minute and 5 minute samples were 7.2 ± 3.0 % and 6.5 ± 2.0%, respectively (Table 2). There was no significant difference between the 2 minute and 5 minutes samples as well as between the SC mg and 99.9% Mg control samples. The porosity of the 99.9% Mg 2 minute and 5 minute samples were 7.0 ± 3.1 % and 6.9 ± 0.6%, respectively (Table 2).

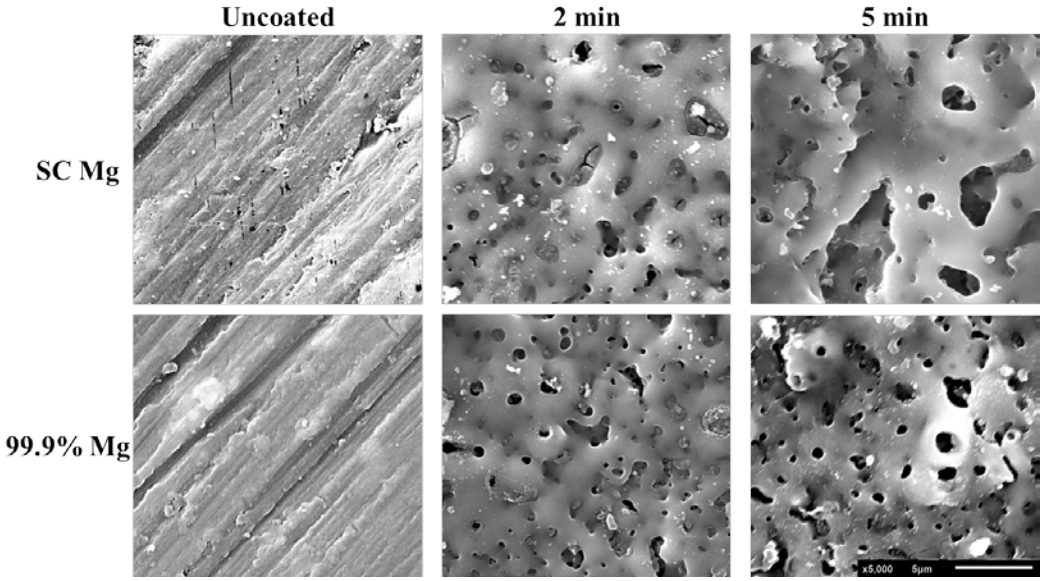

Figure 29: SEM Images (5000X) of SC Mg and 99.9% Mg disks uncoated and coated for 2 and 5 minutes

Table 2: Porosity (%) of SC Mg and 99.9% Mg disks uncoated and coated for 2 and 5 minutes

	Uncoated	2 min	5 min
SC Mg	----	7.2 ± 3.0	6.5 ± 2.0
99.9% Mg	----	7.0 ± 3.1	6.9 ± 0.6

4.3.4 Hardness

The Vickers Hardness of the uncoated and coated Mg samples was recorded (Table 3). The hardness of the uncoated, 2 minute, and 5 minute samples of SC Mg was 46 ± 8, 96 ± 14, and 101 ± 18, respectively. The hardness of the uncoated, 2 minute, and 5 minute samples of 99.9% Mg was 42 ± 2, 83 ± 3, and 90 ± 2, respectively. There was no significant difference between the SC Mg and 99.9% Mg groups. The MAO coating increased the hardness of the substrate by 2 times (Figure 30).

Table 3: Hardness (HV) of SC Mg and 99.9% Mg disks uncoated and coated for 2 and 5 minutes

	Uncoated	**2 min**	**5 min**
SC Mg	46 ± 8	96 ± 14	101 ± 18
99.9% Mg	42 ± 2	83 ± 3	90 ± 2

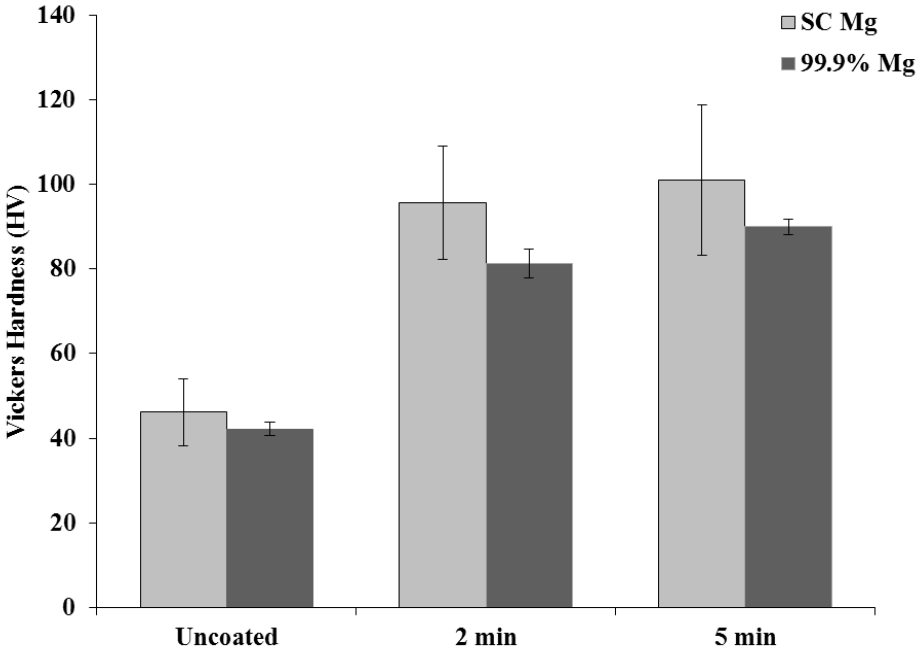

Figure 30: Hardness (HV) of SC Mg and 99.9% Mg disks uncoated and coated for 2 and 5 minutes

4.3.5 Roughness

The average roughness of the uncoated and coated Mg samples was recorded (Table 4). The average roughness of the uncoated, 2 minute, and 5 minute samples of SC Mg was 133 ± 15 μm, 320 ± 44 μm, and 510 ± 85 μm, respectively. The hardness of the uncoated, 2 minute, and 5 minute samples of 99.9% Mg was 129 ± 29 μm, 226 ± 33 μm, and 513 ± 43 μm, respectively. There was no significant difference between the SC Mg and 99.9% Mg groups. The MAO coating increased the roughness of the substrate by approximately 250% for the 2 minute group and 400% for the 5 minute group (Figure 31).

Table 4: Average roughness (R_a, µm) of SC Mg and 99.9% Mg disks uncoated and coated for 2 and 5 minutes

	Uncoated	2 min	5 min
SC Mg	133 ± 15	320 ± 44	510 ± 85
99.9% Mg	129 ± 21	226 ± 33	513 ± 43

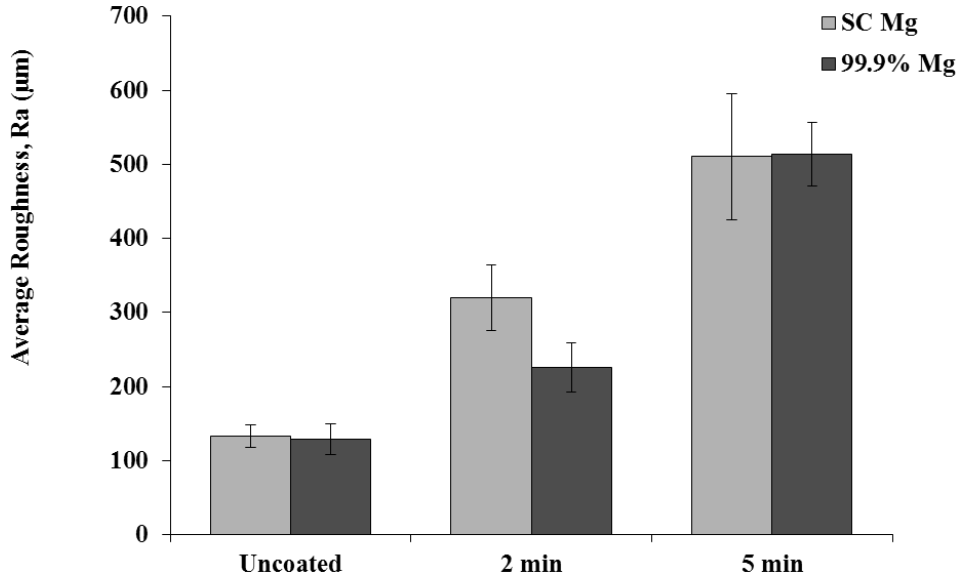

Figure 31: Average roughness (R_a, µm) of SC Mg and 99.9% Mg disks uncoated and coated for 2 and 5 minutes

4.3.6 Contact Angle Measurement

The contact angle of the uncoated and coated Mg samples was recorded as an indication of hydrophilicity (Figure 32). The contact angle of the uncoated, 2 minute, and 5 minute samples of SC Mg was 62 ± 8, 7 ± 2, and 10 ± 2, respectively (Table 5). The contact angle of the uncoated, 2 minute, and 5 minute samples of 99.9% Mg was 74 ± 7, 11 ± 5, and 29 ± 18, respectively. There was no significant difference between the SC Mg and 99.9% Mg groups.

The MAO coating decreased the contact angle for the substrate by approximately 80% for both the 2 minute and 5 minute groups; thus, increasing the hydrophilicity (Figure 32).

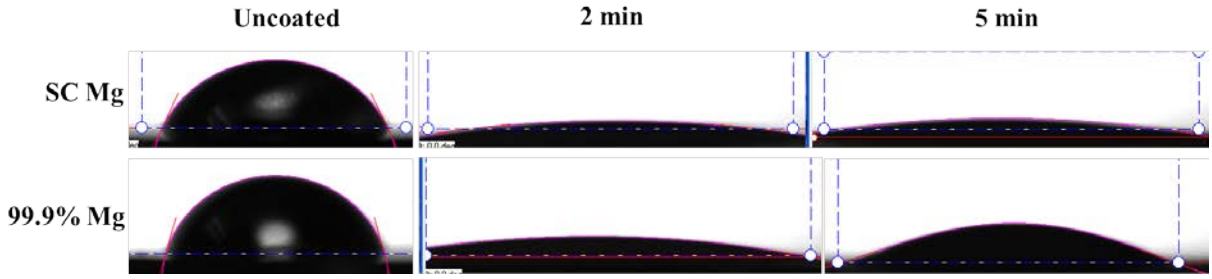

Figure 32: Images of contact angle (in degrees) of SC Mg and 99.9% Mg disks uncoated and coated for 2 and 5 minutes

Table 5: Contact angle (in degrees) of SC Mg and 99.9% Mg disks uncoated and coated for 2 and 5 minutes

	Uncoated	2 min	5 min
SC Mg	62 ± 8	7 ± 2	10 ± 2
99.9% Mg	74 ± 7	11 ± 5	29 ± 18

4.4 DISCUSSION

In recent years, there has been a renewed interest in the use of Mg for biomedical applications because of its mechanical properties and it can be resorbed by the body and replaced by native tissue [201, 202]. These properties make it especially promising for a wide range of uses such as orthopaedics, cardiovascular, and so on. However, the specific needs of different applications vary making it challenging to optimize an ideal Mg substrate. Thus, there is vast amount of research on engineering the corrosion rate. Such methods include but are not limited to grain

refinement, alloying, and coating. Further consideration must be given to how the strategies for controlling the corrosion rate affect the biocompatibility and mechanical properties.

For ACL healing, a Mg substrate that could resist corrosion in the early stages (3-6 weeks) and degrade completely by 12 weeks *in vivo* was an established goal. Additionally, a Mg substrate with high ductility is especially advantageous for an implant in an articulating joint to allow for deformation without damage to the articular cartilage, menisci, and other soft tissues. Also, the absence of alloying elements and minimization of defect concentrations as discussed above in regards to dislocations and stacking faults was desired to ensure the desired biocompatibility and ease of clinical translation. Thus, a single crystal substrate devoid of any alloying elements was selected because the monocrystalline structure allows for greater corrosion resistance, and higher ductility.

In addition to the single crystal Mg substrate, we employed a coating to further resist the corrosion at early stages and then allow for complete resorption of the Mg ring implant. MAO deposits a biocompatible coating that is able to yield implant degradation and allow for favorable cell interaction. MAO coating is characterized by a dense layer that resists infiltration in an aqueous environment and is beneath a porous layer that is attractive to cells. The composition of the coating is dependent on the electrolytic solution, the porosity of the coating is dependent on the applied voltage, and the thickness of the coating is dependent on the coating time. In Specific Aim 1, we aimed to characterize the coating parameters and the resulting coating in order to establish a benchmark for future development of the material-coating combination.

In previous *in vivo* studies of ECM + Mg ring repair of a transected ACL in a goat model at 12 weeks of healing, stifle joints in which the Mg ring implant was resorbed by the endpoint had more likelihood of favorable healing. Contrarily, if the implant was still present after 12

weeks of healing, it appeared as though the implant may have been physically blocking the healing of the ACL. Thus, in Specific Aim 1, we aimed to match the *in vitro* degradation profile of a Mg ring implant used in the previous study with favorable results. The degradation profile obtained from hydrogen evolution measurements seemed to be slow during the first 60 hours followed by accelerated corrosion. While we cannot make a direct relationship between the *in vitro* degradation and the potential *in vivo* degradation, the likelihood that the *in vivo* result would be similar to previous implants is greater if the *in vitro* degradation is the same. Thus, MAO coating of single crystal Mg for 2 minutes closely matched the *in vitro* degradation of the Mg ring implant from previous studies. However, there was variability of the corrosion rates observed within the groups for each coating time which could be indicative that the coating method was likely not consistent enough to produce repeatable results. The methodology for MAO coating is not trivial and close attention should be given to the preparation of the electrolytic solution, and moreover, the single crystal substrate preparation (i.e. materials purity, crystal orientation, machining that tends to result in creation of defects (grain boundaries, stacking faults and dislocations, etc.), polishing, temperature during processing, etc.), application of voltage, and coating timing in order to get consistent results. In the same set of hydrogen evolution measurements, it appears that the uncoated single crystal degrades slower than the coated single crystal Mg. This is unexpected because it is expected that uncoated Mg will likely exhibit rapid corrosion immediately and subsequently, with the formation of a passivation layer it is likely that the coating would cause the corrosion rate to be reduced and eventually plateau out. However, it is observed herein that coated Mg degrades exhibiting an opposite trend, displaying slow corrosion initially and faster once the coating is no longer effective. These trends are observed in the very early stages of the hydrogen evolution measurements but become

questionable over the course of 2 weeks. It is possible that the coating structure (density, distribution of porosity and pore size distribution, adhesion strength) is not consistent enough due to the variability in the substrate preparation stage. As a result, a consistent and reproducible corrosion resistant layer that is characteristic of MAO coating is not adequately formed during the short coating times selected for this study. Thus, the layer formed is likely very porous rendering the Mg substrate more susceptible to corrosion as the HBSS was able to infiltrate and initiate corrosion.

In Specific Aim 1, further characterization of the corrosion of MAO coated single crystal Mg was conducted with a commercially available 99.9% pure Mg control. It was shown that the single crystal Mg is more resistant to early corrosion than polycrystalline Mg as indicated by Mg ion concentration, pH, and mass measurements. Ultimately, these three measurements should provide similar trends on the corrosion rate. The polycrystalline Mg started degrading within the first week and continued throughout the 4 week time period. Contrarily, the single crystal Mg had minimal change in the Mg ion concentration, pH, and mass which indicates minimal corrosion. This further supports the use of MAO coated single crystal for the ACL healing application.

In addition to observing the corrosion of the single crystal Mg, characterization of the coating was also done to gain insight to additional advantages of using MAO coating. The MAO coating was more porous, harder, rougher, and more hydrophilic than uncoated single crystal Mg and 99.9% Mg. Each of these parameters provide an environment far more favorable for cellular interactions. Hardness is strongly dependent on the coating thickness, interface strength, and the pore size as well as pore size distribution. Increased hardness results in an increased cell proliferation, especially fibroblasts and osteoblasts [233-236]. Similarly, the surface roughness

has been shown to increase with coating time and cell attachment is influenced by the roughness of the surface. Cell spreading and differentiation are known to be influenced by both micro scale roughness and wettability [237-240]. The contact angle measurement showed that uncoated Mg is less hydrophilic than the MAO coated Mg, which supports the common practice of coating metallic implants regardless of coating method in order to enhance cell adhesion and proliferation [241-243]. Further investigation of these coating and surface properties in relationship to cell response could be achieved through a series of cell culture experiments which could also help establish acceptable ranges for the parameters of interests.

There were no significant differences between the two substrates or the coating times. Perhaps the differences between coating the substrates for 2 min and 5 min were not pronounced enough. In many published studies, investigators research coating for up to many hours. However, they sought to increase the corrosion resistance much more than what is desired for ACL healing.

There are number of unexpected results and limitations of the materials characterization step conducted herein. For example, with the hydrogen evolution measurements, the uncoated samples did not seem to corrode faster than the coated samples while the opposite trend was observed with the *in vitro* immersion testing. However, these non-electrochemical methods for determining corrosion rate should provide similar trends from the results. There are a number of varying parameters between the setup and implementation for each testing protocol that could have led to these observed discrepancies such as the amount of HBSS used, method of temperature control implemented, and so on. For future studies, it would be advantageous to use the same testing parameters across all experiments. Also, changing the solution daily would also give more reliable results as the solution could become saturated by the 2 week and/or 4 week

time periods of interest. Saturation of the solution could yield likely false corrosion rate indications and hence, also provide results that deviate from the naturally occurring corrosion process.

The results from the characterization of the coating and surface followed previously reported trends in literature. However, there were minimal differences between the 2 minute and 5 minute coating times. In future studies, it might be most beneficial to select coating times with a more determined time lapse between them. Also, the contact angle measurements obtained may have been misleading as the water droplet seemed to sink into the pores which may also indicate that the porosity of the coating layer is variable and an adequately dense layer may not have had adequate time to form. As previously mentioned, this may further explains why in some instances the coating seemed to increase the corrosion rate as opposed to slow it as expected. In future studies, cross sectional analysis could be used to determine if both, dense and porous layers are present. Additionally, electrochemical evaluation (i.e. potentiodynamic polarization (PDP) testing, electrochemical impedance spectroscopy) could provide additional understanding of the corrosion properties and the molecular effects of MAO coating [219].

Despite these limitations, completion of the characterization of the single crystal Mg and 99.9% Mg sets a benchmark for the coating parameters of the Mg ring implant. As the development of the ECM + Mg ring repair continues, considerations of how to improve the implant can be determined based on these parameters. For example, if a more porous coating is desired, the voltage should be increased. However, increasing the coating time may not be advisable if the other parameters should remain nearly constant. Also, further establishing a desired range for stiffness, ductility, and malleability would be helpful for knowing what properties are ideal to avoid damage to the inter-articular structures of the knee. Ultimately, the

MAO coated single crystal substrate was determined to be sufficient for this initial proof of concept study.

5.0 LONG TERM *IN VIVO* STUDY OF ECM + MG RING REPAIR FOR REGENERATION OF A TRANSECTED ACL IN A GOAT MODEL

5.1 INTRODUCTION

As summarized in Section 2.2.6.3, “ECM + Mg-ring repair” combines biological augmentation and mechanical augmentation using an extracellular matrix (ECM) sheet and hydrogel along with a novel metallic implant made with Mg and shaped like a cylinder, or a Mg ring designed to bridge the gap between the two ends of a torn ACL.

The biological augmentation is provided by ECM. ECM scaffolds consist of the structural and functional molecules secreted by the resident cells of the tissue and organ from which they are prepared. There are numerous advantages to using ECM scaffolds for tissue engineering applications. First, they provide a temporary structural scaffold upon which regeneration can occur [244]. Second, rapid degradation of the scaffold results in generation of chemotactic and mitogenic cryptic peptides [245-250]. Third, modulation of the innate immune response toward repair and regeneration (i.e. M2 profile) has been shown to result from the use of ECM scaffolds [251]. Lastly, they recruit multipotential progenitor cells to the site of interest [252]. The use of the ECM hydrogel allows for immediate activity to incite healing while the ECM sheets permit continuous activity throughout early stages of healing [253]. ECM has been

successfully used for the healing of ligaments and tendons including the MCL [254, 255], patellar tendon (PT) defect [256], and ACL [19].

The mechanical augmentation is provided by the Mg ring. The Mg ring serves to bridge the gap between the separate ends of the ACL. *In vivo*, it can also help to protect from the synovial fluid and restrict destructive motion of the ligament. Also, the Mg ring can restore stability to the knee joint immediately post-operatively and load the healing ligament throughout the healing process preventing disuse atrophy of the insertion sites [21, 186]. Additionally, the entire ECM + Mg ring repair construct can be resorbed by the body as the healing tissue begins to bear load. It has been shown that mechanical augmentation would stabilize the knee immediately after surgery and could work synergistically to help the biological augmentation to stimulate and accelerate healing the ACL.

As a next step, a long-term *in vivo* study of ECM + Mg ring repair of a transected ACL was conducted in a goat model and assessed after 26 weeks of healing. A total of 14 goats underwent ECM + Mg ring repair. One specimen was designated for histological evaluation while the remaining were assessed for joint stability, ligament function, and structural properties. The objective was to determine if the success of previous *in vivo* studies would persist to 26 week post-operatively as characterized by continuous collagen fibers without atrophy of the insertion sites as well as resorption of the implant.

5.2 METHODS

5.2.1 Animal Model

Skeletally mature (4-6 years of age), female Spanish goats were used. This animal model has a large size and robust activity level that make it well-suited for studies of the knee. Additionally, the goat has been successfully used historically in our research center and others for studies of ACLR as well as healing of other ligaments and tendons.

A number of *in vivo* animal models have been used to investigate healing of ligaments and tendons. Rodent models were not frequently used because of their small size making it difficult to perform surgical repair accurately. For ACL reconstruction, large animals such as dogs, pigs, goats and sheep are preferred. Based on a comparative study of the stifle joint of a number of experimental animals, the goat is a good choice partly because there are large volumes of data in the literature that could be used for comparison [187, 257, 258].

5.2.2 Preparation of Mg Ring Devices

For *in vivo* experiments, SC Mg was used due to its known biocompatibility as well as ductility. It was machined according to Section 4.2.1.2 and MAO coated according to Section 4.2.2. Following the application of the MAO coating, Mg ring devices were sterilized for surgery using ethylene oxide.

5.2.3 Preparation of ECM Bioscaffolds

ECM sheets and pre-gel digests from the porcine urinary bladder matrix (UBM) was provided by Dr. Badylak's laboratory. Well-established protocols were used to prepare the scaffolds from urinary bladders of market-weight pigs. Briefly, the bladders were cut open and the urothelial, serosal, and musculolayers were scraped away. The remaining tissue (basement membrane and tunica propria) were treated with a 0.1% peracetic acid/4% ethanol solution and then lyophilized. 5 x 40 mm sheets were cut and sterilized with ethylene oxide.

To prepare the UBM hydrogels, additional lyophilized UBM was powdered using a Wiley Mill and filtered through a 40 mesh screen. Then, the UBM powder was enzymatically digested under continuous stirring using 1 mg/ml pepsin in 0.01 M HCl for 72 hours, and the resulting pre-gel digest (10 mg ECM/ml (dry weight)) was frozen at -20°C. On the day of surgery, the pre-gel digest was thawed in 2.5 ml aliquots during the operation, and neutralized by adding one-tenth volume of 0.1 M NaOH, one-ninth the volume of 10X PBS, and then diluting to a final concentration of 6 gm/ml using 1X PBS. The hydrogel was passed through a sterile filter and stored on ice until injection *in vivo*.

5.2.4 Surgical Procedure

The surgical protocol was approved by the University of Pittsburgh's Institutional Animal Care and Use Committee (IACUC). All procedures were performed with sterile techniques using general endotracheal anesthesia. In all animals, the ECM + Mg ring repair was performed on the right stifle joint and the left served as a sham-operated control.

A longitudinal incision was made on the midline of the stifle joint from 1-2 cm above the patella to just below the tibial insertion of the patellar tendon. Then, an arthrotomy was performed medially to the patellar tendon, such that the patellar tendon could be minimally retracted in the lateral direction and the ACL exposed (Figure 33). With clear visualization of the ACL, four bone tunnels were drilled in the femur and tibia using a 1.5 mm guide wire. On the tibial side, tunnels were made medial and lateral to the ACL's insertion, while on the femoral side, two parallel tunnels were made anterior to the insertion. Then, two sets of "repair sutures" (Vicryl 2-0, Ethicon) and "fixation sutures" (Ethibond Excel #2, Ethicon) were attached to each end of the transected ACL. Then, the Mg ring implant was attached to the ACL with the repair sutures passing directly through the ring and tied around it. The fixation sutures were passed through the suture holes and bone tunnels and fixed on the outside of the bones using a knot tied over an Endobutton on the femoral side (Smith & Nephew, Andover, MA) and a double-spiked plate and fixation post on the tibial side (Smith & Nephew, Andover, MA) (Figure 5B). Before femoral and tibial fixation outside the bone tunnels, the 5 x 40 mm UBM sheet sutured to a similarly-sized fibrin sponge (Surgifoam, Ethicon, Inc., Bridgewater, NJ) was wrapped around the Mg ring implant. After fixation of the Mg ring, additional UBM hydrogel (~4 ml) was injected directly into the injury site. A local analgesic (Bupivacaine, 1 mg/kg) was injected subcutaneously, and the wounds were closed.

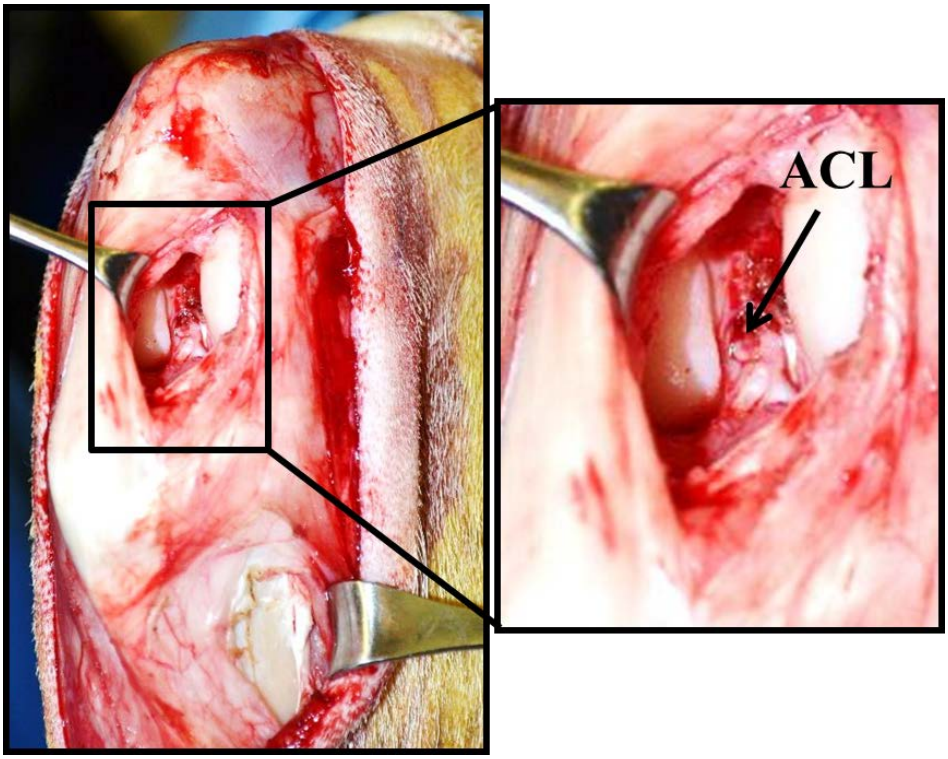

Figure 33: Medial incision and visualization of the ACL

5.2.5 Post-Operative Care

Following surgery, the animals were allowed free cage activity. For pain management, Banamine was administered twice daily subcutaneously (1.1 mg/kg) for 6 days post-surgery, and Metacam was administered every 3-5 days subsequently as deemed necessary by the animal facility veterinarian. Animals were assessed daily for general health and the weight bearing status of the treated joint. A scale was used for qualitative assessment of lameness (Table 6). At the 4, 5, and 6 month time points, manual anterior drawer exams were conducted under twilight sedation (5 mg/kg Ketamine) to assess ACL functionality throughout healing using a qualitative scale (Table 7). Furthermore, x-rays of the ECM + Mg ring repaired joint were taken to observe the presence of the Mg ring implant as well as any abnormalities such as joint space narrowing.

Table 6: Lameness scoring scale

Score	Weight-bearing status
0	Three-legged walking
1	Clear walking lameness/toe-touching
2	Mild walking lameness, clear during running
3	Minimal running lameness
4	Normal

At the end point of the study (26 weeks), animals were humanely euthanized. They were first sedated using an intramuscular injection of Ketamine/Xylazine (7 mg/kg Ketamine, 0.1 mg/kg Xylazine), followed by a lethal injection of sodium pentobarbital (1 mg (390 mg)/10 lbs). Both treated and sham-operated legs were harvested using a scalpel by disarticulation of the hip joint. Of the harvested joints (N=24, 12 goats at the study endpoint), two joints were used for histology and the remaining joint specimen were used for biomechanical evaluation.

Table 7: Qualitative scale for the anterior drawer exam

Score	Description	
A	Normal	• No or very little anterior translation of the tibia • Less than 3 mm
B	Near Normal	• Little anterior translation of the tibia with a firm endpoint • Less than 5 mm
C	Abnormal	• More anterior translation of the tibia with a firm endpoint • More than 5 mm
D	ACL Deficient	• A lot of anterior translation of the tibia with no endpoint • More than 10 mm

5.2.6 Gross Morphology

The gross morphology of the healing ACL was assessed following the dissection of the femur-ACL-tibia complex (FATC). The size, shape, color, alignment, and continuity of the healing tissue were recorded. The articulating surfaces of the patella and the femoral condyles were inspected for the presence of chondral lesions, and the healing of the bone tunnels was also assessed. Degradation of the Mg ring implant as well as the presence of the fibrin sponge and ECM sheet were noted.

5.2.7 Histological Evaluation

In the stifle joints designated for histological evaluation (N=2, an experimental and a contralateral sham operated control), the FATC was dissected and trimmed immediately after harvest. It was submerged in 10% neutral-buffered formalin (Sigma Aldrich, St. Louis, MO) for 48 hours and then stored in 70% ethanol prior to histology. Histology was performed at Alizee Pathology, LLC (Thurmont, MD). The treated FATC was embedded in methylmethacralate (MMA) and the sham-operated FATC was embedded in an oversized paraffin block after decalcification. Then, the samples were sectioned sagittally to generate three serial sections that were ground, polished, and stained with hematoxylin and eosin (H&E), Stevenel's Blue (SB) and Herovici stain. The Herovici staining was used to determine collagen type and maturity [259]. The sections were evaluated using light microscopy.

5.2.8 Analysis of Synovial Fluid

Approximately 1 ml samples of synovial fluid were collected from the treated and sham-operated stifle joints immediately after sacrifice using an 18-guage needed. A small amount (~100-200 μl) of each sample was used to smear a glass slide, and the JorVet Dip Quick Stain (Jorgensen Laboratories, Inc., Loveland, CO) was used to qualitatively assess cytology. After air drying the prepared slide, it was dipped into methanol for fixation, followed by polychromatic stains (eosin and thiazine) to allow detection and visualization of nucleic acids, protein eosinophil granules, and mast cell and basophil granules. Once prepared, the slides were observed under light microscopy. Additionally, the total protein content was measured using a refractometer.

5.2.9 Robotic Testing

The robotic manipulator has a position and orientation repeatability of 0.2 mm and 0.2°, respectively. This testing system can be operated in force control mode to measure the 6 DOF joint kinematics in response to externally applied loads. It can also be used in position control mode to repeat previously recorded 6 DOF kinematics such that the in-situ forces in ligaments and other soft tissue structures can be determined to within a few Newtons of accuracy [260-262]. For the past twenty years, the robotic/ UFS testing system has been successfully used to accurately determine the multiple DOF (translations and rotations) of knee joints as well as in-situ forces of soft tissues in response to externally applied loads when the knee undergoes unrestricted motion.

The robotic/UFS testing system was used to assess joint stability and the in-situ forces in the healing ACL upon external loads (N=20, 10 experimental and 10 contralateral sham operated

control). The UFS system (Model Theta; ATI Industrial Automation, Apex, North Carolina, USA) has a capacity of 1500 N of force and 240 Nm of torque and can measure 3 forces and 3 moments in a Cartesian coordinate system fixed with respect to the sensor with repeatability of 0.5 N for force and 0.05 Nm for torque. The robotic manipulator (KUKA Model KR 210; KUKA Robotics Corp., Shelby Township, Michigan, USA) is capable of recording and reproducing the relative positions between the femur and tibia in the 3-dimensional space with an accuracy of less than 0.1 mm and 0.1° with full 6-DOF of motion. For this study, the robotic/UFS testing system was operated in force, position, and hybrid control to obtain joint kinematics of the repaired stifle joint as well as the forces carried by the healing ACL.

The goat stifle joint was thawed at room temperature the day before testing. Then, it was prepared for testing by cutting the femur and tibia about 20 mm from the joint line, and removing soft tissues approximately 10 mm away from the joint line, such that the femur and tibia were potted in a cylindrical epoxy mold (Everglass, Evercoat, Cincinnati, OH). Then, the specimen was mounted onto the robotic/UFS testing system (Figure 34). The path of passive flexion-extension was determined by flexing the joint at 1° increments, finding the position that minimizes the resulting forces and moments. This path provided the starting position at each angle of flexion for the application of external loads for the remainder of the test and served as the reference position by which to measure knee kinematics. The stifle joint was subjected to (1) 67 N anterior-posterior load and (2) 5 Nm varus-valgus moment (force control). The resulting kinematics including anterior-posterior tibial translation (APTT) of the stifle joint were measured at 30°, 60°, and 90° of joint flexion. The intact kinematics were replayed for the FATC (position control) as each of the following knee structures were removed: medial collateral ligament (MCL), soft tissue and lateral collateral ligament (LCL), medial meniscus, lateral meniscus,

posterior cruciate ligament (PCL), and bony contact. The corresponding in-situ force in each structure in the joint were calculated using the principle of superposition and the final set of forces measured with only the FATC represents the in-situ forces in the ACL. The cross sectional area (CSA) and shape of the ACL were measured quantitatively using a laser reflectance system developed in our research center [66].

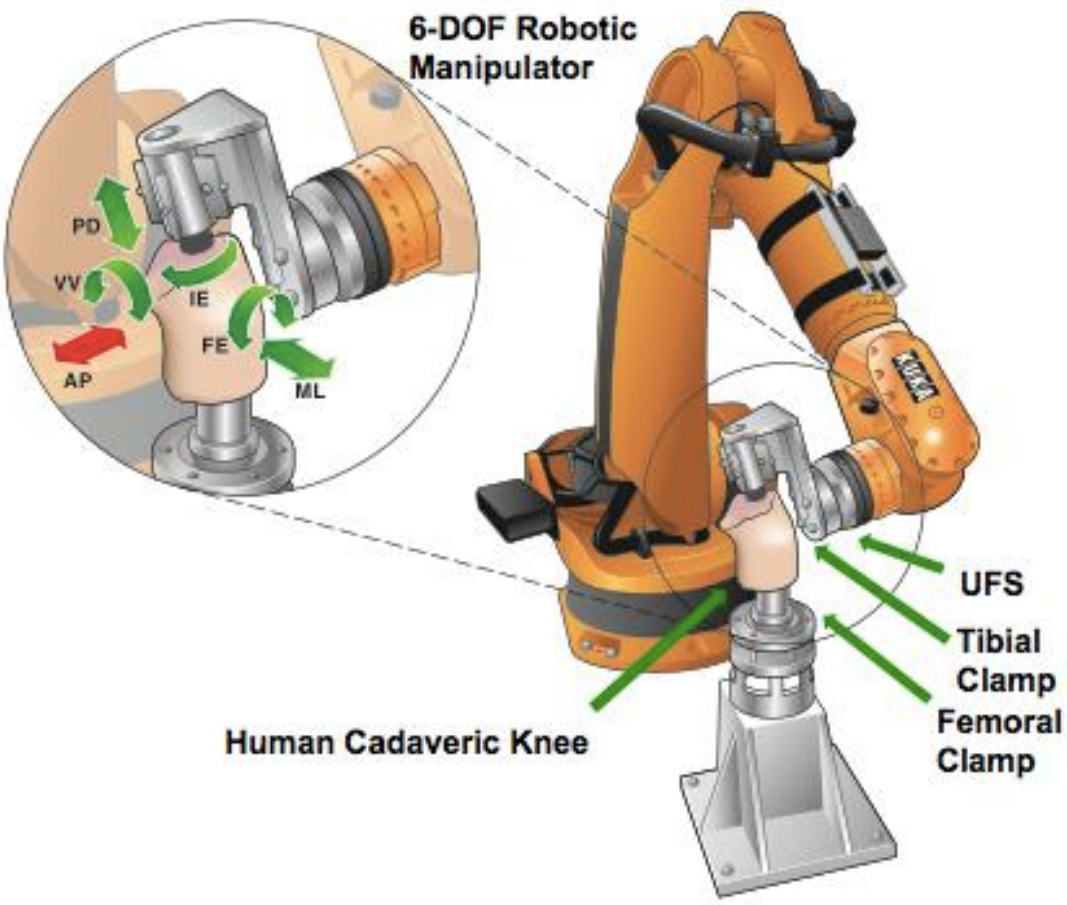

Figure 34: Schematic of the robotic UFS testing system [84]

5.2.10 Tensile Testing

After testing on the robotic/UFS testing system, uniaxial tensile testing was performed on each FATC to determine its structural properties. The FATC was mounted to a materials testing machine (Model 4052, Instron, Canton, MA) in custom clamps such that the ACL was aligned anatomically in its natural direction of tensile loading (Figure 35). Then, it was preloaded to 3N, and the gauge length will be reset. Then, it underwent cyclic preconditioning between 0 – 1 mm of elongation, which is in the toe region of the long-elongation curve, for 10 cycles, at a crosshead speed of 50 mm/min. Finally, the 3 N preload was reapplied and the FATC was loaded to failure at the crosshead speed of 10 mm/min. From the resulting load-elongation curve, the structural properties of the FATC were determined, including the stiffness, ultimate load, and ultimate elongation.

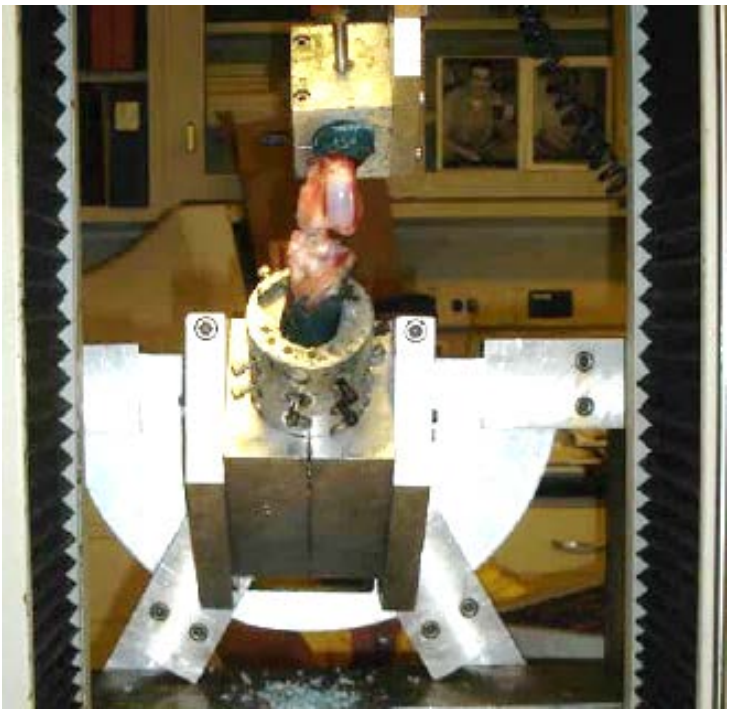

Figure 35: Photograph of set-up of the materials testing machine

5.2.11 Data Analysis

For the *in vivo* evaluation at 26 weeks of healing, a two-way ANOVA was used to analyze the results from the robotic/UFS testing system including APTT and in-situ forces of the ACL. For the data from the tensile testing following the robotic testing including stiffness, ultimate load, and ultimate elongation, student's t-test was performed to compare the treated and sham-operated specimen. Statistical significance was defined as $p<0.05$.

5.3 RESULTS

All goats were mobile and weight-bearing on the treated joints by 2 hours post-operatively. The goats were housed individually for the first 2 weeks to limit motion and reduce the likelihood of injury. During the course of the study, two goats were euthanized before the end point. The first experienced a broken tibia during recovery (ET# 913) and the second had unsatisfactory recovery and was removed from the study at 12 weeks (ET# 891). The remaining 12 goats recovered well. However, Goat ET#914 was excluded from testing as a result of poor scoring during the series of manual AP exams which was indicative of failure.

5.3.1 Post-Operative Drawer Scores and X-Rays

For the first 6 weeks, the site of surgery was vulnerable and the goats exhibited lameness during walking and running. By 12 weeks, the goats had normal gait with no evidence of limping during walking or running. Thus, the lameness scoring system was used as an indication of

recovery but could not be used to determine the quality of the ACL healing. The anterior drawer exam was employed as a qualitative assessment of the ligament function throughout the second half of the *in vivo* study. Less motion of the tibia was an indication of better healing (Table 7). The + and – were added to the score as an indication of the variation between the specimen. The orthopaedic surgical fellow provided a score for the anterior motion of the tibia with respect to the femur (Table 8). Eight of the 12 goats' scores were near normal (score of B or better) at 4 months. By the study endpoint, only 2 remained near normal while the remaining 10 had anterior drawer motion large enough to be considered abnormal.

Table 8: Manual anterior drawer exam results, scores with an asterisks were taken at the 3 month time point

Goat ET#	4 months	5 months	6 months	Implant Visible (X-Ray)?
895	B+	C+	C	Yes
896	C	C+	C-	No
869	B-	B	B	No
863	B	B+	C	No
904	B+	B+	C	Yes
906	C	B-	C	Yes
882	B	B+	B	No
902	B+	B	C	Yes
881	C	B-	C	No
900	B*	B-	C	No
903	A*	C	C-	No
914	C	C+	C	Yes

At the same time the anterior drawer exam was performed, x-ray images were taken of the ECM + Mg ring repaired joint. The presence of the Mg ring implant was noted as well as any radiographic evidence of joint abnormalities such as joint narrowing and osteoarthritis. Seven of the x-ray images showed no evidence of the Mg ring implant by 6 months (26 weeks). Thus, the Mg implant had degraded into very small fragments not detectable by x-ray or completely in those stifle joints.

At 4 months, it seemed as though there was a relationship between the presence of the ring and the anterior drawer score suggesting that if the ring is not present, the anterior drawer score was be favorable and vice versa. However, by the endpoint that relationship is not sustained. Goat ET# 895 is an example of a stifle joint with no radiographic evidence of the Mg ring implant that had a favorable score at 4 months and by the endpoint the score is abnormal (Figure 36). There is also evident of potential joint narrowing. Goat ET# 895 was used for histological analysis.

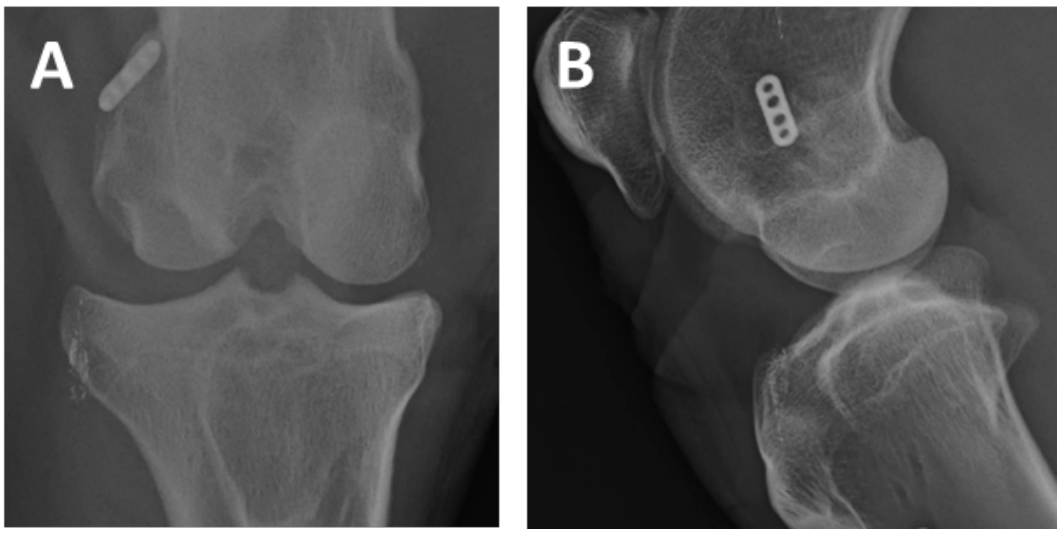

Figure 36: Radiographs of goat ET# 895 after 26 weeks of healing; Anterior-Posterior view (A) and Medial-Lateral view (B)

5.3.2 Gross Morphology of the Healing ACL

After 26 weeks of healing, the stifle joints were found to be stable upon manual manipulations. There were no signs of swelling of inflammation. The gross anatomical observation of the healing ACL showed a variation of the healing ACL. Most specimen were robustly healed ligaments that were mostly white and opaque in color (Figure 37). Others were not as robust with the primary structure of the ACL being composed of the nonresorbable fixation sutures. The geometry of the healing ACL was oblong in shape and was slightly hypertrophic. The cross-sectional areas determined by the laser reflectance system was increased from 33 ± 15 mm^2 in the sham-operated ACL to 59 ± 26 mm^2 in the healing ACL (Figure 38). However, the difference was not statistically significant. Visual inspection of the articular cartilage showed no evidence of degenerative defects. There were very small remnants of the Mg ring remaining in seven of the 10 specimen located in varying locations within the ACL and surrounding tissue. No adverse effects seemed to result from the presence of the remnants.

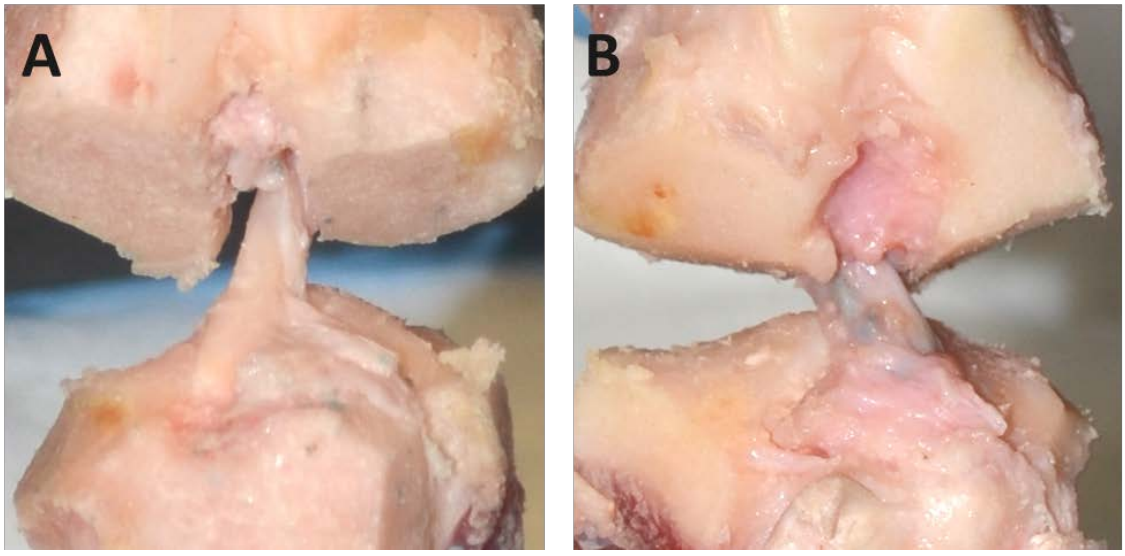

Figure 37: The sham-operated ACL (A) and ECM + Mg ring repaired ACLs with robust neo-tissue (B)

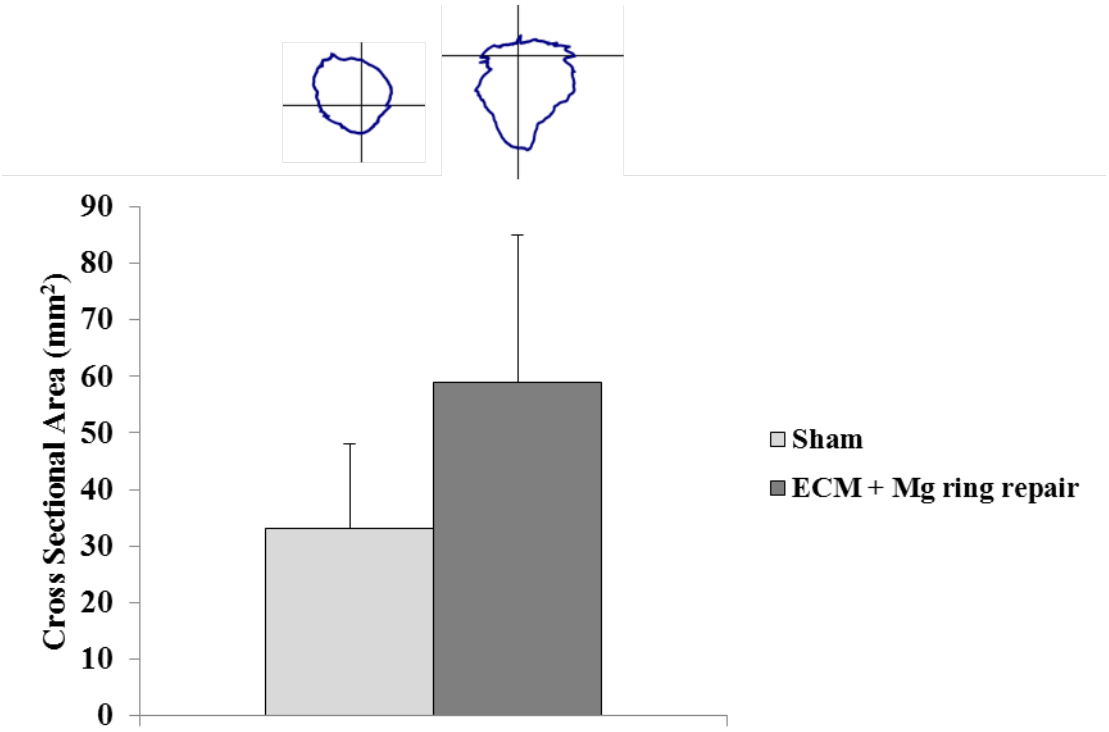

Figure 38: Cross-sectional area of sham and ECM + Mg ring repair ACLs

5.3.3 Histological Evaluation

The histology of the sham-operated ACL was found to be within normal limits with no evidence of inflammation, fibrosis, or synovial hyperplasia noted. The healing FATC was effectively repaired and healed with fibrous connective tissue and a low-grade foreign body reaction to the presence of the suture material and remaining Mg material as evident by the H&E (Figure 39) and SB (Figure 40) stains. The transected ends of the ACL were not readily discernable due to the fibrous tissue present. The bone tunnel sites on both the femur and tibia contained suture material with a mild foreign body reaction and fibrosis. Additionally, the tibial insertion site contained a small amount of chondrocyte metaplasia that lined the edges and occasionally the center of the suture material (Figure 41A).

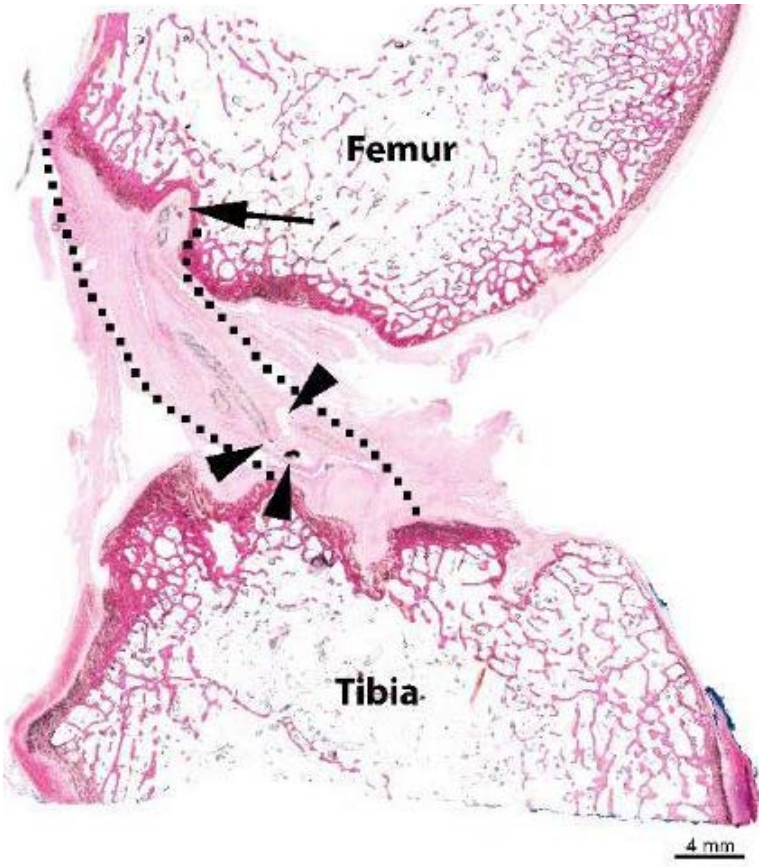

Figure 39: H&E staining of the healing FATC where the dotted line outlines the ACL, the arrow points to the femoral bone tunnel containing suture material and the arrowheads show small remnants of Mg

A small amount of Mg ring was found on the H&E slide (Figure 39) and a larger amount of Mg ring material was evident on the SB slides (Figure 40). The Mg ring material was surrounded by low numbers of macrophages (low grade foreign body reaction) and a moderate amount of dense fibrous connective tissue. Occasionally, small aggregates of clear space were noted within the fibrous connective tissue in the ACL midsubstance. Within the layer of inflammation surrounding one aggregate of clear space was an area with multiple small particles of mineralization (Figure 41B). The black aggregates of Mg material appeared to be surrounded by several layers of mineralization as well (Figure 41C). The synovium was within normal limits without evidence of synovial hyperplasia or inflammation.

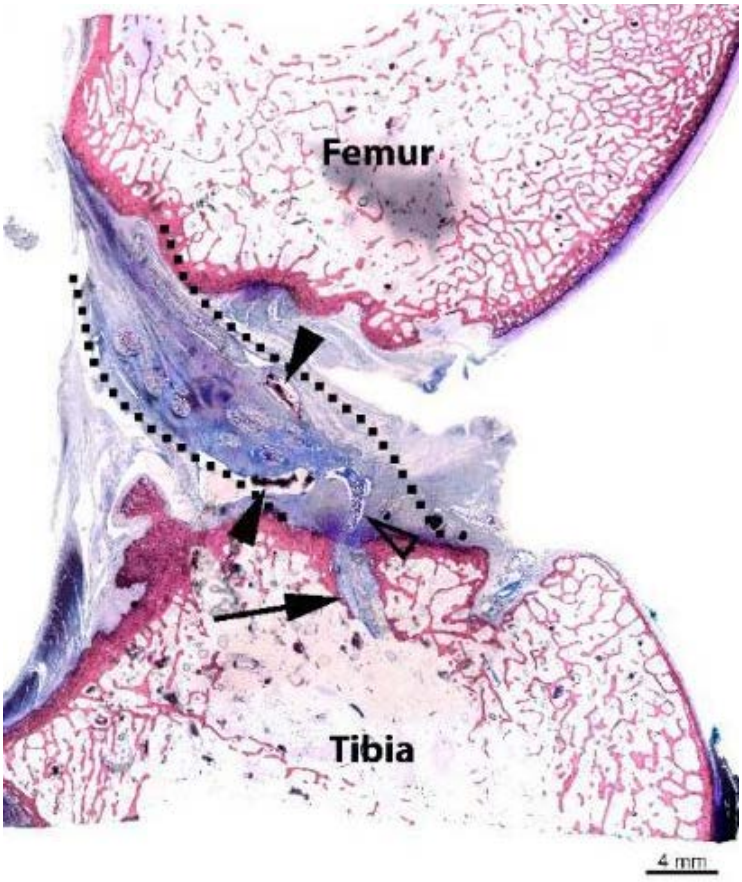

Figure 40: SB staining of the healing FATC where the dotted line outlines the ACL, the arrow points to the tibial bone tunnel containing suture material and the arrowheads show small remnants of Mg

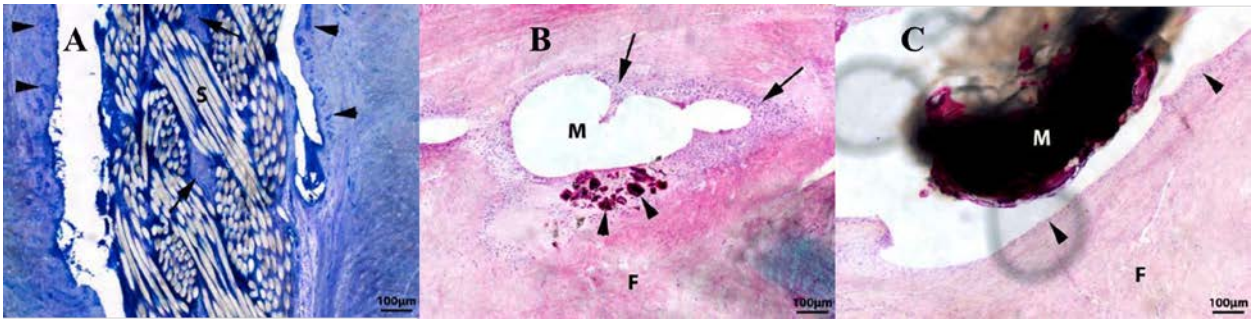

Figure 41: Small amount of chondrocyte metaplasia lining edges of suture material (A), small particles of mineralization within the aggregates of clear space located in the ACL midsubstance (B), and minimal inflammatory response composed of low numbers of macrophages surrounding Mg remnants (C)

As a result of Herovici staining, the PCL (indicated as an asterisk in Figure 42) stained dark purple-blue which is indicative of mature collagen. In contrast, the fibrous connective tissue throughout the ACL stained light blue-green-yellow representing immature collagen with occasional areas of darker blue-purple-red staining surrounding the suture material (Figure 42). The collagen surrounding the Mg remnants was light yellow-green-blue.

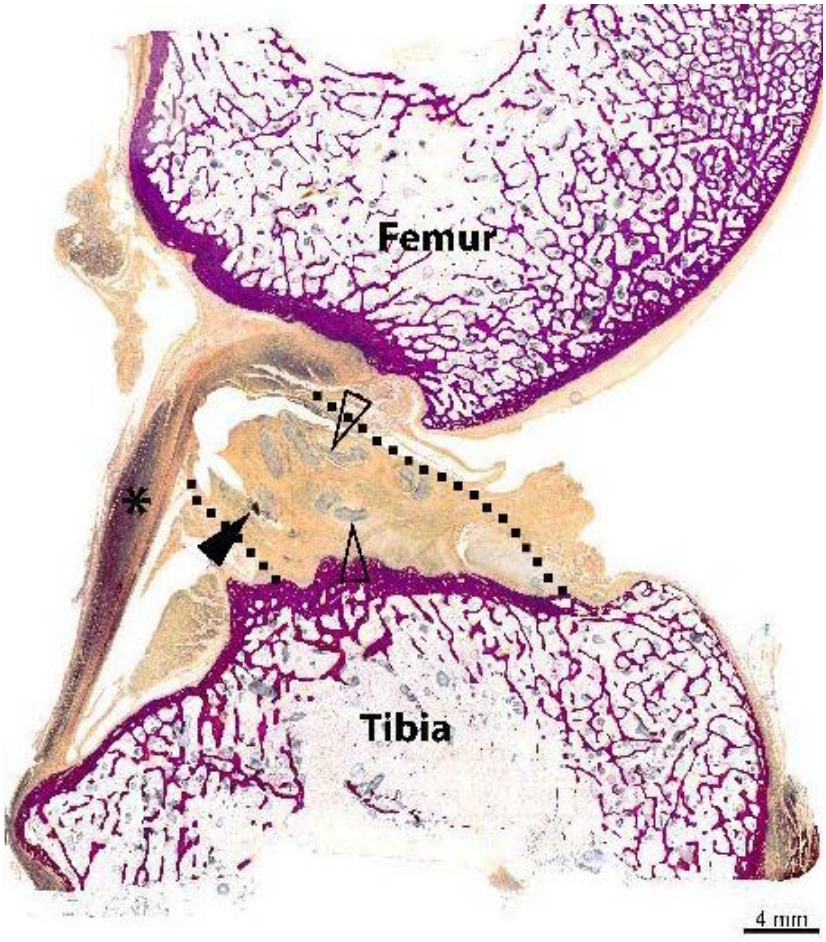

Figure 42: Herovici staining of the healing FATC with dotted lines highlighting the edge of fibrous connective tissue surrounding the ACL

5.3.4 Cytology and Total Protein Content of Synovial Fluid

The synovial fluids in the sham-operated and healing stifle joints were clear with a sticky consistency. There was no visual difference between the 2 samples. However, the synovial fluid was easier to collect from the healing joints and in greater volume. Similarly, the cytology of the synovial fluid from the sham-operated and healing joints were similar. In both groups, there was low cellularity. However, the synovial fluid from the healing joint had slightly higher synovial cells as well as few macrophages. There were no signs of infection.

The total protein content in the synovial fluid from the sham-operated joints was 2.0 ± 0.2 g/dl, which was similar to the value of the value of 2.4 g/dl estimated for normal joint synovial fluid in goats (one-third of the total blood serum protein content) (Figure 43) [263]. The total protein content in the synovial fluid from the healing joints was 2.5 ± 0.4 g/dl. There was not significant difference between the two groups.

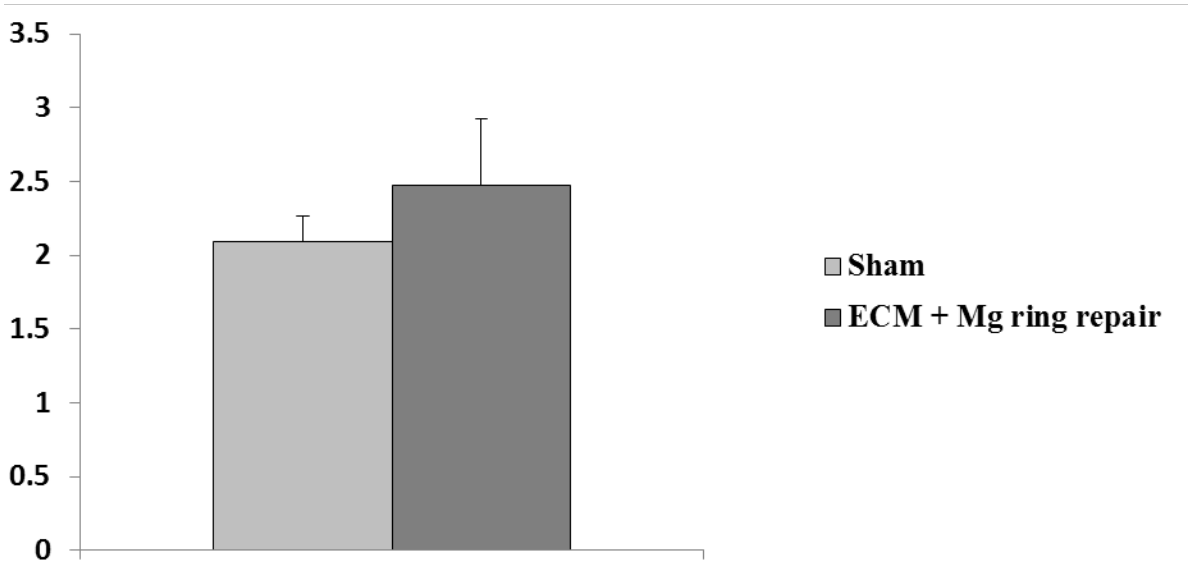

Figure 43: Total protein content in synovial fluid from sham-operated and healing goat stifle joints after 26 weeks of healing

5.3.5 Joint Stability and In Situ Forces

The curves representing the average APTT in the sham-operated and ECM + Mg ring repaired stifle joints is shown in Figure 44. Results at 30° of joint flexion are shown as the results were similar at all tested joint flexion angles. In the graph, elongation begins at the point of maximum posterior tibial translation and continues to the point of maximum anterior tibial translation. The posterior tibial translation in response to the 67-N posterior tibial load was similar between groups because the PCL left intact in both groups. The curve for the sham-operated group continued with a near linear slope through the application of the 67-N anterior tibial load. However, near the neutral position (~30 N posterior tibial load), the ECM + Mg ring repaired joint became less stable and began to experience higher translation in response to small increases in loading. The continued until 20 N of anterior tibial loading after which joint structures were engaged to prevent further translation.

The APTT in response to the 67-N anterior-posterior tibial load is shown in Table 9. For both the sham-operated and ECM + Mg ring repaired joints, The APTT increased from 30° to 60° of stifle joint flexion, then decreased at 90°. The APTT in the sham-operated group ranged from 3.3 to 3.8 mm, and was within the range of previously reported values for a normal goat stifle joint. At all flexion angles, the APTT in the ECM + Mg ring repaired joint was about 2.5 times that in the sham-operated joint.

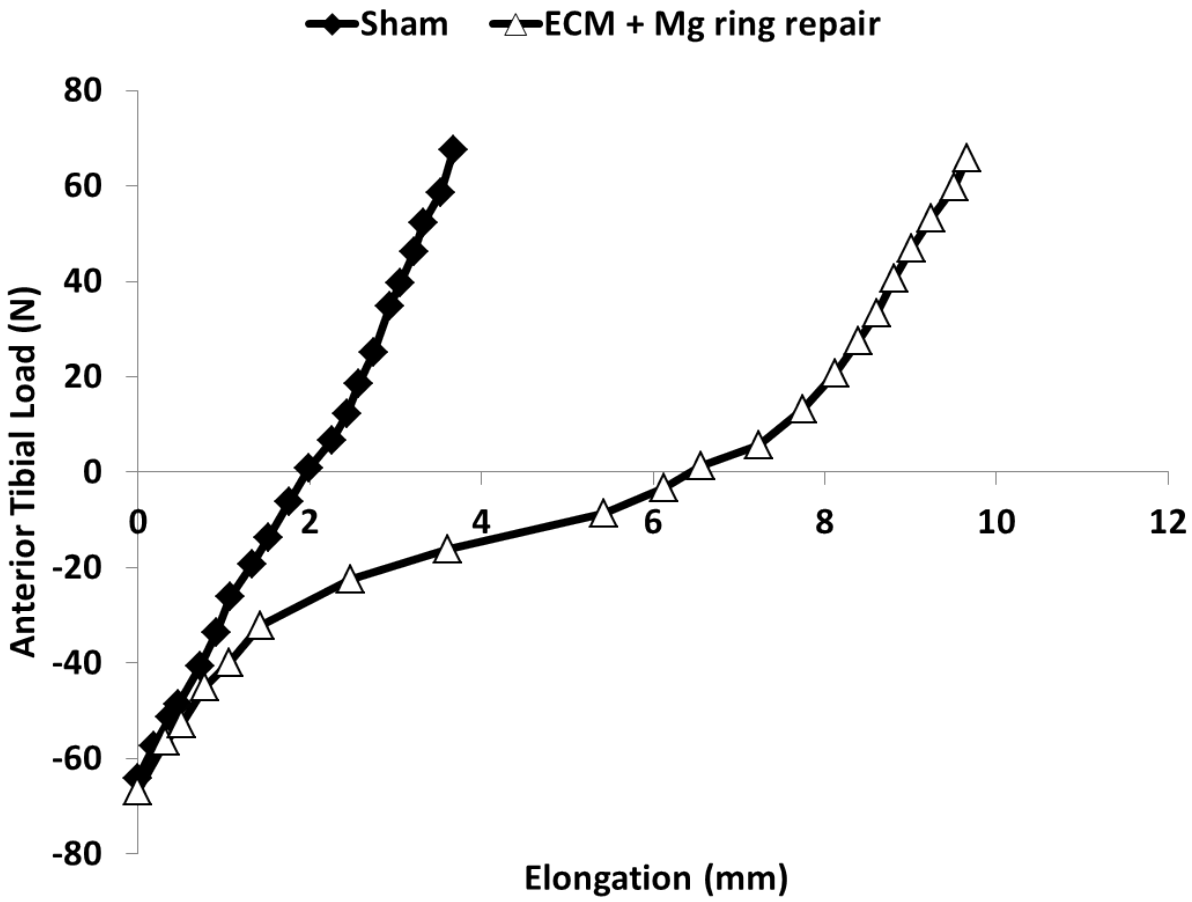

Figure 44: Average curves for the elongation in the sham-operated and ECM + Mg ring repaired joints at 30° of joint flexion under 67 N anterior tibial load

The in-situ forces in the ECM + Mg ring repaired ACL in response to the 67-N anterior-posterior tibial load is also shown in Table 9. The in-situ force in the ACL in the sham-operated joint was close to the applied load and ranged from 56 to 70 N. The in-situ force in the ECM + Mg ring repaired ACL was close to that of the sham-operated ACL at 30° of flexion, and decrease by approximately 20 N at 60° of flexion. At 90° of joint flexion, the in-situ force in the ECM + Mg ring repaired ACL decreased again by approximately 40 N.

Table 9: Anterior-posterior tibial translation (A) and in-situ forces in the ACL (B) of the sham-operated and ECM + Mg ring repaired goat stifle joints at 30°, 60°, and 90° of joint flexion

	Flexion Angle		
	30°	**60°**	**90°**
A. Anterior-posterior tibial translation (mm)			
Sham-operated group	3.4 ± 0.5	3.8 ± 0.6	3.3 ± 1.1
ECM + Mg ring repaired group	9.2 ± 2.7	9.9 ± 2.7	8.0 ± 1.9
B. In-Situ forces in the ACL (N)			
Sham-operated group	70 ± 13	60 ± 10	56 ± 10
ECM + Mg ring repaired group	56 ± 23	43 ± 23	17 ± 16

To better understand the differences between the function of the sham-operated and ECM + Mg ring repaired joints, the in-situ forces in the other structures in the knee were compared (Figure 45). The force distribution differed between the groups as well as based on the flexion angle. At 30° of joint flexion, the majority of the in-situ force in response to 67-N anterior-posterior tibial load was in the ACL in both the sham-operated and ECM + Mg ring repaired groups. In the sham-operated joints, there were also smaller forces in the lateral meniscus (~40 N) and bony contact (~30 N), but in the ECM + Mg ring repaired joints the forces shifted to the medial meniscus (~40 N). At 60° of joint flexion, the majority of force in the sham-operated group was also carried by the ACL, and the forces carried by the lateral meniscus decreased by half and that of the bony contact remained approximately the same. In contrast, in the ECM + Mg ring repaired joints, the in-situ force in the ACL was decreased, with forces also carried by the medial meniscus. Finally, at 90° of flexion, the in-situ forces in the sham-operated joints were also carried mostly by the ACL, with smaller forces carried by the MCL and medial meniscus. Alternatively, in the ECM + Mg ring repaired joints, the ACL carried much smaller

forces while the other joint structures carried equal or higher forces including the MCL, soft tissue, and medial meniscus.

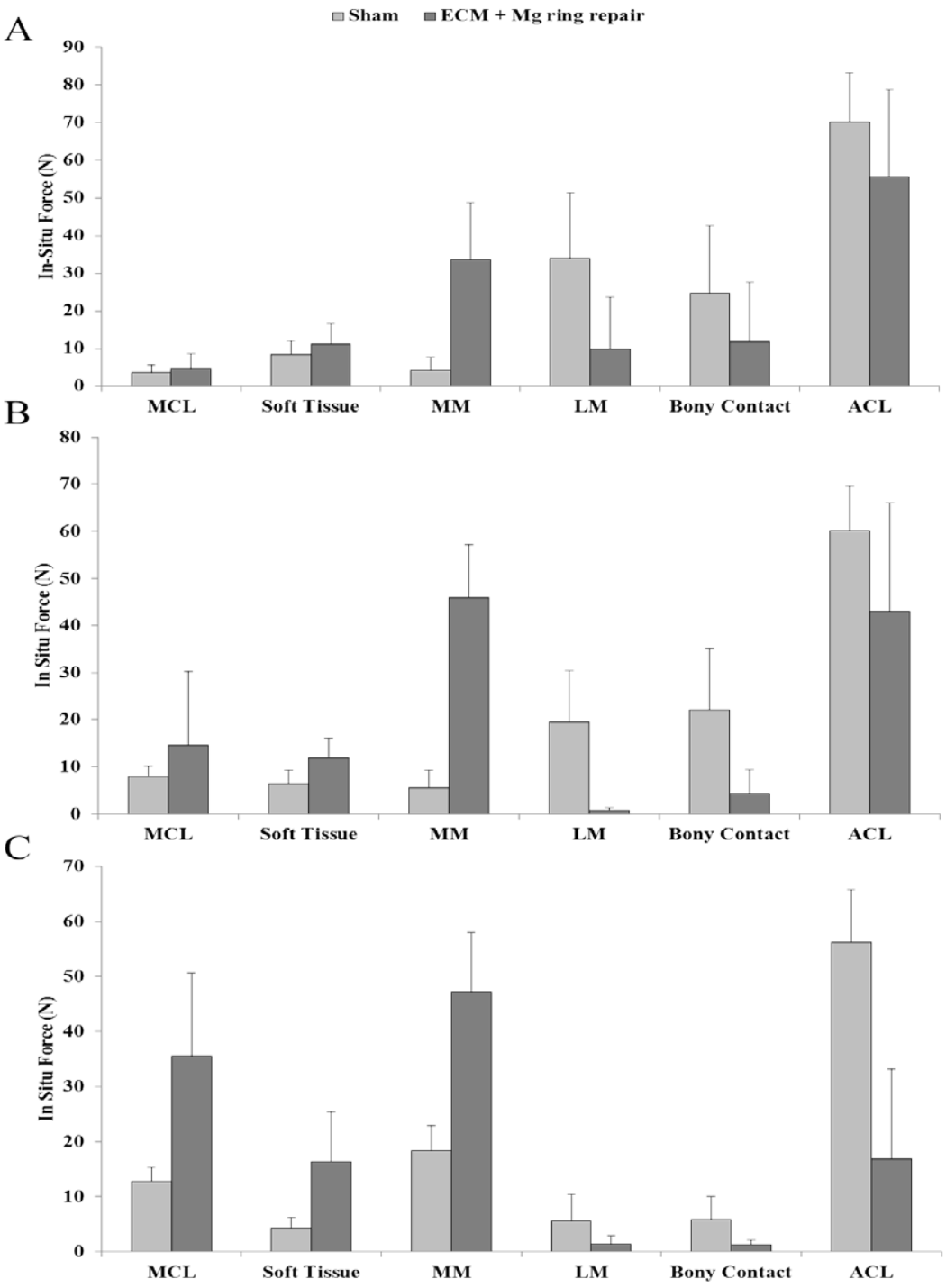

Figure 45: In-situ forces in the MCL, soft tissue, medial meniscus, lateral meniscus, bony contact, and ACL in the sham-operated and ECM + Mg ring repaired goat stifle joints at 30° (A), 60° (B), and 90° (C) of joint flexion

5.3.6 Tensile Properties

The load-elongation curve for the sham-operated and ECM + Mg ring repaired FATCs were obtained from the uniaxial tensile testing and were characterized by the toe region followed by a linear region prior to failure. The structural properties of the FATC are shown in Table 10. The stiffness values of the ECM + Mg ring repaired FATCs ranged between 30 and 129 N/mm with an average stiffness of about 50% of that of the sham-operated group. The average ultimate load was about 30% of the sham-operated group. The maximum ultimate load obtained was 981 N which is 75 % of the average ultimate load of the sham-operated group. The average ultimate elongation in the ECM + Mg ring repaired group was about 60% of the sham-operated group.

Table 10: Structural properties of the sham-operated and ECM + Mg ring repaired joints

	Sham	ECM + Mg ring repaired
Stiffness (N/mm)	124 ± 19	64 ± 33
Ultimate Load (N)	1309 ± 164	390 ± 265
Ultimate Elongation (mm)	12.6 ± 2.0	7.6 ± 2.6

After loading the FATCs to failure, the failure mode was noted. The ECM + Mg ring repaired FATCs failed in the ligament midsubstance in 6 out of 10 specimen whereas the others failed at the insertion sites. Figure 46 illustrates the midsubstance failure of the healing ACL.

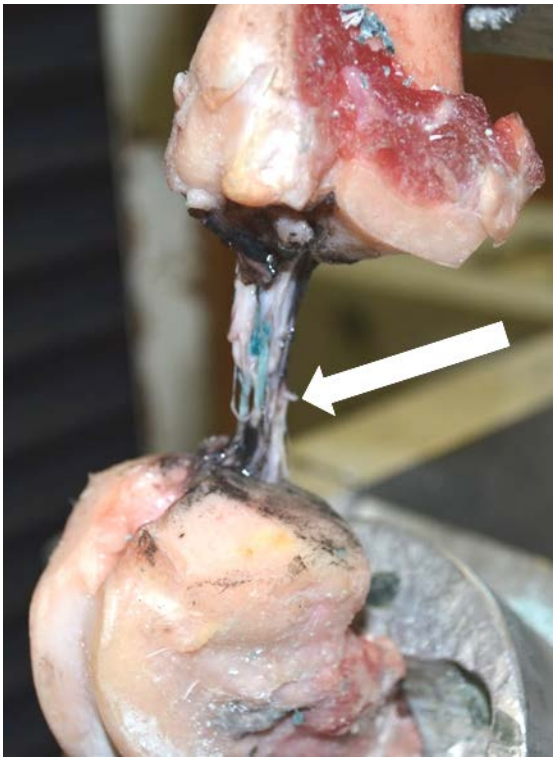

Figure 46: Failure mode of 60% of the specimen was at the midsubstance of the healing ACL

5.3.7 Time Course Comparison of ECM + Mg Ring Repair

To further highlight the advantages of ECM + Mg ring repair, the gross morphology, joint kinematics, in-situ forces in the healing ACL, and tensile properties were compared at time-zero and after 12 and 26 weeks of healing. Figure 47 shows the gross morphology of Mg ring repair at time-zero and ECM + Mg ring repaired ACLs after 6, 12, and 26 weeks of healing. At time-zero, the transected end of the ACL are held together by the Mg ring and sutures. After 6 weeks of healing, the Mg ring started to degrade and had fractured. Neo tissue was observed and there was a very small gap (~1 mm) between the transected ends [264]. At 12 weeks of healing, complete resorption of the Mg ring was observed in most specimen and there was continuous

tissue with no evidence of the initial transection. Similar results were observed at 26 weeks of healing. It is important to note that the healing results varied after 12 and 26 weeks of healing.

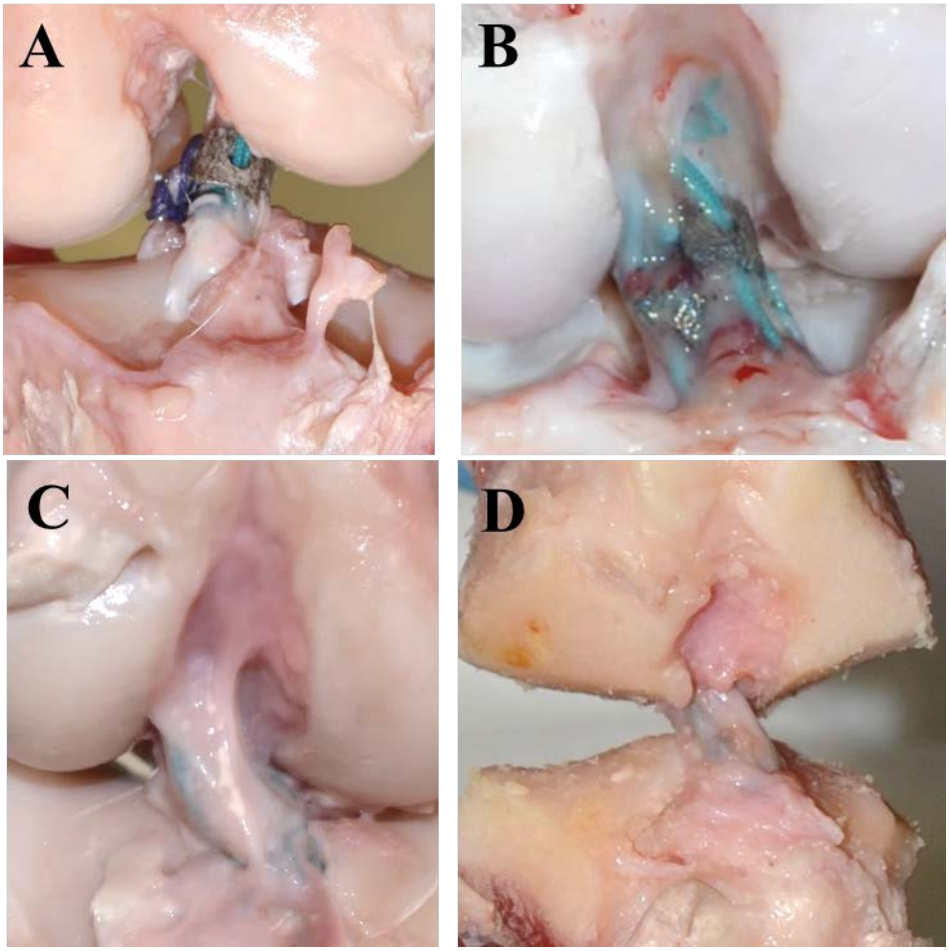

Figure 47: Gross morphology of ECM + Mg ring repair at time- zero (A) and after 6 weeks (B), 12 weeks (C) and 26 weeks of healing (D)

To compare the quantitative values of various studies, values were normalized by the sham-operated control values (experimental/control or e/c) in order to reduce interspecimen variability. Figure 48 illustrates the normalized APTT of ECM + Mg ring repair at time-zero and after 12 and 26 weeks of healing. At time-zero, the normalized APTT was about 1.5 at all

flexion angles. The APTT ranged between 2 and 3 times that of the sham-operated control after 12 weeks of healing and a similar trend was maintained up to 26 weeks of healing.

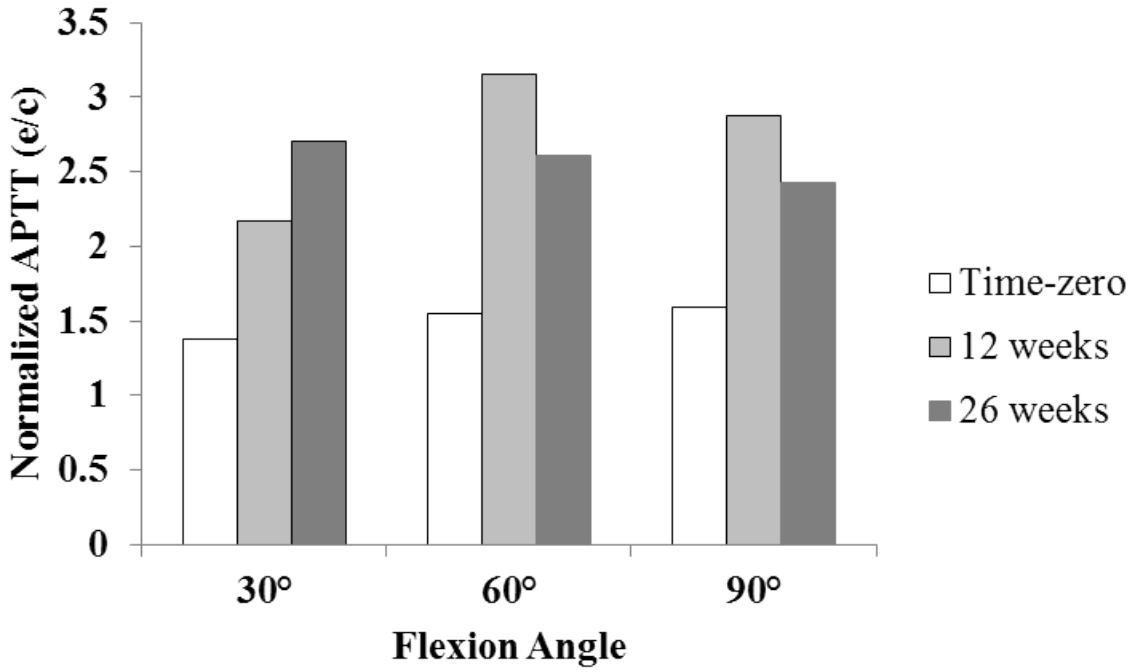

Figure 48: Normalized APTT (e/c) of ECM + Mg ring repair at time-zero and after 12 and 26 weeks of healing at 30°, 60°, and 90° of joint flexion

Figure 49 illustrates the normalized in-situ force of ECM + Mg ring repair at time-zero and after 12 and 26 weeks of healing. At 30° of flexion, the in-situ force of the ACL was near that of the sham-operated control at time-zero and after 12 and 26 weeks of healing. The normalized in-situ force of approximately 1 was maintained at 60° and 90° of joint flexion at time-zero. Contrarily, the normalized in-situ force decreased from 30° to 60° of flexion, and further decreased from 60° to 90° of joint flexion for ECM + Mg ring repaired ACLs after both 12 and 26 weeks of healing.

Figure 50 illustrates the normalized structural properties. At time-zero, both the stiffness and ultimate load were about 20% of the intact joint. After 12 weeks of healing the normalized stiffness was 0.6 and the normalized ultimate load was 0.4. These values were maintained up to 26 weeks of healing.

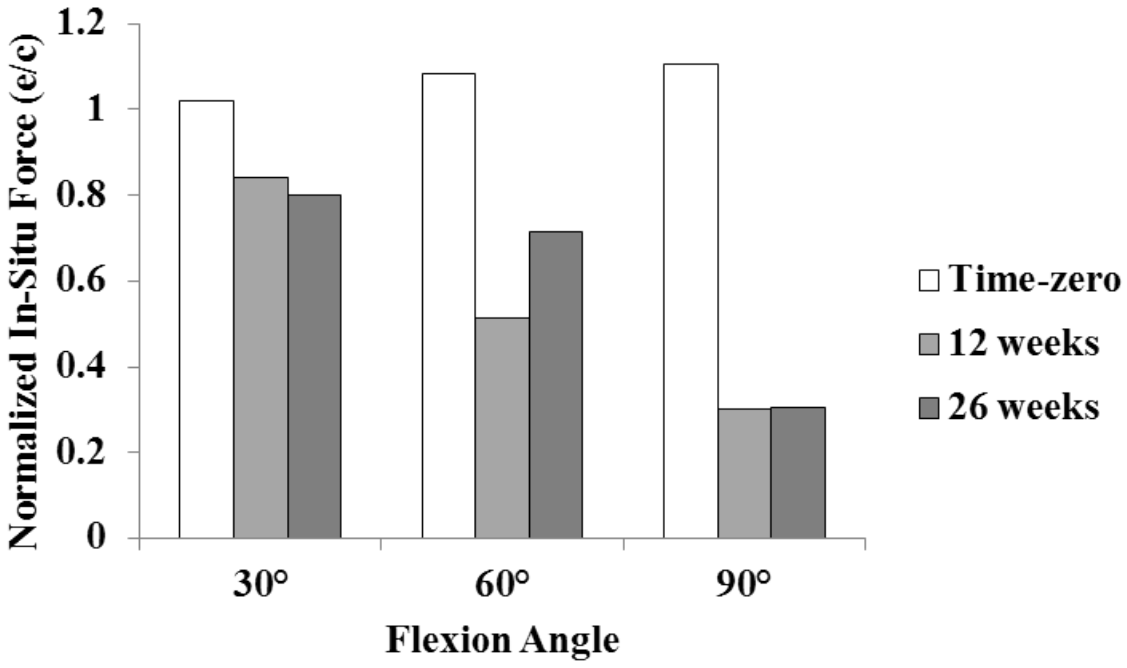

Figure 49: Normalized in-situ force (e/c) of ECM + Mg ring repair at time-zero and after 12 and 26 weeks of healing at 30°, 60°, and 90° of joint flexion

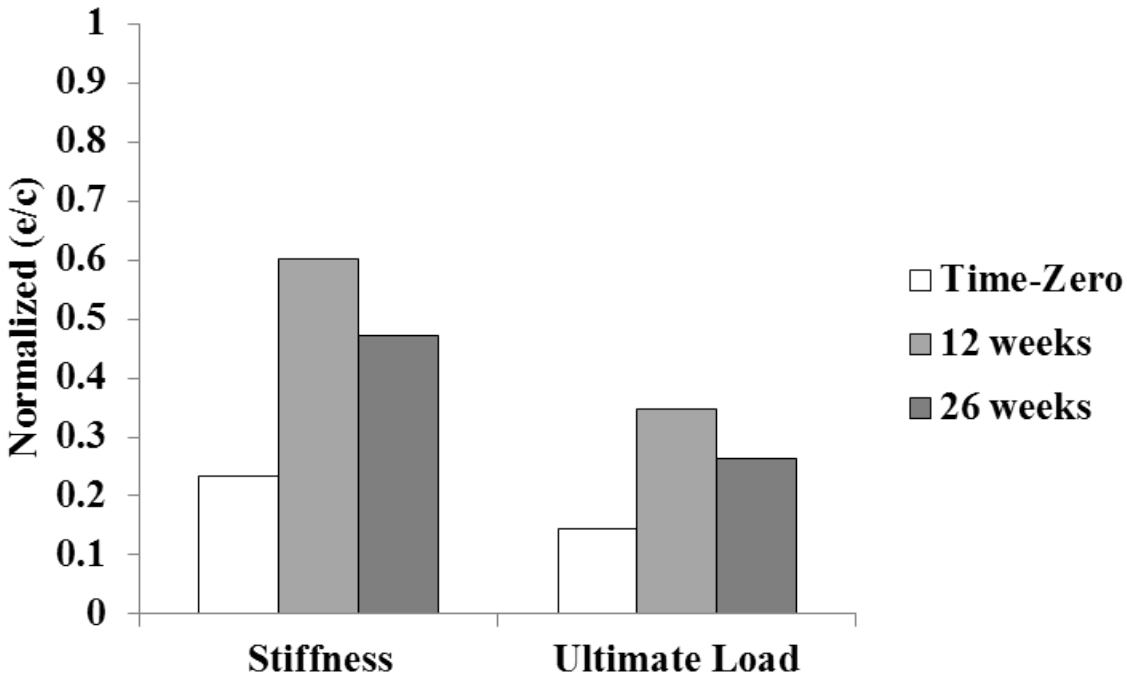

Figure 50: Normalized stiffness and ultimate load (e/c) of ECM + Mg ring repair at time-zero and after 12 and 26 weeks of healing

5.3.8 Comparison to Previous ACL Studies

To further assess the advantages of ECM + Mg ring repair, the time course of the tensile properties were compared to that of ACLR in the rabbit [265], canine [266], and goat [187] models as well as ACL healing by ECM only treatment in the goat model [19]. Table 11 is a compilation of the stiffness of experimental and control joints in the aforementioned animal models up to 1 year post-operatively. The normalized stiffness of the reconstructed ACL in the rabbit model was 15% at time-zero, 11% at 6 weeks, 24% at 26 weeks, and 13% at 52 weeks. ACLR in the canine model resulted in a normalized stiffness that reached 22% after 1 year. In the goat model, the normalized stiffness of the reconstructed ACL was 12% at time-zero, 13% at 6 weeks, 12% at 12 weeks, and increased to 21% by 26 weeks and 35% by 52 weeks. ECM only

treatment in the goat model resulted in a normalized stiffness of 47% at 12 weeks and 63% at 26 weeks. Similarly, the normalized stiffness of ECM + Mg ring repaired ACL was 24% at time-zero and increased to 46% by 12 weeks and was maintained to 51% at 26 weeks of healing. These results show that the healing approaches reached stiffness values closer to the sham-operated control faster than ACLR.

Table 12 is a compilation of the ultimate load of experimental and control joints in the aforementioned animal models up to 1 year post-operatively. The normalized ultimate load of the reconstructed ACL in the rabbit model was 7% at time-zero, 7% at 6 weeks, 15% at 26 weeks, and 11% at 52 weeks. ACLR in the canine model resulted in a normalized ultimate load that reached 16% after 1 year. In the goat model, the normalized ultimate load of the reconstructed ACL was 11% at time-zero, 17% at 6 weeks, 17% at 12 weeks, 17% by 26 weeks and increased to 31% by 52 weeks. ECM only treatment in the goat model resulted in a normalized ultimate load of 15% at 12 weeks and 15% at 26 weeks. Finally, the normalized ultimate load of ECM + Mg ring repaired ACL was 15% at time-zero and increased to 25% by 12 weeks and was maintained to 30% at 26 weeks of healing. These results show that the ECM + Mg ring repair approach reached ultimate load values closer to the sham-operated control faster than the others.

Lastly, the normalized tensile properties for ACLR and ECM + Mg ring repair in a goat model after 26 weeks of healing are shown in Figure 51. The normalized stiffness of the ECM + Mg ring repaired ACL was approximately 10% greater than that of the reconstructed ACL in the same animal model. An even greater difference was seen from the normalized ultimate load with the ECM + Mg ring repaired ACL more than twice that of the reconstructed ACL. These trends

are especially interesting as they show that ECM + Mg ring repair is able to reach values better than ACLR which is the gold standard for treatment of ACL injuries.

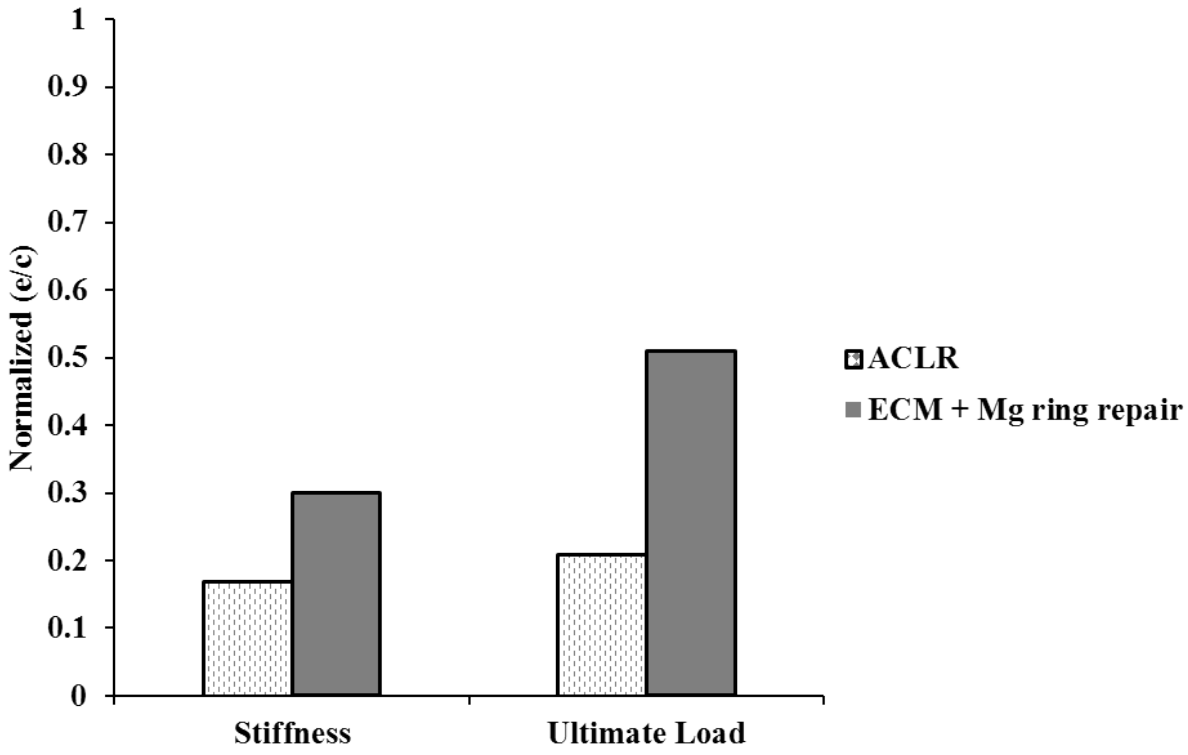

Figure 51: Normalized stiffness and ultimate load of ACLR and ECM + Mg ring repair after 26 weeks of healing in a goat model

Table 11: Stiffness of reconstructed or repaired ACLs in various animal models up to 1 year post-operatively

		Post-Operative Timing (Weeks)				
		0	6	12	26/30	52
ACL – Rabbit [265]	e					
	c					
	e/c	15%	11%		24%	13%
ACLR – Canine [266]	e					45 ± 19
	c					202 ± 41
	e/c					22%
ACLR – Goat [187]	e	36 ± 15	39 ± 18	37 ± 22	66 ± 24	108 ± 51
	c	306 ± 67	306 ± 67	306 ± 67	306 ± 67	306 ± 67
	e/c	12%	13%	12%	21%	35%
ECM Treatment – Goat [19]	e			53 ± 19	71 ± 9	
	c			112 ± 21	112 ± 2	
	e/c			47%	63%	
ECM + Mg ring repair – Goat [264]	e	22 ± 5		59 ± 38	64 ± 33	
	c	92 ± 27		127 ± 21	124 ± 19	
	e/c	24%		46%	51%	

Table 12: Ultimate Load of reconstructed or repaired ACLs in various animal models up to 1 year post-operatively

		Post-Operative Timing (Weeks)				
		0	6	12	26/30	52
ACL – Rabbit [265]	e	26 ± 5	22 ± 4		63 ± 19	51 ± 6
	c					
	e/c	7%	7%		15%	11%
ACLR – Canine [266]	e					304 ± 223
	c					1867 ± 324
	e/c					16%
ACLR – Goat [187]	e	165 ± 68	268 ± 77	269 ± 176	260 ± 71	486 ± 236
	c	1547 ± 464	1547 ± 464	1547 ± 464	1547 ± 464	1547 ± 464
	e/c	11%	17%	17%	17%	31%
ECM Treatment – Goat [19]	e			249 ± 129	266 ± 28	
	c			1624 ± 235	1820 ± 290	
	e/c			15%	15%	
ECM + Mg ring repair – Goat [264]	e	166 ± 41		287 ± 227	390 ± 265	
	c	1144 ± 282		1137 ± 320	1309 ± 164	
	e/c	15%		25%	30%	

5.4 DISCUSSION

With a Mg ring implant having acceptable corrosion properties for ACL healing, ECM + Mg ring repair of a transected ACL was performed in a goat model and assessed after 26 weeks of healing. The overall goal of the *in vivo* study was to determine if the success of the previous *in vivo* study would persist for 26 weeks. The healed ACL was assessed by observing the gross morphology, joint stability, ligament function and structural properties.

After implantation of the Mg ring *in vivo,* the goats recovered very well which could be attributed to minimal incision through which to perform the surgery. This increased the difficulty of the surgical procedure. However, there were limited adverse events after surgery. The goats were actually walking and running with no evidence of a pain or limping by 12 weeks. Therefore, the lameness scores could not be used as an indicator of the quality of the healing. In order to gauge the progress of the healing throughout the study, the orthopaedic surgery resident performed anterior drawer tests at 4 months, 5 months, and 6 months post operatively. Over the course of those three months, the anterior drawer scores seemed to get worse, moving from near normal to abnormal. This was not evident of poor healing. However, it may suggest that the repair construct remains strong at the earlier time points. By the end point, there may have been suture elongation as well as elongation of the healing ligament. The use of x-rays to visualize the Mg ring implant was also employed. It was very difficult to visualize if the implant was present. But, the x-rays provided confidence that the Mg ring implant has been mostly resorbed which had been shown to be beneficial for allowing the ligament to heal.

Prior to dissection, analysis of the synovial fluid suggested there was no evidence of inflammation. The total protein content and cytology of the synovial fluid was near normal and improved compared to previous 12 week of healing studies [264]. In terms of gross morphology, there was continuous new tissue formation after 26 weeks of healing in all samples. The cross sectional area of the healed ACL was slightly hypertrophic. Noticeably, there was variation between specimen. The results varied between having robust tissue to being mostly the lingering fixation sutures with translucent tissue. Nonetheless, ECM + Mg ring repair successfully healed the transected ACL. This was confirmed by the histological evaluation where the transected ends of the ACL were not detectable. Additionally, Herovici staining was used as an indicator of the maturity of the collagen. The results showed that the entire length of the ACL appeared to have immature collagen. Thus was unexpected as it was thought that the ACL stumps would appear to have mature collagen with a gradient to immature collagen at the transection site. It is thought that the tissue that underwent Herovici staining was from the fibrous connective tissue that formed around the ACL as opposed to the midsubstance of healing ACL. Thus, future histology of ECM + Mg ring repair should employ Herovici staining of the appropriate region of interest observe the maturity of the healing tissue. Observing how the quantity of immature and/or mature collagen changes over time would be interesting as well.

After completion of testing using the robotic/UFS testing system, the APTT for the ECM + Mg ring repair group was 37% of that of the sham-operated group. This was comparable to ECM + Mg ring repair at 12 weeks of healing. Similarly, there were no significant difference between the normalized in-situ force of the repaired ACL between ECM + Mg ring repair healing at 12 weeks and ECM + Mg ring repair at 26 weeks. However, it was noticeable that the in-situ force decreased significantly at 90° of joint flexion. There are several possible reasons for

the low in-situ force including that the joint functions best at full extension because the repair construct is fixed at full extension. Also, the animals do not undergo any rehabilitation protocol and the surrounding structures compensate for the function of the healing ACL.

The structural properties obtained for ECM + Mg ring repair at 12 weeks and 26 weeks had a similar trend. The normalized ultimate load of the ECM + Mg ring repaired ACL after 12 weeks was slightly larger than at 26 weeks. However, it is important to consider the difference of the ultimate load of the sham-operated control. The results suggest that the biomechanical evaluation of ECM + Mg ring repair is comparable at 12 weeks and 26 weeks of healing. These findings confirm the hypothesis that the advantages seen at 12 week if healing would persist to 12 weeks of healing. Additionally, the failure modes observed from the majority of ECM + Mg ring repaired ACLs was at the midsubstance, both at 12 weeks and 26 weeks. Thus, ECM + Mg ring repair can successfully prevent disuse atrophy at the insertion sites.

The comparisons of ECM + Mg ring repair to previous ACL studies further highlight the success of the combined approach. The structural properties of the reconstructed ACL's seemed to remain constant and increase after 6 months or even up to a year. ECM + Mg ring repair had normalized structural properties better than ACLR which is the gold standard for treatment of ACL injuries.

ECM + Mg ring repair has been successful because of the combined biological and mechanical augmentation strategy that attempts to address the challenges of healing the ACL and capture the advantages of ligaments that have the innate healing capabilities. The biological augmentation provided by the ECM sheet and bioscaffold is effective because they provide an early scaffold for tissue healing, the constructive remodeling of the ECM incite tissue growth and the degradation products of the ECM are bioactive as well [253]. Additionally, the ECM

sheet provides a temporary synovium that protect the healing tissue. Since the ECM degrades very quickly in vivo, perhaps multiple sheets of ECM would provide a protective barrier longer. Future studies of ECM + Mg ring repair could also employ the use of matrix-bound nanovesicles [267, 268]. Matrix bound nanovesicles carry proteins and RNA to the region of interest and have been shown to regulate the macrophasge phenotype and other cellular responses.

In addition to the biological augmentation, mechanical augmentation is required to support ACL healing. Indeed, the Mg ring is an integral part of the repair construct. Since there are no bone-to-bone augmentation sutures, the Mg ring helps maintain the stability of the repair construct; thus, the mechanical stabilization of the joint at the earlier time points. As the sutures begin to elongate and the Mg ring degrades, the corrosion products from the Mg ring implant may also be bioactive for soft tissue healing. The success of ECM + Mg ring repair is highly dependent on the transition of the loading from the repair construct to the healing tissue at an appropriate timing where the loading is not pulling weak tissue apart but strengthening healing tissue that can endure the loading.

By protecting the healing tissue, providing bioactive stimulants from the ECM bioscaffolds and the Mg implant as well as allowing for helpful loading of the ligament, there are some similarities to the healing of the MCL. While it is hoped, that the strength of the healing ACL would improve with time, it seemed to remain similar to that from short-term studies which is also seen with MCL healing. As the MCL heals, there is hypotrophy to accommodate for the less quality healing tissue. Additionally, the MCL has intrinsic healing ability, but doesn't appear to return to the preinjury strength. Perhaps, that is what is being observed with ACL healing from 12 weeks of healing to 26 weeks of healing.

Specific Aim 2 demonstrated the ACL healing capacity of ECM + Mg ring repair and that it can persist to 26 week of healing. The healing tissue is characterized by continuous neo-tissue and the transection site is no longer visible. The biomechanical outcomes were better than ACLR and similar to the short term ECM + Mg ring repair study.

6.0 DEVELOPMENT FOR USE IN HUMANS

6.1 INTRODUCTION

The use of ECM + Mg ring repair has been shown to successfully heal a transected ACL in a goat model. With these promising results, translation of this healing approach could be designed for the human ACL. Previously, the Mg ring had been designed considering the geometry of the goat ACL. Next, a similar design can be made for the human ACL. Considering the geometry of the human ACL, the Mg ring implant was scaled up and evaluated in a preliminary *in vitro* study of Mg ring repair in cadaveric human knee joints. Also, a finite element model was developed of the Mg ring implanted in the human knee which can be used as a vehicle for future design and development of the Mg ring for the human ACL.

6.2 DESIGN OF MG RING DEVICE FOR HUMAN ACL

The geometry of the human ACL has been studied for many years (Figure 52). The ACL is characterized as a fan shaped structure with cross section areas and lengths that widely vary based on gender and other anatomical factors. The cross sectional area of human ACL can vary between 25 and 60 mm^2. Additionally, the length of the ACL can range between 20 mm and 20 mm. Initially, the strategy for designing a Mg ring implant for the human ACL was to scale up

the design parameter according to the differences from the goat ACL and the human ACL as highlighted in Table 13.

Figure 52: Human ACL

Table 13: Relationship between goat ACL and human ACL to scale up Mg ring implant

Design Parameter	Dimensions for Goat Implant	Human ACL relation to Goat ACL	Dimensions for Human Implant
Height	5 mm	Length: 4X greater	15-20 mm
Circumference	22 mm (F) 25 mm (T)	Diameter: ~Equivalent	25-30 mm
Thickness	0.5 mm	In Situ Force: 2X greater	1 mm

After considering the large range of the dimensions for the human ACL, it was not possible to create on device for ACLs of all sizes. Thus, the ring was redesigned in 3 sizes: small, medium, and large (Figure 53 and Table 14). The design features of the original Mg ring implant were maintained including the cylindrical shape with a larger tibial diameter, holes through which sutures can pass and notches for stabilizing sutures. The 3 designs vary by the

femoral and tibial diameters where the smaller design may be most appropriate for children and more petite women and the larger design for men.

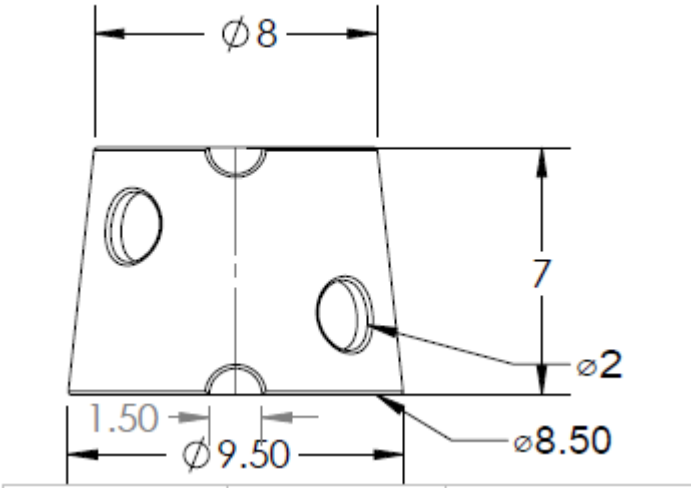

Figure 53: Mg Ring Design for Human ACL

Table 14: Dimensions for the Mg ring implants designed for Human ACL

Mg Ring Implant for Human ACL	Dimensions		
	Femoral Diameter (mm)	Tibial Diameter (mm)	Height (mm)
Small	8	9.5	7
Medium	8.75	10.25	7
Large	9.25	10.75	7

6.3 *IN VITRO* EVALUATION OF MG RING REPAIR FOR HUMAN ACL

6.3.1 Experimental Design

As a second evaluative method of the Mg ring implant for use in humans, a preliminary *in vitro* study was conducted in cadaveric human knees (N=2). The Mg ring implant was implanted after the same surgery approach from Section 5.2.4. Then, the robotic/UFS system was used to evaluated the Mg ring repair ability to restore joint stability and ligament function. Afterwards, these values were compared to the success of Mg ring repair in the goat model as well as ACL reconstruction, the current gold standard treatment for ACL injuries.

6.3.2 Robotic Testing

The cadaveric knee joint was thawed at room temperature the day before testing. Then, it was prepared for testing as previously described with the epoxy putty (Everglass, Evercoat, Cincinnati, OH). Then, the specimen was mounted onto the robotic/UFS testing system (Figure 6). The path of passive flexion-extension was determined by flexing the joint at 1° increments, finding the position that minimizes the resulting forces and moments. This path provided the starting position at each angle of flexion for the application of external loads for the remainder of the test and served as the reference position by which to measure knee kinematics. The knee joint was subjected to a (1) 134 N anterior tibial load (2) 134 N anterior tibial load with a 200 N compression and (3) 10 NM valgus and 5 NM internal tibial torque (force control). The resulting kinematics including anterior tibial translation (ATT) of the knee joint was measured at 30°, 60°, and 90° of joint flexion. Next, the ACL was transected through its midsubstance using a medial

parapatellar incision. The previously recorded kinematics of the joint with an intact ACL were repeated, while the UFS recorded new forces and moments. The in situ forces of the intact ACL were determined in response to the loading condition using the principle of superposition.

Then, Mg ring repair of the ACL was performed as described in Section 5.2.4. Once complete, the kinematics of the repaired joint were obtained using the loading condition. Finally, the ring was removed and the previously recorded kinematics were repeated to obtain in situ forces in the Mg ring repaired ACL. The protocol is detailed in Table 15.

Table 15: Robotic Protocol for Mg ring repair in Human Knee Joint

		Data Acquired	
Knee State	**Load/Kinematics Applied**	**Kinematics**	**In-Situ Force**
1. Intact	Path of passive flexion/extension Applied Loads (15°, 30°, 60°, 90°) 1. 134 N Anterior Tibial Load (ATL) 2. 134 N ATL + 200 N Compression 3. 10 Nm valgus + 5 Nm internal tibial torque	Intact ACL (A)	
2. ACL Deficient	Repeat Intact Kinematics (A) Applied Loads 1, 2, 3	ACL Deficient	Intact ACL
3. Mg Ring Repaired	Applied Loads 1, 2, 3	Mg Ring Repaired (B)	
4. ACL Deficient (remove implant)	Repeat Mg Ring Repaired Kinematics (B)		Mg Ring Repaired ACL

6.3.3 Data Analysis

For the *in vitro* analysis on the cadaveric human knees, APTT and in situ forces in the ACL were averaged between specimen. Two-way ANOVA was used to compare the values of APTT or in situ forces in response to the loading condition with the independent factors being joint state

(intact, ACL-deficient, or Mg ring repaired) and flexion angle (30°, 60°, 90°). Statistical significance will be defined as $p<0.05$.

6.3.4 Results

The ATT of the intact ACL increased between 15° and 60° and decreased at 90° (Figure 54A). The ATT of the knee with an intact ACL ranged between 4 mm at 15° to 10 mm at 60° of flexion. After transection of the ACL, the ATT increase as much as 300% and ranged between 12.6 to 24.3 mm. After Mg ring repair, the ATT was restored within 4 mm of the intact state (Figure 54 B). The kinematic data of the intact, ACL-deficient, and Mg ring repaired knee joint under 134 N anterior tibial load and 134 N anterior tibial load with 200 compression is shown in Table 17.

With the addition of 200 N axial compression to the 134 N anterior tibial load, the anterior tibial translation of the intact knee decreased at all flexion angles (Table 16). For the ACL-deficient joint, these values also decreased at 15° and 30° and remained relatively the same at 60° and 90°. After Mg ring repair, the anterior tibial translation was reduced to within 3.5 mm of the intact knee.

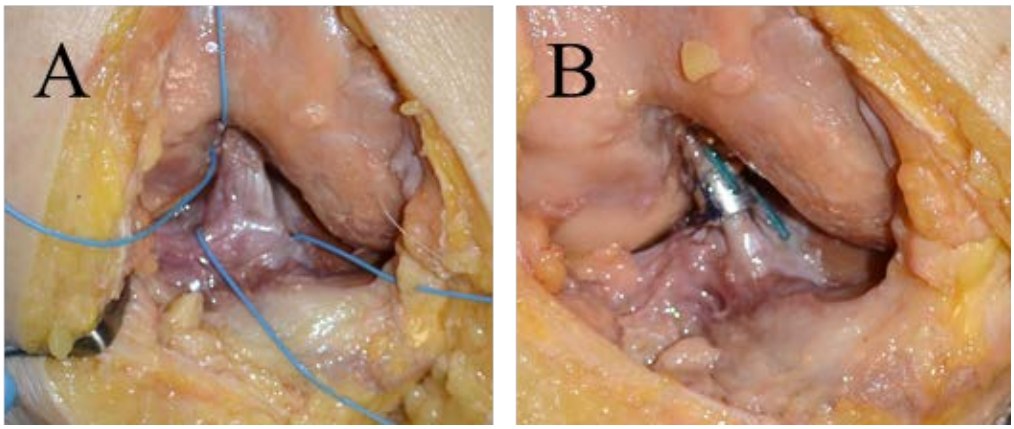

Figure 54: The intact human ACL (A) and the Mg ring repaired human ACL (B)

Table 16: Anterior tibial translation of the intact, ACL-deficient and Mg ring repaired knee joint in response to a 134 N anterior tibial load and a 134 N anterior tibial load combined with a 200 N axial compression

	Flexion Angle			
Translation, mm	15°	30°	60°	90°
134-N anterior tibial load				
Intact	4.3 ± 0.5	6.8 ± 1.2	7.8 ± 3.1	6.3 ± 1.7
ACL deficient	13.3 ± 0.9	19.3 ± 1.6	19.4 ± 6.9	14.7 ± 2.5
Mg ring repaired	8.0 ± 1.4	10.3 ± 0.5	11.6 ± 4.0	5.7 ± 2.3
134-N anterior tibial load + 200-N axial compression				
Intact	4.0 ± 0.3	4.3 ± 0.13	5.0 ± 2.4	5.1 ± 2.8
ACL deficient	7.9 ± 3.1	11.8 ± 3.1	19.7 ± 10.6	13.3 ± 5.8
Mg ring repaired	5.5 ± 1.4	6.4 ± 2.3	8.5 ± 5.3	8.0 ± 4.6

The magnitude of the in-situ force of the intact ACL decreased from 15° to 90°, ranging from 85 N to 170 N under 134 N anterior tibial load (Table 17). A similar trend was seen with the Mg ring repaired ACL, decreasing with an increase in flexion angle of the joint. With the addition of 200 N axial compression, the in situ force of the both the intact and Mg ring repaired ACL increased across all angles of joint flexion.

Table 17: In-situ force of intact ACL and Mg ring repaired ACL in response to a 134 N anterior tibial load and a 134 N anterior tibial load combined with 200 N axial compression

	Flexion Angle			
In-Situ Force, N	15°	30°	60°	90°
134-N anterior tibial load				
Intact	153 ± 26	116 ± 13	97 ± 4	94 ± 12
Mg ring repaired	107 ± 6	98 ± 10	77 ± 22	73 ± 33
134-N anterior tibial load + 200-N axial compression				
Intact	165 ± 20	132 ± 10	103 ± 10	77 ± 11
Mg ring repaired	117 ± 18	114 ± 2	123 ± 8	110 ± 8

Under the combined rotatory load, anterior tibial translation decreased (became more negative indicating a posterior direction) from 15° to 30° of knee flexion with all knee conditions (Table 198. After transection of the ACL, the anterior tibial translation increased by up to 2 mm compared to intact knee. After Mg ring repair, anterior tibial translation was within 1 mm of the intact joint at both 15° and 30°. The tibial rotation also increased from 15° to 30° of knee flexion (Table 18). After Mg ring repair, the tibial rotation was within 2 mm of the intact knee. The magnitude of the in-situ force in the ACL under the combined rotatory load decreased from 15° to 30° of knee flexion. This was also seen with the Mg ring repaired ACL (Figure 55).

Table 18: Knee Kinematics of the Intact and Mg ring repaired knee joint in response to a combined 10 Nm valgus tibial torque and 5 Nm internal tibial torque

	ACL-Intact Knee	ACL-Deficient Knee	Mg ring repaired Knee
Anterior tibial translation,mm			
15 of flexion	-0.5 ± 0.8	0.8 ± 3.7	-1.4
30 of flexion	-1.0 ± 0.4	0.8 ± 3.2	-2.2
Internal tibial rotation, deg			
15 of flexion	6.3 ± 1.0	3.1 ± 2.8	5
30 of flexion	7.0 ± 2.2	2.0 ± 2.9	5.3

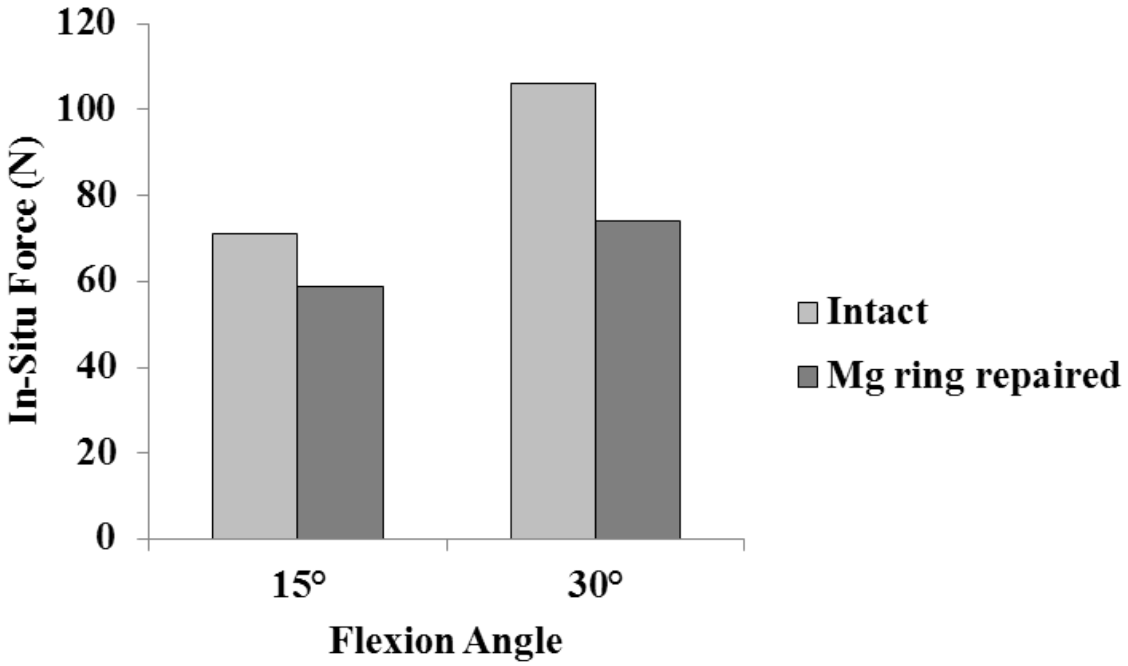

Figure 55: Average in-situ force of the intact and Mg ring repaired ACL at 15 and 30 of knee flexion in response to a combined 10 Nm valgus and 5 Nm internal tibial torque

In order to evaluate the Mg ring repair of the ACL in the human knee, the joint kinematics and in-situ force of the ligament were normalized and compared with previous in vitro studies conducted in the goat model and ACLR in human cadaveric knee joints (Figure 56) [21, 84]. The normalized ATT of Mg ring repair in the goat model increase from 30° to 90° and ranged from 2 to 2.5. The Mg ring repair in the human knee remained constant across all angles of knee flexion at approximately 1.5. The normalized ATT of the reconstructed ACL using QT in human knee ranged from 0.8 to 1.0 and also increased from 30° to 90°.

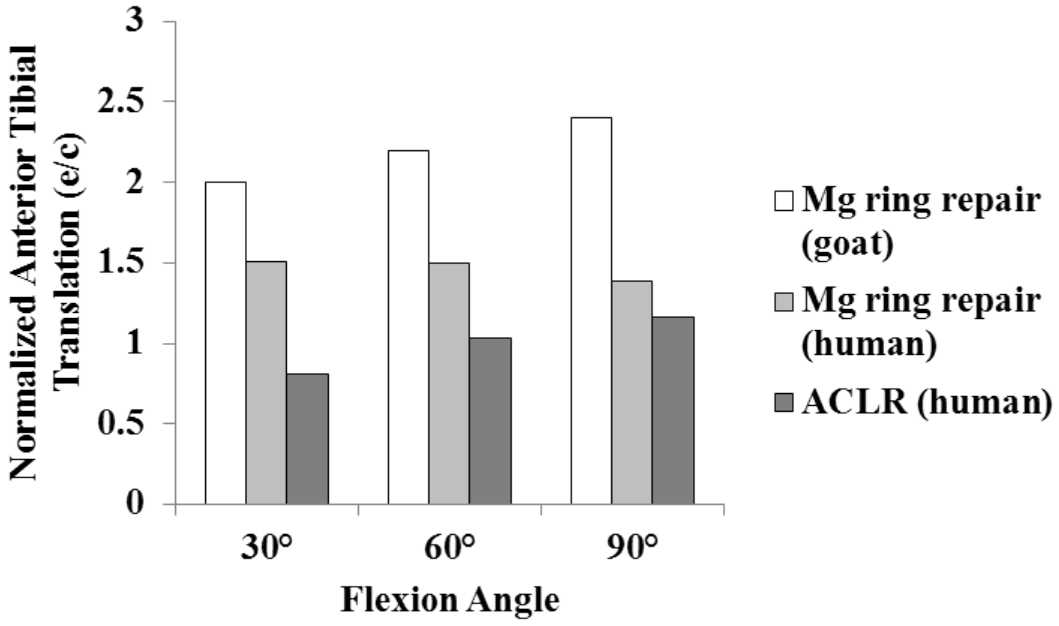

Figure 56: Normalized anterior tibial translation in response to 134 N anterior tibial load

The normalized in-situ force of the Mg ring repaired ACL in the goat model increased from 30° to 90° of knee flexion ranging from 1.0 to 1.2 (Figure 57). For Mg ring repair in the human knee, the normalized in-situ force of the repaired ACL remained constant across all angles of knee flexion at approximately 0.8. These values were closer to the in-situ force of intact ACL than the ACL reconstructed with QT having normalized values that increased from 30° to 90° of knee flexion ranging from 0.6 to 0.8.

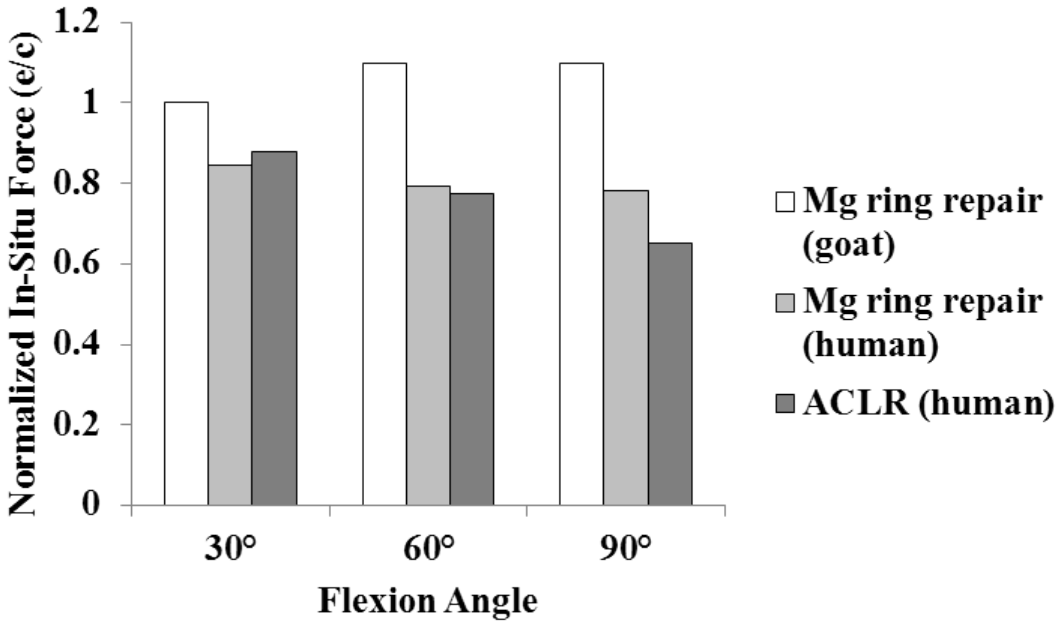

Figure 57: Normalized in-situ force in response to 134 N anterior tibial load

6.4 FINITE ELEMENT ANALYSIS

6.4.1 Model Development

With the design of the Mg ring implant for the human ACL, finite element analysis (FEA) was employed to assess the potential of the implant for ACL healing application. The FE model could be used to confirm that the implant could bridge the gap between the two end of the ACL and the repair construct which includes the sutures can load the ACL.

The FE model used for these simulations was adopted from the OpenKnee project (SimTK.org). This project is a model of the human knee including bones (femur and tibia), menisci, and major ligaments (ACL, PCL, LCL, MCL) in addition to layers of articular cartilage. With the femur fixed and motion limited in all directions, a 134 N force was applied to the tibia

in the anterior direction, boundary and loading conditions adopted from the robotic protocol. The resulting kinematics were recorded. Then, the model was modified to include the femur, tibia, transected ACL connected with the Mg ring by sutures (Figure 43). Then, the recorded kinematics were applied to the modified FE model. The resulting von Mises stress concentrations were recorded as an indication of the effectiveness of Mg ring repair in the human knee.

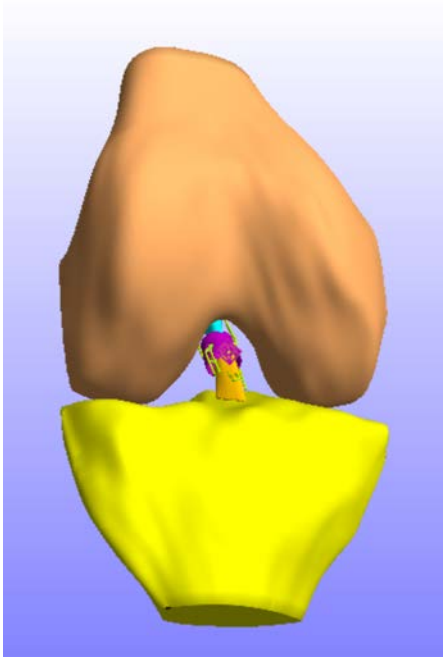

Figure 58: The finite element model of the Mg ring repaired human knee

6.4.2 Finite Element Analysis Results

The von Mises stresses were recorded in the FE model as a result on Mg ring repair. The majority of the stress was seen in the sutures. There was also evidence of stress on the ACL at the contact between the ACL and the sutures as well as in the anterior portion of the

midsubstance. Additionally, there was stress concentrated on the sutures holes of the Mg ring implant. None of the stress values exceeded the yield strength of the structures within the FE model. Future validation and use of the FE model can be used throughout the iterative design process of the Mg ring implant for use in humans.

6.5 DISCUSSION

With the potential of ECM + Mg ring repair, clinical translation of this healing approach is the next logical step. So, the Mg ring implant device was redesigned for the human ACL. After reviewing literature on the ACL geometry, it was not possible to make one Mg ring implant. Therefore, a small, medium, and large implant was designed.

As we moved forward with *in vitro* analysis of the Mg ring implant in human cadaver knees, we noticed the wide range of ACL sizes. Using the same sutures and surgical implantation as developed for the goat model, the Mg ring was implanted on human cadaver ACL. One of the strengths of the repair construct is the ability to restore joint stability at time zero. This was also demonstrated in the human knee joint even under the 134 N anterior tibial load. The ATT and in-situ force results were superior to ACLR construction studies of similar experimental design.

Finally, the development of a finite element model of the Mg ring implant in the human knee has confirmed the loading mechanism of the repair construct. Future validation of the finite element model would make it especially useful for future redesign of the Mg ring implant. Particularly, the actual design of the implant may need to deviate from the ring shape. If so, the finite element model could be used as an initial assessment tool.

7.0 OVERALL DISCUSSION AND CONCLUSIONS

In this dissertation, further research and development of the ECM + Mg ring repair method was pursued. First, the novel MAO coated single crystal Mg was characterized for corrosion, coating, and surface properties. This was accomplished through in vitro degradation testing and measurement of corrosion rate as determined by monitoring the Mg ion concentration, change in pH, and change in mass over 4 weeks. Additionally, the porosity, hardness, roughness, hydrophilicity of the coating were measured in order to make assumptions about cell interaction with the implant and to establish a benchmark for which further modifications can be based. Then, the MAO coated Mg ring implant, made with single crystal Mg, was used to repair a transected ACL in a goat model. The healing was assessed after 26 weeks of healing by observing the gross morphology and through extensive biomechanical evaluation to determine the joint stability, ligament function, and structural properties of the healed ACL. Lastly, with the exciting results, the Mg ring implant was designed for the human ACL. Maintaining the same design characteristics including suture holes and a larger tibial diameter, three Mg ring implants of varying size were designed to account for the wide variation of ACL geometry. Then, finite element analysis was used to model the implantation of the Mg ring implant in the human knee. Finally, the Mg ring implant underwent in vitro evaluation in cadaveric human knees using the robotic/UFS testing system as an initial step toward clinical translation of the ECM + Mg ring repair.

7.1 LIMITATIONS

There several limitations of this dissertation research. First, the corrosion scenario in real biomedical applications is always more complex than in laboratory experiments. For instance, the hydrodynamic condition around the implant surface influences mass transfer. Consequently, the local surface chemistry evolves with time and can be drastically different under static conditions. Thus, dynamic in vitro degradation testing may be more realistic. However, *in vitro* testing cannot be directly related to *in vivo* response.

Secondly, *in vivo* animal study provides great insight to the healing of the ACL. However, the sample size is smaller and there is no control group. With the challenges and expenses associated with large animal studies, we were limited to fewer animals. Additionally, an ACL reconstruction control group would be ideal as ACLR is the current standard of care.

Thirdly, the goat model cannot be extrapolated to human treatment. However, extensive ACL research has been conducted in the goat model. Thus, the trends between studies and the results of this research provide insight and inspiration for ACL healing. This research has high translational potential as ACL healing would be an advantageous alternative to ACLR.

Fourthly, the surgical implantation technique in the goat model as well as the preliminary study in the human cadaveric knee was an open surgery. The current standard for knee surgery is arthroscopy. Thus, the implantation technique is not directly translatable. However, the orthopaedic surgeons were able to make the goat surgeries as minimal invasive as possible and the goats recovered very well with no adverse effects due to surgical implantation.

7.2 CONCLUSIONS

7.2.1 Clinical Implications

ECM + Mg ring repair is a strategy for healing an injured ACL. ACL healing is an advantageous alternative treatment option to ACLR. Patients would experience better short and long term outcomes, as many of the complications associated with ACLR would be eliminated. Furthermore, this would benefit patients, as well s surgeons, hospitals, and insurance companies because of reduced time in the operating room as graft harvesting is not required and potentially comparable in cost to ACLR. The successful development of the ACL healing strategy has the potential to shift the paradigm of ACL treatment. Also, this approach could be extended to other "hard to heal" ligaments and tendons.

7.2.2 Scientific/Engineering Significance

The method of evaluating joint stability and ligament function using the robotic UFS testing system is state-of-the art. The precision provided and the repeatable results is especially valuable. The use of advanced protocol and accurate tools allows for efficient comparison of treatment options. Furthermore, development of the finite element model allows for early evaluation of implant design and implementation.

7.3 FUTURE DIRECTIONS

The overall goal of this dissertation research was to evaluate the ECM + Mg ring repair of a transected ACL and begin efforts toward clinical translation. In the future, other strategies can be evaluated against these results. Since ACL healing is such a complex process, a more multi-faceted approach to evaluating the healing is advisable (including histology, biomechanics, etc.). Finally, continuous modifications to the design and implantation technique are essential. To prepare this approach for human application, it must meet the current standard of care which is arthroscopy.

BIBLIOGRAPHY

1. Woo, S. and J. Wayne, *Mechanics of the anterior cruciate ligament and it contribution to knee kinematics.* 1990.

2. Woo, S.L., et al., *Use of robotic technology for diathrodial joint research.* Journal of Science and Medicine in Sport, 1999. **2**(4): p. 283-297.

3. Ali, N. and G. Rouhi, *Barriers to predicting the mechanisms and risk factors of non-contact anterior cruciate ligament injury.* The open biomedical engineering journal, 2010. **4**: p. 178.

4. Shimokochi, Y. and S.J. Shultz, *Mechanisms of noncontact anterior cruciate ligament injury.* Journal of athletic training, 2008. **43**(4): p. 396-408.

5. Beynnon, B.D., et al., *Treatment of anterior cruciate ligament injuries, part I.* The American journal of sports medicine, 2005. **33**(10): p. 1579-1602.

6. Neuman, P., et al., *Prevalence of Tibiofemoral Osteoarthritis 15 Years After Nonoperative Treatment of Anterior Cruciate Ligament Injury A Prospective Cohort Study.* The American journal of sports medicine, 2008. **36**(9): p. 1717-1725.

7. Zätterström, R., et al., *Early rehabilitation of acute anterior cruciate ligament injury—a randomized clinical trial.* Scandinavian journal of medicine & science in sports, 1998. **8**(3): p. 154-159.

8. Allen, C.R., et al., *Injury and reconstruction of the anterior cruciate ligament and knee osteoarthritis.* Osteoarthritis and Cartilage, 1999. **7**(1): p. 110-121.

9. Feagin JR, J.A. and W.W. Curl, *Isolated tear of the anterior cruciate ligament: 5-year follow-up study.* The American journal of sports medicine, 1976. **4**(3): p. 95-100.

10. Salmon, L.J., et al., *Long-term Outcome of Endoscopic Anterior Cruciate Ligament Reconstruction With Patellar Tendon Autograft Minimum 13-Year Review.* The American journal of sports medicine, 2006. **34**(5): p. 721-732.

11. Von Porat, A., E. Roos, and H. Roos, *High prevalence of osteoarthritis 14 years after an anterior cruciate ligament tear in male soccer players: a study of radiographic and patient relevant outcomes.* Annals of the rheumatic diseases, 2004. **63**(3): p. 269-273.

12. Kannus, P. and M. Järvinen, *Conservatively treated tears of the anterior cruciate ligament. Long-term results.* J Bone Joint Surg Am, 1987. **69**(7): p. 1007-1012.

13. Johnson, R.J., et al., *The treatment of injuries of the anterior cruciate ligament.* JBJS, 1992. **74**(1): p. 140-151.

14. Meunier, A., M. Odensten, and L. Good, *Long-term results after primary repair or non-surgical treatment of anterior cruciate ligament rupture: A randomized study with a 15-year follow-up.* Scandinavian journal of medicine & science in sports, 2007. **17**(3): p. 230-237.

15. Sandberg, R., et al., *Operative versus non-operative treatment of recent injuries to the ligaments of the knee. A prospective randomized study.* J Bone Joint Surg Am, 1987. **69**(8): p. 1120-1126.

16. Kanaya, A., et al., *Intra-articular injection of mesenchymal stromal cells in partially torn anterior cruciate ligaments in a rat model.* Arthroscopy: The Journal of Arthroscopic & Related Surgery, 2007. **23**(6): p. 610-617.

17. Kimura, Y., et al., *Regeneration of anterior cruciate ligament by biodegradable scaffold combined with local controlled release of basic fibroblast growth factor and collagen wrapping.* Tissue Engineering Part C: Methods, 2008. **14**(1): p. 47-57.

18. Joshi, S.M., et al., *Collagen-platelet composite enhances biomechanical and histologic healing of the porcine anterior cruciate ligament.* The American journal of sports medicine, 2009. **37**(12): p. 2401-2410.

19. Fisher, M.B., et al., *Potential of healing a transected anterior cruciate ligament with genetically modified extracellular matrix bioscaffolds in a goat model.* Knee Surgery, Sports Traumatology, Arthroscopy, 2012. **20**(7): p. 1357-1365.

20. Farraro, K.F., et al., *Revolutionizing orthopaedic biomaterials: The potential of biodegradable and bioresorbable magnesium-based materials for functional tissue engineering.* Journal of biomechanics, 2014. **47**(9): p. 1979-1986.

21. Farraro, K.F., et al., *Magnesium ring device to restore function of a transected anterior cruciate ligament in the goat stifle joint.* Journal of Orthopaedic Research, 2016. **34**(11): p. 2001-2008.

22. Bray, R., R. Rangayyan, and C. Frank, *Normal and healing ligament vascularity: a quantitative histological assessment in the adult rabbit medial collateral ligament.* Journal of anatomy, 1996. **188**(Pt 1): p. 87.

23. Hildebrand, K., C. Frank, and D. Hart, *Gene intervention in ligament and tendon: current status, challenges, future directions.* Gene therapy, 2004. **11**(4): p. 368-378.

24. Lo, I.K., et al., *The cellular networks of normal ovine medial collateral and anterior cruciate ligaments are not accurately recapitulated in scar tissue.* Journal of anatomy, 2002. **200**(3): p. 283-296.

25. Woo, S., et al., *Anatomy, biology, and biomechanics of tendon and ligament.* Orthopaedic basic science, 2000. **2**: p. 581-616.

26. Birk, D.E. and R.L. Trelstad, *Extraceilular Compartments in Matrix Morphogenesis: Collagen Fibril, Formation by Corneal Fibroblasts.* The Journal of cell biology, 1984. **99**: p. 2024-2033.

27. Maffulli, N., *Current Concepts Review-Rupture of the Achilles Tendon.* J Bone Joint Surg Am, 1999. **81**(7): p. 1019-36.

28. Amiel, D., et al., *Tendons and ligaments: a morphological and biochemical comparison.* Journal of Orthopaedic Research, 1983. **1**(3): p. 257-265.

29. Thornton, G., et al., *Medial collateral ligament autografts have increased creep response for at least two years and early immobilization makes this worse.* Journal of orthopaedic research, 2002. **20**(2): p. 346-352.

30. Dyer, R.F. and C.D. Enna, *Ultrastructural features of adult human tendon.* Cell and tissue research, 1976. **168**(2): p. 247-259.

31. Eyden, B. and M. Tzaphlidou, *Structural variations of collagen in normal and pathological tissues: role of electron microscopy.* Micron, 2001. **32**(3): p. 287-300.

32. Goh, J.C.-H., et al., *Tissue-engineering approach to the repair and regeneration of tendons and ligaments.* Tissue Engineering, 2003. **9**(4, Supplement 1): p. 31-44.

33. Oakes, B.W., *Collagen ultrastructure in the normal ACL and in ACL graft.* The anterior cruciate ligament. Current and future concepts, 1993: p. 209-217.

34. Ottani, V., M. Raspanti, and A. Ruggeri, *Collagen structure and functional implications.* Micron, 2001. **32**(3): p. 251-260.

35. Mechanic, G.L., *An automated scintillation counting system with high efficiency for continuous analysis: Cross-links of [3H] NaBH4-reduced collagen.* Analytical biochemistry, 1974. **61**(2): p. 349-354.

36. Tanzer, M.L., *Cross-linking of collagen.* Science, 1973. **180**(4086): p. 561-566.

37. Tanzer, M.L. and J.H. Waite, *Collagen cross-linking.* Collagen and related research, 1982. **2**(2): p. 177-180.

38. Liu, S.H., et al., *Collagen in Tendon, Ligament, and Bone Healing: A Current Review.* Clinical orthopaedics and related research, 1995. **318**: p. 265-278.

39. Birk, D. and R. Mayne, *Localization of collagen types I, III and V during tendon development. Changes in collagen types I and III are correlated with changes in fibril diameter.* European journal of cell biology, 1997. **72**(4): p. 352-361.

40. Linsenmayer, T.F., et al., *Type V collagen: molecular structure and fibrillar organization of the chicken alpha 1 (V) NH2-terminal domain, a putative regulator of corneal fibrillogenesis.* The Journal of Cell Biology, 1993. **121**(5): p. 1181-1189.

41. Niyibizi, C., et al., *Collagens in an adult bovine medial collateral ligament: immunofluorescence localization by confocal microscopy reveals that type XIV collagen predominates at the ligament-bone junction.* Matrix biology, 1995. **14**(9): p. 743-751.

42. Fukuta, S., et al., *Identification of types II, IX and X collagens at the insertion site of the bovine achilles tendon.* Matrix Biology, 1998. **17**(1): p. 65-73.

43. Niyibizi, C., et al., *Identification and immunolocalization of type X collagen at the ligament–bone interface.* Biochemical and biophysical research communications, 1996. **222**(2): p. 584-589.

44. Visconti, C.S., et al., *Biochemical analysis of collagens at the ligament–bone interface reveals presence of cartilage-specific collagens.* Archives of biochemistry and biophysics, 1996. **328**(1): p. 135-142.

45. Cooper, R.R., S. Misol, and P. Stimmel, *Tendon and ligament insertion.* J Bone Joint Surg Am, 1970. **52**(1): p. 1-170.

46. Matyas, J., et al., *Stress governs tissue phenotype at the femoral insertion of the rabbit MCL.* Journal of biomechanics, 1995. **28**(2): p. 147-157.

47. Woo, S.L.-Y., et al., *Structure and Function of Ligaments and Tendons*, in *Basic Orthopaedic Biomechanics and Mechano-Biology*, R.H. Van C. Mow, Editor. 2005. p. 301-342.

48. Benjamin, M. and J. Ralphs, *Tendons and ligaments-an overview.* Histology and histopathology, 1997. **12**(4): p. 1135-1144.

49. Chowdhury, R., J. Matyas, and C. Frank, *The "epiligament" of the rabbit medial collateral ligament: a quantitative morphological study.* Connective tissue research, 1991. **27**(1): p. 33-50.

50. Kastelic, J., A. Galeski, and E. Baer, *The multicomposite structure of tendon.* Connective tissue research, 1978. **6**(1): p. 11-23.

51. Hast, M., A. Zuskov, and L. Soslowsky, *The role of animal models in tendon research.* Bone and Joint Research, 2014. **3**(6): p. 193-202.

52. Figgie, H.E., et al., *The effects of tibial-femoral angle on the failure mechanics of the canine anterior cruciate ligament.* Journal of biomechanics, 1986. **19**(2): p. 89-91.

53. Woo, S., et al., *The biomechanical and morphological changes in the medial collateral ligament of the rabbit after immobilization and remobilization.* J Bone Joint Surg Am, 1987. **69**(8): p. 1200-1211.

54. Laros, G.S., et al., *Influence of physical activity on ligament insertions in the knees of dogs.* JBJS, 1971. **53**(2): p. 275-286.

55. Woo, S., et al., *Measurement of mechanical properties of ligament substance from a bone-ligament-bone preparation.* Journal of Orthopaedic Research, 1983. **1**(1): p. 22-29.

56. Woo, S.L.-Y., et al., *Functional Tissue Engineering of Ligament and Tendon Injuries-Chapter 54.*

57. Woo, S.L.-Y., et al., *Tensile properties of the human femur-anterior cruciate ligament-tibia complex The effects of specimen age and orientation.* The American journal of sports medicine, 1991. **19**(3): p. 217-225.

58. Woo, S.L.-Y., et al., *Effects of postmortem storage by freezing on ligament tensile behavior.* Journal of biomechanics, 1986. **19**(5): p. 399-404.

59. Woo, S.L.-Y., et al., *Temperature dependent behavior of the canine medial collateral ligament.* Journal of biomechanical engineering, 1987. **109**(1): p. 68-71.

60. Larsen, N.P., M.R. Forwood, and A.W. Parker, *Immobilization and retraining of cruciate ligaments in the rat.* Acta Orthopaedica Scandinavica, 1987. **58**(3): p. 260-264.

61. Woo, S., et al., *Mechanical properties of tendons and ligaments. II. The relationships of immobilization and exercise on tissue remodeling.* Biorheology, 1981. **19**(3): p. 397-408.

62. Ellis, D., *A shadow amplitude method for measuring cross-sectional areas of biological specimens.* Houston, TX, 1968. **51**: p. 175-186.

63. Gupta, B., et al., *Tensile strength of canine cranial cruciate ligaments.* American journal of veterinary research, 1971. **32**(1): p. 183.

64. Iaconis, F., R. Steindler, and G. Marinozzi, *Measurements of cross-sectional area of collagen structures (knee ligaments) by means of an optical method.* Journal of biomechanics, 1987. **20**(10): p. 10031009-10071010.

65. Njus, G. and N. Njus. *A noncontact method for determining cross-sectional area of soft tissues*. in *Transactions of the 32nd Meeting, Orthopaedic Research Society*. 1986.

66. Moon, D.K., S.D. Abramowitch, and S.L.-Y. Woo, *The development and validation of a charge-coupled device laser reflectance system to measure the complex cross-sectional shape and area of soft tissues.* Journal of biomechanics, 2006. **39**(16): p. 3071-3075.

67. Weiss, J.A., J.C. Gardiner, and C. Bonifasi-Lista, *Ligament material behavior is nonlinear, viscoelastic and rate-independent under shear loading.* Journal of biomechanics, 2002. **35**(7): p. 943-950.

68. Abramowitch, S.D., et al., *A biomechanical and histological evaluation of the structure and function of the healing medial collateral ligament in a goat model.* Knee Surgery, Sports Traumatology, Arthroscopy, 2003. **11**(3): p. 155-162.

69. Harner, C.D., et al., *The human posterior cruciate ligament complex: an interdisciplinary study Ligament morphology and biomechanical evaluation.* The American journal of sports medicine, 1995. **23**(6): p. 736-745.

70. Lee, T.Q. and M.I. Danto, *Application of a continuous video digitizing system for tensile testing of bone-soft tissue-bone complex.* Adv Bioeng, 1992. **22**: p. 87-90.

71. Woo, S., *Mechanical properties of tendons and ligaments. I. Quasi-static and nonlinear viscoelastic properties.* Biorheology, 1982. **19**(3): p. 385.

72. Woo, S.L., et al., *Biomechanics of knee ligaments.* The American journal of sports medicine, 1999. **27**(4): p. 533-543.

73. Lam, T., C. Frank, and N. Shrive, *Calibration characteristics of a video dimension analyser (VDA) system.* Journal of biomechanics, 1992. **25**(10): p. 1227-1231.

74. Scheffler, S.U., et al., *Structure and function of the healing medial collateral ligament in a goat model.* Annals of biomedical engineering, 2001. **29**(2): p. 173-180.

75. Smutz, W., et al., *Accuracy of a video strain measurement system.* Journal of Biomechanics, 1996. **29**(6): p. 813-817.

76. Yin, F.C., et al., *A video-dimension analyzer.* IEEE Transactions on Biomedical Engineering, 1972(5): p. 376-381.

77. Butler, D.L., F. Noyes, and E. Grood, *Ligamentous restraints to anterior-posterior drawer in the human knee. A biomechanical study.* JBJS, 1980. **62**(2): p. 259-270.

78. Furman, W., J. Marshall, and F. Girgis, *The anterior cruciate ligament. A functional analysis based on postmortem studies.* J Bone Joint Surg Am, 1976. **58**(2): p. 179-185.

79. Ahmed, A., et al., *Ligament tension pattern in the flexed knee in combined passive anterior translation and axial rotation.* Journal of Orthopaedic Research, 1992. **10**(6): p. 854-867.

80. Grood, E.S., et al., *Biomechanics of the knee-extension exercise. Effect of cutting the anterior cruciate ligament.* J Bone Joint Surg Am, 1984. **66**(5): p. 725-734.

81. Hollis, J., et al., *The effects of knee motion and external loading on the length of the anterior cruciate ligament (ACL): a kinematic study.* Journal of biomechanical engineering, 1991. **113**(2): p. 208-214.

82. Takai, S., et al., *Determination of the in situ loads on the human anterior cruciate ligament.* Journal of Orthopaedic Research, 1993. **11**(5): p. 686-695.

83. Woo, S.L., et al., *Biomechanics of the ACL: measurements of in situ force in the ACL and knee kinematics.* The Knee, 1998. **5**(4): p. 267-288.

84. Sasaki, N., et al., *Biomechanical evaluation of the quadriceps tendon autograft for anterior cruciate ligament reconstruction: a cadaveric study.* The American journal of sports medicine, 2014. **42**(3): p. 723-730.

85. Rudy, T., et al., *A combined robotic/universal force sensor approach to determine in situ forces of knee ligaments.* Journal of biomechanics, 1996. **29**(10): p. 1357-1360.

86. Livesay, G.A., et al., *Evaluation of the effect of joint constraints on the in situ force distribution in the anterior cruciate ligament.* Journal of Orthopaedic Research, 1997. **15**(2): p. 278-284.

87. Allen, C.R., et al., *Importance of the medial meniscus in the anterior cruciate ligament-deficient knee.* Journal of Orthopaedic Research, 2000. **18**(1): p. 109-115.

88. Papageorgiou, C.D., et al., *The biomechanical interdependence between the anterior cruciate ligament replacement graft and the medial meniscus.* The American journal of sports medicine, 2001. **29**(2): p. 226-231.

89. Woo, S.L.-Y., et al., *Biomechanics of knee ligaments: injury, healing, and repair.* Journal of biomechanics, 2006. **39**(1): p. 1-20.

90. Bone, U.S. and J. Decade, *The burden of musculoskeletal diseases in the United States.* Rosemont, IL: American Academy of Orthopaedic Surgeons, 2008.

91. Fukuda, Y., et al., *A quantitative analysis of valgus torque on the ACL: a human cadaveric study.* Journal of Orthopaedic Research, 2003. **21**(6): p. 1107-1112.

92. Kanamori, A., et al., *The forces in the anterior cruciate ligament and knee kinematics during a simulated pivot shift test: a human cadaveric study using robotic technology.* Arthroscopy: The Journal of Arthroscopic & Related Surgery, 2000. **16**(6): p. 633-639.

93. Kanamori, A., et al., *The effect of axial tibial torque on the function of the anterior cruciate ligament: a biomechanical study of a simulated pivot shift test.* Arthroscopy: The Journal of Arthroscopic & Related Surgery, 2002. **18**(4): p. 394-398.

94. Livesay, G.A., et al., *Determination of thein situ forces and force distribution within the human anterior cruciate ligament.* Annals of biomedical engineering, 1995. **23**(4): p. 467-474.

95. Sakane, M., et al., *In situ forces in the anterior cruciate ligament and its bundles in response to anterior tibial loads.* Journal of Orthopaedic Research, 1997. **15**(2): p. 285-293.

96. Arnoczky, S.P., *Anatomy of the anterior cruciate ligament.* Clinical orthopaedics and related research, 1983. **172**: p. 19-25.

97. Duthon, V., et al., *Anatomy of the anterior cruciate ligament.* Knee Surgery, Sports Traumatology, Arthroscopy, 2006. **14**(3): p. 204-213.

98. Haus, J. and H. Refior, *A study of the synovial and ligamentous structure of the anterior cruciate ligament.* Int Orthop, 1987. **11**(2): p. 117-124.

99. Amiel, D., et al., *Synovial fluid nutrient delivery in the diathrial joint: an analysis of rabbit knee ligaments.* Journal of Orthopaedic research, 1986. **4**(1): p. 90-95.

100. Arnoczky, S., *Blood supply to the anterior cruciate ligament and supporting structures.* The Orthopedic clinics of North America, 1985. **16**(1): p. 15-28.

101. Bray, R., A. Fisher, and C. Frank, *Fine vascular anatomy of adult rabbit knee ligaments.* Journal of anatomy, 1990. **172**: p. 69.

102. Kobayashi, S., et al., *Microvascular system of anterior cruciate ligament in dogs.* Journal of orthopaedic research, 2006. **24**(7): p. 1509-1520.

103. Murakami, Y., et al., *Permeation from the synovial fluid as nutritional pathway for the anterior cruciate ligament in rabbits.* Acta physiologica scandinavica, 1996. **158**(2): p. 181-187.

104. Scapinelli, R., *Vascular anatomy of the human cruciate ligaments and surrounding structures.* Clinical anatomy, 1997. **10**(3): p. 151-162.

105. Beaty, J., *Knee and leg: soft tissue trauma.* OKU orthopaedic knowledge update, 1999. **442**.

106. Cole, D.W., et al., *Cost comparison of anterior cruciate ligament reconstruction: autograft versus allograft.* Arthroscopy: The Journal of Arthroscopic & Related Surgery, 2005. **21**(7): p. 786-790.

107. Griffin, L.Y., et al., *Understanding and preventing noncontact anterior cruciate ligament injuries a review of the Hunt Valley II meeting, January 2005.* The American journal of sports medicine, 2006. **34**(9): p. 1512-1532.

108. Buckley, S.L., R.L. Barrack, and A.H. Alexander, *The natural history of conservatively treated partial anterior cruciate ligament tears.* The American journal of sports medicine, 1989. **17**(2): p. 221-225.

109. Daniel, D.M., et al., *Fate of the ACL-injured patient: a prospective outcome study.* The American journal of sports medicine, 1994. **22**(5): p. 632-644.

110. Kanamori, A., et al., *In-situ force in the medial and lateral structures of intact and ACL-deficient knees.* Journal of orthopaedic science, 2000. **5**(6): p. 567-571.

111. Sakane, M., et al., *Relative contribution of the ACL, MCL, and bony contact to the anterior stability of the knee.* Knee Surgery, Sports Traumatology, Arthroscopy, 1999. **7**(2): p. 93-97.

112. Giove, T.P., et al., *Non-operative treatment of the torn anterior cruciate ligament.* J Bone Joint Surg Am, 1983. **65**(2): p. 184-192.

113. Clancy, W., J. Ray, and D. Zoltan, *Acute tears of the anterior cruciate ligament. Surgical versus conservative treatment.* J Bone Joint Surg Am, 1988. **70**(10): p. 1483-1488.

114. Kostogiannis, I., et al., *Activity Level and Subjective Knee Function 15 Years After Anterior Cruciate Ligament Injury A Prospective, Longitudinal Study of Nonreconstructed Patients.* The American journal of sports medicine, 2007. **35**(7): p. 1135-1143.

115. Kessler, M., et al., *Function, osteoarthritis and activity after ACL-rupture: 11 years follow-up results of conservative versus reconstructive treatment.* Knee Surgery, Sports Traumatology, Arthroscopy, 2008. **16**(5): p. 442-448.

116. McDANIEL, W.J. and T. Dameron, *Untreated ruptures of the anterior cruciate ligament. A follow-up study.* J Bone Joint Surg Am, 1980. **62**(5): p. 696-705.

117. Andersson, C., M. Odensten, and J. Gillquist, *Knee function after surgical or nonsurgical treatment of acute rupture of the anterior cruciate ligament: a randomized study with a long-term follow-up period.* Clinical orthopaedics and related research, 1991. **264**: p. 255-263.

118. Odensten, M., et al., *Surgical or Conservative Treatment of the Acutely Torn Anterior Cruciate Ligament: A Randomized Study with Short-term Follow-up Observations.* Clinical orthopaedics and related research, 1985. **198**: p. 87-93.

119. O'donoghue, D.H., et al., *Repair of the anterior cruciate ligament in dogs.* JBJS, 1966. **48**(3): p. 503-519.

120. Engebretsen, L., et al., *A prospective, randomized study of three surgical techniques for treatment of acute ruptures of the anterior cruciate ligament.* The American journal of sports medicine, 1990. **18**(6): p. 585-590.

121. Noyes, F.R., et al., *Biomechanical analysis of human ligament grafts used in knee-ligament repairs and reconstructions.* J Bone Joint Surg Am, 1984. **66**(3): p. 344-352.

122. Beynnon, B.D., et al., *Anterior cruciate ligament replacement: comparison of bone-patellar tendon-bone grafts with two-strand hamstring grafts.* J Bone Joint Surg Am, 2002. **84**(9): p. 1503-1513.

123. Feller, J.A. and K.E. Webster, *A randomized comparison of patellar tendon and hamstring tendon anterior cruciate ligament reconstruction.* The American Journal of Sports Medicine, 2003. **31**(4): p. 564-573.

124. Spindler, K.P., et al., *Anterior cruciate ligament reconstruction autograft choice: bone-tendon-bone versus hamstring does it really matter? A systematic review.* The American journal of sports medicine, 2004. **32**(8): p. 1986-1995.

125. Järvelä, T., P. Kannus, and M. Järvinen, *Anterior knee pain 7 years after an anterior cruciate ligament reconstruction with a bone-patellar tendon-bone autograft.* Scandinavian journal of medicine & science in sports, 2000. **10**(4): p. 221-227.

126. Kartus, J., T. Movin, and J. Karlsson, *Donor-site morbidity and anterior knee problems after anterior cruciate ligament reconstruction using autografts.* Arthroscopy: The Journal of Arthroscopic & Related Surgery, 2001. **17**(9): p. 971-980.

127. Colombet, P., et al., *Anterior cruciate ligament reconstruction using four-strand semitendinosus and gracilis tendon grafts and metal interference screw fixation.* Arthroscopy: The Journal of Arthroscopic & Related Surgery, 2002. **18**(3): p. 232-237.

128. Marder, R.A., J.R. Raskind, and M. Carroll, *Prospective evaluation of arthroscopically assisted anterior cruciate ligament reconstruction: patellar tendon versus semitendinosus and gracilis tendons.* The American Journal of Sports Medicine, 1991. **19**(5): p. 478-484.

129. Yasuda, K., et al., *Anatomic reconstruction of the anteromedial and posterolateral bundles of the anterior cruciate ligament using hamstring tendon grafts.* Arthroscopy: The Journal of Arthroscopic & Related Surgery, 2004. **20**(10): p. 1015-1025.

130. Akoto, R. and J. Hoeher, *Anterior cruciate ligament (ACL) reconstruction with quadriceps tendon autograft and press-fit fixation using an anteromedial portal technique.* BMC musculoskeletal disorders, 2012. **13**(1): p. 161.

131. Chen, C.-H., et al., *Arthroscopic anterior cruciate ligament reconstruction with quadriceps tendon autograft: clinical outcome in 4–7 years.* Knee Surgery, Sports Traumatology, Arthroscopy, 2006. **14**(11): p. 1077-1085.

132. DeAngelis, J.P. and J.P. Fulkerson, *Quadriceps tendon—A reliable alternative for reconstruction of the anterior cruciate ligament.* Clinics in sports medicine, 2007. **26**(4): p. 587-596.

133. Theut, P.C., et al., *Anterior cruciate ligament reconstruction utilizing central quadriceps free tendon.* Orthopedic Clinics of North America, 2003. **34**(1): p. 31-39.

134. Drogset, J.O., et al., *A sixteen-year follow-up of three operative techniques for the treatment of acute ruptures of the anterior cruciate ligament.* J Bone Joint Surg Am, 2006. **88**(5): p. 944-952.

135. Jomha, N.M., et al., *Long Term Osteoarthritic Changes in Anterior Cruciate Ligament Reconstructed Knees.* Clinical Orthopaedics and related research, 1999. **358**: p. 188-193.

136. Selmi, T.A.S., D. Fithian, and P. Neyret, *The evolution of osteoarthritis in 103 patients with ACL reconstruction at 17 years follow-up.* The Knee, 2006. **13**(5): p. 353-358.

137. Frank, C., et al., *Medial collateral ligament healing: a multidisciplinary assessment in rabbits.* The American journal of sports medicine, 1983. **11**(6): p. 379-389.

138. Inoue, M., et al., *Effects of surgical treatment and immobilization on the healing of the medial collateral ligament: a long-term multidisciplinary study.* Connective tissue research, 1990. **25**(1): p. 13-26.

139. Woo, S.L., et al., *The response of ligaments to injury: Healing of the collateral ligaments.* Knee ligaments: structure, function, injury, and repair, 1990: p. 351-64.

140. Woo, S.L.-Y., et al., *Treatment of the medial collateral ligament injury II: Structure and function of canine knees in response to differing treatment regimens.* The American journal of sports medicine, 1987. **15**(1): p. 22-29.

141. Frank, C.B., et al., *Soft Tissue Healing*, in *Knee surgery*, F.H. Fu, C.D. Harner, and Vince Kelly G., Editors. 1994, Williams & Wilkins: Baltimore, MD. p. 189-229.

142. Murphy, P.G., et al., *Influence of exogenous growth factors on the synthesis and secretion of collagen types I and III by explants of normal and healing rabbit ligaments.* Biochemistry & Cell Biology, 1994. **72**(9-10): p. 403-9.

143. Frank, C., et al., *Collagen fibril diameters in the healing adult rabbit medial collateral ligament.* Connective Tissue Research, 1992. **27**(4): p. 251-63.

144. Hart, R.A., S.L. Woo, and P.O. Newton, *Ultrastructural morphometry of anterior cruciate and medial collateral ligaments: an experimental study in rabbits.* J Orthop Res, 1992. **10**(1): p. 96-103.

145. Adachi, E. and T. Hayashi, *In vitro formation of hybrid fibrils of type V collagen and type I collagen. Limited growth of type I collagen into thick fibrils by type V collagen.* Connect Tissue Res, 1986. **14**(4): p. 257-66.

146. Birk, D.E., et al., *Collagen fibrillogenesis in vitro: interaction of types I and V collagen regulates fibril diameter.* Journal of Cell Science, 1990. **95**(Pt 4): p. 649-57.

147. Marchant, J.K., et al., *Reduction of type V collagen using a dominant-negative strategy alters the regulation of fibrillogenesis and results in the loss of corneal-specific fibril morphology.* Journal of Cell Biology, 1996. **135**(5): p. 1415-26.

148. Doillon, C.J., et al., *Collagen fiber formation in repair tissue: development of strength and toughness.* Coll Relat Res, 1985. **5**(6): p. 481-92.

149. Parry, D., G. Barnes, and A. Craig, *A comparision of the size distribution of collagen fibrils in connective tissues as a function of age and a possible relation between fibril size distribution and mechanical properties.* Proc. R. Soc. Lond., 1978. **(Biol).** p. 305-321.

150. Clayton, M.L., J.S. Miles, and M. Abdulla, *Experimental investigations of ligamentous healing.* Clin Orthop Relat Res, 1968. **61**: p. 146-53.

151. O'Donoghue, D.H., et al., *Repair and reconstruction of the anterior cruciate ligament in dogs. Factors influencing long-term results.* J Bone Joint Surg Am, 1971. **53**(4): p. 710-8.

152. Tipton, C.M., et al., *Influence of exercise on strength of medial collateral knee ligaments of dogs.* Am J Physiol, 1970. **218**(3): p. 894-902.

153. Woo, S.L., et al., *Treatment of the medial collateral ligament injury. II: Structure and function of canine knees in response to differing treatment regimens.* Am J Sports Med, 1987. **15**(1): p. 22-9.

154. Woo, S.L., et al., *The effects of transection of the anterior cruciate ligament on healing of the medial collateral ligament. A biomechanical study of the knee in dogs.* J Bone Joint Surg Am, 1990. **72**(3): p. 382-92.

155. Inoue, M., et al., *Effects of surgical treatment and immobilization on the healing of the medial collateral ligament: a long-term multidisciplinary study.* Connect Tissue Res, 1990. **25**(1): p. 13-26.

156. Weiss, J.A., et al., *Evaluation of a new injury model to study medial collateral ligament healing: primary repair versus nonoperative treatment.* Journal of Orthopaedic Research, 1991. **9**(4): p. 516-28.

157. Indelicato, P.A., *Non-operative treatment of complete tears of the medial collateral ligament of the knee.* J Bone Joint Surg Am, 1983. **65**(3): p. 323-9.

158. Reider, B., et al., *Treatment of isolated medial collateral ligament injuries in athletes with early functional rehabilitation. A five-year follow-up study.* Am J Sports Med, 1994. **22**(4): p. 470-7.

159. Musahl, V., et al., *Tensile properties of an anterior cruciate ligament graft after bone–patellar tendon–bone press-fit fixation.* Knee Surgery, Sports Traumatology, Arthroscopy, 2003. **11**(2): p. 68-74.

160. Amiel, D., et al., *Injury of the anterior cruciate ligament: the role of collagenase in ligament degeneration.* Journal of Orthopaedic Research, 1989. **7**(4): p. 486-493.

161. Warren, R.F., *Primary repair of the anterior cruciate ligament.* Clinical orthopaedics and related research, 1983. **172**: p. 65-70.

162. Hefti, F.L., et al., *Healing of the transected anterior cruciate ligament in the rabbit.* J Bone Joint Surg Am, 1991. **73**(3): p. 373-383.

163. Kobayashi, D., et al., *Effect of basic fibroblast growth factor on the healing of defects in the canine anterior cruciate ligament.* Knee Surgery, Sports Traumatology, Arthroscopy, 1997. **5**(3): p. 189-194.

164. Murray, M.M., et al., *Histological changes in the human anterior cruciate ligament after rupture.* J Bone Joint Surg Am, 2000. **82**(10): p. 1387-1387.

165. Murray, M.M., et al., *Use of a collagen-platelet rich plasma scaffold to stimulate healing of a central defect in the canine ACL.* Journal of Orthopaedic Research, 2006. **24**(4): p. 820-830.

166. Wiig, M.E., et al., *The early effect of high molecular weight hyaluronan (hyaluronic acid) on anterior cruciate ligament healing: an experimental study in rabbits.* Journal of Orthopaedic Research, 1990. **8**(3): p. 425-434.

167. Frank, C., D. Amiel, and W. Akeson, *Healing of the medial collateral ligament of the knee: a morphological and biochemical assessment in rabbits.* Acta Orthopaedica Scandinavica, 1983. **54**(6): p. 917-923.

168. Indelicato, P.A., *Isolated medial collateral ligament injuries in the knee.* Journal of the American Academy of Orthopaedic Surgeons, 1995. **3**(1): p. 9-14.

169. Weiss, J.A., et al., *Evaluation of a new injury model to study medial collateral ligament healing: primary repair versus nonoperative treatment.* Journal of Orthopaedic Research, 1991. **9**(4): p. 516-528.

170. Nagineni, C.N., et al., *Characterization of the intrinsic properties of the anterior cruciate and medial collateral ligament cells: an in vitro cell culture study.* Journal of orthopaedic research, 1992. **10**(4): p. 465-475.

171. Lee, J., et al., *Growth factor expression in healing rabbit medial collateral and anterior cruciate ligaments.* The Iowa orthopaedic journal, 1998. **18**: p. 19.

172. Wiig, M., et al., *Type I procollagen gene expression in normal and early healing of the medial collateral and anterior cruciate ligaments in rabbits: an in situ hybridization study.* Journal of orthopaedic research, 1991. **9**(3): p. 374-382.

173. Kobayashi, K., et al., *Novel method for the quantitative assessment of cell migration: a study on the motility of rabbit anterior cruciate (ACL) and medial collateral ligament (MCL) cells.* Tissue engineering, 2000. **6**(1): p. 29-38.

174. Fukui, N., et al., *Metabolic activity in disrupted human anterior cruciate ligament. Evaluation of procollagen mRNA expression in 29 patients.* Joint Bone Spine, 2001. **68**(4): p. 318-326.

175. Steadman, J.R., et al., *Outcomes following healing response in older, active patients: a primary anterior cruciate ligament repair technique.* Journal of Knee Surgery, 2012. **25**(03): p. 255-260.

176. Murray, M.M., et al., *Enhanced histologic repair in a central wound in the anterior cruciate ligament with a collagen–platelet-rich plasma scaffold.* Journal of Orthopaedic Research, 2007. **25**(8): p. 1007-1017.

177. Gobbi, A., L. Bathan, and L. Boldrini, *Primary repair combined with bone marrow stimulation in acute anterior cruciate ligament lesions results in a group of athletes.* The American journal of sports medicine, 2009. **37**(3): p. 571-578.

178. Murray, M.M., et al., *Collagen-platelet rich plasma hydrogel enhances primary repair of the porcine anterior cruciate ligament.* Journal of Orthopaedic Research, 2007. **25**(1): p. 81-91.

179. Nguyen, D.T., et al., *Histological characteristics of ligament healing after bio-enhanced repair of the transected goat ACL.* Journal of experimental orthopaedics, 2015. **2**(1): p. 4.

180. Nguyen, D.T., et al., *Healing of the goat anterior cruciate ligament after a new suture repair technique and bioscaffold treatment.* Tissue Engineering Part A, 2013. **19**(19-20): p. 2292-2299.

181. Fleming, B.C., et al., *Can suture repair of ACL transection restore normal anteroposterior laxity of the knee? An ex vivo study.* Journal of Orthopaedic Research, 2008. **26**(11): p. 1500-1505.

182. Fisher, M.B., et al., *Evaluation of bone tunnel placement for suture augmentation of an injured anterior cruciate ligament: effects on joint stability in a goat model.* Journal of Orthopaedic Research, 2010. **28**(10): p. 1373-1379.

183. Fisher, M.B., et al., *Suture augmentation following ACL injury to restore the function of the ACL, MCL, and medial meniscus in the goat stifle joint.* Journal of biomechanics, 2011. **44**(8): p. 1530-1535.

184. Fisher, M.B., Kim, K.E., Jung, H-J., and P.J. McMahon, Woo, S.L-Y., *Mechanical Augmentation Using Sutures to Stimulate Healing of the ACL in the Goat Model.* International Symposium on Ligaments and Tendons – XI, 2011: p. 42.

185. Farraro, K.F., et al., *Magnesium ring device to restore function of a transected anterior cruciate ligament in the goat stifle joint.* Journal of Orthopaedic Research, 2016.

186. Kathryn F. Farraro, A.P., Jonquil R. Mau, Savio L-Y. Woo, *A Novel Magnesium Ring Device Can Enhance Anterior Cruciate Ligament Healing*, in *Orthopaedic Reseach Society Annual Meeting*. 2016: Orlando, Florida.

187. Ng, G.Y., et al., *Biomechanics of patellar tendon autograft for reconstruction of the anterior cruciate ligament in the goat: Three-year study.* Journal of orthopaedic research, 1995. **13**(4): p. 602-608.

188. Geetha, M., et al., *Ti based biomaterials, the ultimate choice for orthopaedic implants – A review.* Progress in Materials Science, 2009. **54**(3): p. 397-425.

189. Jacobs, J.J., et al., *Metal release in patients who have had a primary total hip arthroplasty. A prospective, controlled, longitudinal study.* J Bone Joint Surg Am, 1998. **80**(10): p. 1447-58.

190. Songür, M., et al., *Electrochemical corrosion properties of metal alloys used in orthopaedic implants.* Journal of Applied Electrochemistry, 2009. **39**(8): p. 1259.

191. Wang, J.Y., et al., *Titanium, chromium and cobalt ions modulate the release of bone-associated cytokines by human monocytes/macrophages in vitro.* Biomaterials, 1996. **17**(23): p. 2233-2240.

192. Butler, D.L., S.A. Goldstein, and F. Guilak, *Functional tissue engineering: the role of biomechanics.* Ann Arbor, 2000. **1001**(48109-0486): p. 77-78.

193. Ge, Z., et al., *Biomaterials and scaffolds for ligament tissue engineering.* Journal of biomedical materials research Part A, 2006. **77**(3): p. 639-652.

194. Navarro, M., et al., *Biomaterials in orthopaedics.* Journal of the Royal Society Interface, 2008. **5**(27): p. 1137-1158.

195. Drury, J.L. and D.J. Mooney, *Hydrogels for tissue engineering: scaffold design variables and applications.* Biomaterials, 2003. **24**(24): p. 4337-4351.

196. Lu, H.H. and S. Thomopoulos, *Functional attachment of soft tissues to bone: development, healing, and tissue engineering.* Annual review of biomedical engineering, 2013. **15**: p. 201-226.

197. Smith, C.A., et al., *Fracture of Bilok interference screws on insertion during anterior cruciate ligament reconstruction.* Arthroscopy: The Journal of Arthroscopic & Related Surgery, 2003. **19**(9): p. e115-e117.

198. Johnston, M., et al., *Resorption and Remodeling of Hydroxyapatite–Poly-L-Lactic Acid Composite Anterior Cruciate Ligament Interference Screws.* Arthroscopy: The Journal of Arthroscopic & Related Surgery, 2011. **27**(12): p. 1671-1678.

199. Walton, M. and N.J. Cotton, *Long-term in vivo degradation of poly-L-lactide (PLLA) in bone.* Journal of Biomaterials Applications, 2007. **21**(4): p. 395-411.

200. Tecklenburg, K., et al., *Prospective evaluation of patellar tendon graft fixation in anterior cruciate ligament reconstruction comparing composite bioabsorbable and*

allograft interference screws. Arthroscopy: The Journal of Arthroscopic & Related Surgery, 2006. **22**(9): p. 993-999.

201. Witte, F., *Reprint of: The history of biodegradable magnesium implants: A review.* Acta biomaterialia, 2015. **23**: p. S28-S40.

202. Staiger, M.P., et al., *Magnesium and its alloys as orthopedic biomaterials: a review.* Biomaterials, 2006. **27**(9): p. 1728-1734.

203. Zheng, Y., X. Gu, and F. Witte, *Biodegradable metals.* Materials Science and Engineering: R: Reports, 2014. **77**: p. 1-34.

204. Witte, F., et al., *Degradable biomaterials based on magnesium corrosion.* Current opinion in solid state and materials science, 2008. **12**(5): p. 63-72.

205. Cao, J.D., et al., *Quantitative in vitro assessment of Mg65Zn30Ca5 degradation and its effect on cell viability.* Journal of Biomedical Materials Research Part B: Applied Biomaterials, 2013. **101**(1): p. 43-49.

206. Kirkland, N., et al., *A survey of bio-corrosion rates of magnesium alloys.* Corrosion Science, 2010. **52**(2): p. 287-291.

207. Li, N., et al., *Corrosion resistance and cytotoxicity of a MgF2 coating on biomedical Mg–1Ca alloy via vacuum evaporation deposition method.* Surface and Interface Analysis, 2013. **45**(8): p. 1217-1222.

208. Li, Z., et al., *The development of binary Mg–Ca alloys for use as biodegradable materials within bone.* Biomaterials, 2008. **29**(10): p. 1329-1344.

209. Chou, D.-T., et al., *In vitro and in vivo corrosion, cytocompatibility and mechanical properties of biodegradable Mg–Y–Ca–Zr alloys as implant materials.* Acta biomaterialia, 2013. **9**(10): p. 8518-8533.

210. Hong, D., et al., *In vitro degradation and cytotoxicity response of Mg–4% Zn–0.5% Zr (ZK40) alloy as a potential biodegradable material.* Acta biomaterialia, 2013. **9**(10): p. 8534-8547.

211. Witte, F., et al., *In vivo corrosion of four magnesium alloys and the associated bone response.* Biomaterials, 2005. **26**(17): p. 3557-3563.

212. Wei, J., et al., *Hierarchically microporous/macroporous scaffold of magnesium–calcium phosphate for bone tissue regeneration.* Biomaterials, 2010. **31**(6): p. 1260-1269.

213. Joshia, M., et al., *Magnesium Single Crystal as a Biodegradable Implant Material.* Biomaterials Science: Processing, Properties and Applications V: Ceramic Transactions, 2015. **254**: p. 97.

214. Liu, M., et al., *The effect of crystallographic orientation on the active corrosion of pure magnesium.* Scripta Materialia, 2008. **58**(5): p. 421-424.

215. Shin, K., et al., *Characterization of biodegradable magnesium single crystals with various crystallographic orientations.* Eur. Cells Mater, 2013. **26**(4).

216. Shin, K.S., M.Z. Bian, and N.D. Nam, *Effects of crystallographic orientation on corrosion behavior of magnesium single crystals.* Jom, 2012. **64**(6): p. 664-670.

217. Song, G.-L. and Z. Xu, *Crystal orientation and electrochemical corrosion of polycrystalline Mg.* Corrosion Science, 2012. **63**: p. 100-112.

218. White, L.G., *Investigation of Coatings with Controlled Degradation for Biodegradable Magnesium Implants*, in *Department of Mechanical Engineering*. 2014, North Carolina Agricultural & Technical State University. p. 209.

219. Esmaily, M., et al., *Fundamentals and Advances in Magnesium Alloy Corrosion.* Progress in Materials Science, 2017.

220. Chen, Y., et al., *Recent advances on the development of magnesium alloys for biodegradable implants.* Acta biomaterialia, 2014. **10**(11): p. 4561-4573.

221. Zhang, L.-N., et al., *The effect of selected alloying element additions on properties of Mg-based alloy as bioimplants: A literature review.* Frontiers of Materials Science, 2013. **7**(3): p. 227-236.

222. Hofstetter, J., et al., *Assessing the degradation performance of ultrahigh-purity magnesium in vitro and in vivo.* Corrosion Science, 2015. **91**: p. 29-36.

223. Hartwig, A., *Role of magnesium in genomic stability.* Mutation Research/Fundamental and Molecular Mechanisms of Mutagenesis, 2001. **475**(1): p. 113-121.

224. Lewis III, J., *Water, electrolyte, mineral, and acid-base metabolism.* The Merck manual of diagnosis and therapy. Whitehouse Station, NJ: Merck Research Laboratories, 1999: p. 120-64.

225. Okuma, T., *Magnesium and bone strength*. 2001, Elsevier.

226. Saris, N.-E.L., et al., *Magnesium: an update on physiological, clinical and analytical aspects.* Clinica chimica acta, 2000. **294**(1): p. 1-26.

227. Vormann, J., *Magnesium: nutrition and metabolism.* Molecular aspects of medicine, 2003. **24**(1): p. 27-37.

228. Wolf, F.I. and A. Cittadini, *Chemistry and biochemistry of magnesium.* Molecular aspects of medicine, 2003. **24**(1): p. 3-9.

229. Witte, F., et al., *Characterization of degradable magnesium alloys as orthopedic implant material by synchrotron-radiation-based microtomography. 2001*.

230. Ernstberger, T., G. Buchhorn, and G. Heidrich, *Artifacts in spine magnetic resonance imaging due to different intervertebral test spacers: an in vitro evaluation of magnesium versus titanium and carbon-fiber-reinforced polymers as biomaterials.* Neuroradiology, 2009. **51**(8): p. 525-529.

231. Willbold, E., et al., *Corrosion of magnesium alloy AZ31 screws is dependent on the implantation site.* Materials Science and Engineering: B, 2011. **176**(20): p. 1835-1840.

232. Curran, J. and T. Clyne, *Porosity in plasma electrolytic oxide coatings.* Acta Materialia, 2006. **54**(7): p. 1985-1993.

233. Bordji, K., et al., *Cytocompatibility of Ti-6Al-4V and Ti-5Al-2.5 Fe alloys according to three surface treatments, using human fibroblasts and osteoblasts.* Biomaterials, 1996. **17**(9): p. 929-940.

234. Hussein, R., X. Nie, and D. Northwood, *Plasma electrolytic oxidation coatings on Mg-alloys for improved wear and corrosion resistance.* Corrosion: Material Performance and Cathodic Protection, 2017. **99**: p. 133.

235. Luo, H., et al., *Effect of (NaPO 3) 6 concentrations on corrosion resistance of plasma electrolytic oxidation coatings formed on AZ91D magnesium alloy.* Journal of Alloys and Compounds, 2008. **464**(1): p. 537-543.

236. Sun, X., et al., *Composition and mechanical properties of hard ceramic coating containing α-Al 2 O 3 produced by microarc oxidation on Ti–6Al–4V alloy.* Thin Solid Films, 2005. **471**(1): p. 194-199.

237. Berglundh, T., et al., *Spontaneous progression of ligature induced peri-implantitis at implants with different surface roughness: an experimental study in dogs.* Clinical Oral Implants Research, 2007. **18**(5): p. 655-661.

238. Sundararajan, G. and L.R. Krishna, *Mechanisms underlying the formation of thick alumina coatings through the MAO coating technology.* Surface and Coatings Technology, 2003. **167**(2): p. 269-277.

239. Tian, J., et al., *Structure and antiwear behavior of micro-arc oxidized coatings on aluminum alloy.* Surface and Coatings Technology, 2002. **154**(1): p. 1-7.

240. White, L., et al., *Enhanced mechanical properties and increased corrosion resistance of a biodegradable magnesium alloy by plasma electrolytic oxidation (PEO).* Materials Science and Engineering: B, 2016. **208**: p. 39-46.

241. Cui, X.-j., et al., *Fabrication and corrosion resistance of a hydrophobic micro-arc oxidation coating on AZ31 Mg alloy.* Corrosion Science, 2015. **90**: p. 402-412.

242. Hezi-Yamit, A., et al., *Impact of polymer hydrophilicity on biocompatibility: implication for DES polymer design.* Journal of Biomedical Materials Research Part A, 2009. **90**(1): p. 133-141.

243. Zhang, L., H. Zeng, and Q. Liu, *Probing Molecular and Surface Interactions of Comb-Type Polymer Polystyrene-graft-poly (ethylene oxide)(PS-g-PEO) with an SFA.* The Journal of Physical Chemistry C, 2012. **116**(33): p. 17554-17562.

244. Nguyen, T.D., et al., *Effects of cell seeding and cyclic stretch on the fiber remodeling in an extracellular matrix–derived bioscaffold.* Tissue Engineering Part A, 2008. **15**(4): p. 957-963.

245. Badylak, S.F., et al., *Marrow-derived cells populate scaffolds composed of xenogeneic extracellular matrix.* Experimental hematology, 2001. **29**(11): p. 1310-1318.

246. Hodde, J., et al., *Fibronectin peptides mediate HMEC adhesion to porcine-derived extracellular matrix.* Biomaterials, 2002. **23**(8): p. 1841-1848.

247. Li, F., et al., *Low-molecular-weight peptides derived from extracellular matrix as chemoattractants for primary endothelial cells*. 2004, Taylor & Francis.

248. McPherson, T., et al., *Galα (1, 3) Gal epitope in porcine small intestinal submucosa.* Tissue engineering, 2000. **6**(3): p. 233-239.

249. Voytik-Harbin, S.L., et al., *Identification of extractable growth factors from small intestinal submucosa.* Journal of cellular biochemistry, 1997. **67**(4): p. 478-491.

250. Zantop, T., et al., *Extracellular matrix scaffolds are repopulated by bone marrow-derived cells in a mouse model of Achilles tendon reconstruction.* Journal of Orthopaedic Research, 2006. **24**(6): p. 1299-1309.

251. Brown, B.N., et al., *Macrophage phenotype and remodeling outcomes in response to biologic scaffolds with and without a cellular component.* Biomaterials, 2009. **30**(8): p. 1482-1491.

252. Agrawal, V., et al., *Recruitment of progenitor cells by an extracellular matrix cryptic peptide in a mouse model of digit amputation.* Tissue engineering Part A, 2011. **17**(19-20): p. 2435-2443.

253. Badylak, S.F., D.O. Freytes, and T.W. Gilbert, *Extracellular matrix as a biological scaffold material: Structure and function.* Acta Biomaterialia, 2009. **5**(1): p. 1-13.

254. Liang, R., et al., *Long-term effects of porcine small intestine submucosa on the healing of medial collateral ligament: A functional tissue engineering study.* Journal of orthopaedic research, 2006. **24**(4): p. 811-819.

255. Musahl, V., et al., *The use of porcine small intestinal submucosa to enhance the healing of the medial collateral ligament—a functional tissue engineering study in rabbits.* Journal of Orthopaedic Research, 2004. **22**(1): p. 214-220.

256. Karaoglu, S., et al., *Use of a bioscaffold to improve healing of a patellar tendon defect after graft harvest for ACL reconstruction: a study in rabbits.* Journal of Orthopaedic Research, 2008. **26**(2): p. 255-263.

257. Abramowitch, S.D., et al., *The effect of initial graft tension on the biomechanical properties of a healing ACL replacement graft: a study in goats.* Journal of orthopaedic research, 2003. **21**(4): p. 708-715.

258. Papageorgiou, C.D., et al., *A multidisciplinary study of the healing of an intraarticular anterior cruciate ligament graft in a goat model.* The American journal of sports medicine, 2001. **29**(5): p. 620-626.

259. Turner, N.J., et al., *Quantitative multispectral imaging of Herovici's polychrome for the assessment of collagen content and tissue remodelling.* Journal of tissue engineering and regenerative medicine, 2013. **7**(2): p. 139-148.

260. Livesay, G.A., et al., *Determination of the in-Situ Forces and Force Distribution within the Human Anterior Cruciate Ligament.* Annals of Biomedical Engineering, 1995. **23**(4): p. 467-474.

261. Rudy, T.W., et al., *A combined robotic/universal force sensor approach to determine in situ forces of knee ligaments.* J Biomech, 1996. **29**(10): p. 1357-1360.

262. Woo, S.L.Y., et al., *The effectiveness of reconstruction of the anterior cruciate ligament with hamstrings and patellar tendon - A cadaveric study comparing anterior tibial and rotational loads.* Journal of Bone and Joint Surgery-American Volume, 2002. **84A**(6): p. 907-914.

263. Alberghina, D., et al., *Analysis of serum proteins in clinically healthy goats (Capra hircus) using agarose gel electrophoresis.* Veterinary Clinical Pathology, 2010. **39**(3): p. 317-321.

264. Farraro, K., *Regeneration of the Anterior Cruciate Ligament Using Resorbable Metallic and Extracellular Matrix Bioscaffolds*. 2015, University of Pittsburgh.

265. Ballock, R.T., et al., *Use of patellar tendon autograft for anterior cruciate ligament reconstruction in the rabbit: A long-term histologic and biomechanical study.* Journal of Orthopaedic Research, 1989. **7**(4): p. 474-485.

266. Beynnon, B.D., et al., *The relationship between anterior-posterior knee laxity and the structural properties of the patellar tendon graft: a study in canines.* The American journal of sports medicine, 1994. **22**(6): p. 812-820.

267. Faust, A., et al., *Urinary bladder extracellular matrix hydrogels and matrix-bound vesicles differentially regulate central nervous system neuron viability and axon growth and branching.* Journal of Biomaterials Applications, 2017. **31**(9): p. 1277-1295.

268. Huleihel, L., et al., *Matrix bound nanovesicles recapitulate extracellular matrix effects on macrophage phenotype.* Tissue Engineering, 2017(ja).